Mathematical modelling of lymphocyte-mediated immune responses

Von der Fakultät für Lebenswissenschaften

der Technischen Universität Carolo-Wilhelmina

zu Braunschweig

zur Erlangung des Grades eines

Doktors der Naturwissenschaften

(Dr. rer. nat.)

genehmigte

D i s s e r t a t i o n

von Aleksei Uvarovskii
aus Velikij Ustyug

1. Referent:	Prof. Dr. Michael Meyer-Hermann
2. Referent:	Prof. Dr. Klemens Rottner
eingereicht am:	29.06.2016
mündliche Prüfung (Disputation) am:	28.11.2016

Druckjahr 2017

Vorveröffentlichungen der Dissertation

Teilergebnisse aus dieser Arbeit wurden mit Genehmigung der Fakultät für Lebenswissenschaften, vertreten durch den Mentor der Arbeit, in folgenden Beiträgen vorab veröffentlicht:

Publikationen

- Hernandez-Vargas, Esteban A., Esther Wilk, Laetitia Canini, Franklin R. Toapanta, Sebastian C. Binder, Alexey Uvarovskii, Ted M. Ross, Carlos A. Guzman, Alan S. Perelson, and Michael Meyer-Hermann. "Effects of Aging on Influenza Virus Infection Dynamics." Journal of virology 88, no. 8 (2014): 4123-4131.
- Halle, Stephan, Kirsten Anja Keyser, Felix Rolf Stahl, Andreas Busche, Anja Marquardt, Xiang Zheng, Melanie Galla et al. "In Vivo Killing Capacity of Cytotoxic T Cells Is Limited and Involves Dynamic Interactions and T Cell Cooperativity." Immunity (2016).

Tagungsbeiträge

- Uvarovskii Alexey, and Michael Meyer-Hermann. "What is the Impact of Germinal Centre Interactions on Germinal Centre Development?" Scandinavian Journal of Immunology. Vol. 80. No. 3. 111 River St, Hoboken 07030-5774, NJ USA: Wiley-Blackwell, 2014.
- Uvarovskii Alexey and Michael Meyer-Hermann. “Modelling of germinal centres interactions”. 12th B cell forum, Kriekenbeck, Germany (2014).
- Uvarovskii Alexey, Nadine Schaadt, Friedrich Feuerhake, Michael Meyer-Hermann. “Modelling of tertiary lymphoid organ development in the context of kidney transplant.” 6th Conference on Systems Biology of Mammalian Cells, Münich, Germany (2016).

Auszüge dieser Arbeit wurden im Rahmen der oben genannten Vorver öffentlichungen in Fachzeitschriften veröffentlicht. Der Abdruck erfolgt mit freundlicher Genehmigung dieser Zeitschriften. Weiterhin wird darauf hingewiesen, dass Abschnitte, Resultate und Abbildungen dieser Dissertation zum Teil oder vollständig in zukünftigen Veröffentlichungen des Autors verwendet werden.

Summary

The adaptive immune response is crucial for defence of organisms against infections. There are two main cell populations of the adaptive immune system, T and B lymphocytes, bearing specific receptors which allow to recognise infection and cancer antigens. Although these cells may play a beneficial role in viral or bacterial infection, in some cases, like autoimmune diseases or organ transplantation, T and B cell responses are undesired.

Chronic graft rejection is associated with the production of donor-specific antibodies by B cells, and is the main reason for late graft failure. Immune cell clusters called tertiary lymphoid organs (TLOs), which develop at chronic inflammation sites, are shown to be related to graft rejection in mice. The stability of these clusters depends on the interactions of lymphocytes with stromal cells via chemokine and cell surface proteins, which is modelled in chapter 3. Besides analytical approach, I implemented a 3D agent-based off-lattice model, which allows to describe cell migration, chemokine diffusion and receptor internalisation dynamics. I show that chemokine degradation by proteolysis does not influence its concentration in the vicinity of a secreting cell. In addition, I study how consumption of the chemokine may change its gradient or even invert it at certain model parameters. Such a framework might help in planning of therapies aimed to destabilize TLOs structure.

In chapter 4, I model interaction of germinal centres (GCs). GCs are organized clusters of immune and stromal cells in secondary and tertiary lymphoid tissue, which are responsible for the generation of B cell clones producing high affinity antibodies. Injected antibodies are shown to mask antigen which is presented to B cells in GCs. It motivates to consider GCs as a system of agents interacting via antibodies. Simulation of a system of interacting GCs suggested the possibility for early GCs to suppress development of the later ones. I hope to provoke new experiments in order to investigate influence of antibodies on the GC reaction course more precisely, which might help to regulate GC responses in different clinical conditions.

Besides antibody responses, a cytotoxic T cell (CTL) activity might also find application in clinics. In chapter 5, I estimated killing rates for CTLs in different experimental set-ups. Using the data from *in vivo* microscopy about target cell fate depending on the contacts with CTLs I show that previous contacts dramatically increase the probability of target cells to die. This kind of modelling may be used for optimization of T cell-based therapies.

Zusammenfassung

Die adaptive Immunantwort ist essentiell für die Verteidigung des Organismus gegen Infektionen. Es gibt zwei wesentliche Zellpopulationen des adaptiven Immunsystems, die T- und B-Lymphozyten, welche spezifische Rezeptoren tragen, die ihnen erlauben, Antigene in Infektionen und Krebs zu erkennen. Obwohl diese Zellen bei viralen oder bakteriellen Erkrankungen hilfreich sind, ist die T- und B-Zell Immunantwort unter bestimmten Bedingungen wie Autoimmunerkrankungen oder Organtransplantationen unerwünscht.

Chronische Transplantatabstoßung geht mit der Produktion spezifischer Antikörper gegen das Spendergewebe einher und ist der Haupgrund für spätes Transplantatatversagen. Verbünde von Immunzellen, genannt tertiäre lymphoide Organe (TLO), die sich an chronischen Entzündungsherden bilden, stehen mit der Transplantatabstoßung in Mäusen im Zusammenhang. Die Stabilität dieser Zellverbünde hängt von über Chemokine und Oberflächenproteine vermittelten Interaktionen ab, die in Kapitel 3 modelliert werden. Neben einem analytischen Ansatz habe ich ein dreidimensionales agentenbasiertes Off-lattice-Modell implementiert, das es uns erlaubt, die Zellmigration, Diffusion von Chemokin und die Dynamik der Rezeptorinternalisierung zu beschreiben. Ich zeige hier, dass die Degradation von Chemokin durch Proteolyse dessen Konzentration in der Umgebung einer chemokinproduzierenden Zelle nicht beeinflusst. Weiterhin untersuche ich, wie der Verbrauch von Chemokin dessen Gradienten unter bestimmten Modellparametern verändern oder sogar umkehren kann. Dieses Framework kann in der Planung von Therapien helfen, die darauf abzielen, TLO-Strukturen zu destabilisieren.

In Kapitel 4 modelliere ich Interaktionen zwischen Keimzentren (GC). GC sind organisierte Verbünde von Immun- und Stromazellen in sekundärem und tertiärem lymphoiden Gewebe, die für die Bildung von B-Zell-Klonen verantwortlich sind, die hochaffine Antikörper produzieren. Es konnte nachgewiesen werden, dass injizierte Antikörper das im GC den B-Zellen präsentierte Antigen bedecken. Dies legt nahe, GC als ein System von interagierenden Akteuren zu betrachten. Simulationen eines Systems interagierender GC weisen darauf hin, dass früh gebildete GC sich später bildende GC unterdrücken könnten. Ich hoffe, damit Anregungen für neue Experimente zu geben, um den Einfluss von Antikörpern auf die Keimzentrumsreaktion genauer zu untersuchen und damit möglicherweise eine Regulation der GC Antwort unter verschiedenen klinischen Bedingungen zu unterstützen.

Neben der Antikörperantwort kann auch die Aktivität cytotoxischer T-Zellen (CTL) für die klinische Anwendung relevant sein. In Kapitel 5 schätze ich die Rate ab, mit der CTL in verschiedenen Experimenten Zellen eliminieren. Anhand von mittels *in vivo*-Mikroskopie generierten Daten zur weiteren Entwicklung von Zellen abhängig von der Zahl der Kontakte mit CTL weise ich nach, dass ein früherer Kontakt mit CTL die Wahrscheinlichkeit für eine Zelle massiv erhöht, bei einem erneuten CTL-Kontakt zu sterben. Dieser Modellierungsansatz könnte für die Optimierung von auf T-Zellen basierten Therapien genutzt werden.

Contents

1

Introduction

1.1 The immune system

To cope with infection, organisms developed a special system of cells and molecules called the immune system. The systems performs a layered defence, starting from nonspecific physical barriers like skin to pathogen specific response such as antibody-mediated immunity. The innate immune system is responsible for the immediate non-specific responses. Surface barriers impede entrance of pathogens and mechanical mechanisms like coughing and flushing (tears) help to get rid of microorganisms. Chemical barriers like antimicrobial peptides and decreased pH of the skin suppress growth of bacteria. The complement system consists of a cascade of proteases which is activated upon the binding to antibody and results in destruction of the cell membrane as well as opsonisation of the microbe and subsequent phagocytosis by immune cells. Cellular components of the innate system are phagocytic cells like macrophages, neutrophils and dendritic cells. They are able to migrate to the infection site, search and eliminate pathogens, secrete regulatory molecules which kill pathogens or provide signals to other cells.

During evolution, multicellular organisms developed a very complex defense system, and in jawed vertebrates the immune response can be shaped by the environment thanks to its recombination-based receptors system. This part of the immune system is called adaptive immune system and is responsible for the more strong and specific responses partially because of the mechanism of the immune memory. The major types of the cells are B and T lymphocytes. T cells have two main subtypes: the killer and the helper T cells. Killer T cells specifically recognize antigen but only in the context of bound major histocompatibility complex (MHC) and having contacted an infected cell they produce cytotoxins and induce apoptosis of the contacted cell. Helper T cells do not possess any cytotoxic activity, but regulate the response by signalling to other immune cells.

B cells are able to recognize antigen without any preprocessing and secrete antibodies which specifically bind to pathogens and mark them for phagocytosis or induce complement response.

The primary immune organs, bone marrow and thymus, are responsible for generation of lymphocytes and early clonal selection. Selection of the best affine B cell clones during adaptive immune

response takes place in structures called germinal centres (GCs) which are located in secondary lymphoid organs (SLOs) like lymph nodes and spleen.

Chronic inflammation induced by infection, cancer or organ transplantation may result in development of new immune organs at the inflammatory site. This type of organs is called tertiary lymphoid organs (TLOs). They are characterised by less organisation in their structure in comparison to SLOs and are supposed to be a transient phenomenon, i.e. they dissolve upon inflammation resolution. Although their presence was shown to be protective in viral infection, in autoimmune diseases or in chronic inflammation in transplanted graft they were shown to be a source of tissue specific antibodies and might contribute to the pathological immune response.

1.2 Aim

In this work I consider several types of immune responses. I start with the review of secondary and tertiary lymphoid organs structure and describe the model of TLO development in the following chapter. Since TLOs may contribute to the disease pathology, investigation of stability of this structures is of interest for fundamental as well as clinical research. Cell organisation in TLOs depends on chemokine secretion and its gradient sensing. Description of this phenomenon may help to investigate in which range of parameters the cluster formation is possible. Another important factor of TLO formation is cell interaction via contact as reviewed in the next chapter. That is why the spatial aspect, i.e. relative cell position in tissue, also influences the frequency of interaction, and, consequently, the probability to get activated. I aim to construct a framework for modelling cell interaction via diffusing chemokines and cell contacts which can describe chemokine distribution and ability to sense its gradient as well as to model cell migration and contacts.

GCs located in follicles in SLOs and in matured TLOs are responsible for specific antibody response which may contribute to the autoimmune disease pathology or may help to fight the infection. Usually GCs are commonly considered to be individual structures and the internal mechanisms of antibody affinity maturation are investigated. However, recently it was shown that there is a possibility of their interaction via secreted antibodies, hence GCs may be treated as a system of interacting agents. The aim of our study is to model such interaction and to investigate how they might change the kinetics of affinity maturation depending on system size and starting time of development.

Finally, the third topic of our study is kinetic analysis of effector T cell responses. Adoptive T cell therapy is a very promising clinical approach to treat infection diseases or cancer. It involves *ex vivo* expansion of killer T cells specific to the target antigen and transfer of this cells into a patient. Knowledge about the killing abilities of the T cells might help in estimation of cell amounts needed for the therapy. However, there is no consent about the magnitude of the killing rate characterising T cells and I aim to estimate this parameter for the *in vivo* system. The initial data were generated

by two-photon microscopy observation lymph node extracted from infected mice. The populations of infected cells were estimated for different T cell densities after one day experiment. In addition, based on the cell contact data I was going to analyse how multiple interactions with T cells influences survival probability of infected cells.

1.3 Methods

The methods, which are used, vary depending on the system and the aim of the problem. For early TLO development events I chose a multiscale agent-based approach to describe spatial cell and molecule distribution and their interactions, because the phenomena happening in the system range from molecular to cellular scale. In order to achieve this, one needs to describe cell contacts, which demands the implementation of a collision detection algorithm. Chemokine diffusion can be described by a diffusion equation, represented by so-called partial differential equation (PDE). In the model migrating cells navigate by sensing the difference of bound receptors at their surface and I implemented receptor dynamics using ordinary differential equations (ODE).

In the model of GCs interaction I neglected spatial distribution patterns of cells and molecules and used an ODEs system to describe cell population dynamics, antibody production, and binding to the antigen.

In the same manner, T cell killing kinetics are simple to describe using a single ODE which was used estimate killing rate for the experimental conditions. Data about cell contacts were used to test the hypothesis of independence of cell death from previous interactions using a probabilistic model for cell death events.

1.4 Results

In this work I constructed a framework for a 3D agent-based simulation. I implemented collision detection, diffusion solver and receptor dynamics at cell surfaces. Such a framework is interesting not only for our present problem in the context of TLO development but also for similar systems where cell migration is governed by secreted chemokines which can be internalized after binding to a receptor. Using an analytical solution and simulations based on the framework, I estimate how chemokine secretion rate, receptor density at the cell surface and degradation rate contribute to chemokine gradient generation. For a given range of receptor densities, cells may decrease chemokine concentration due to receptor internalization, but an increase in receptor number compensates their sensitivity for a gradient generated by a point source. Based on estimation of degradation rates from similar works, it was shown that proteolytic degradation does not substantially change the chemokine concentration at the distances comparable with the cell cluster size.

In simulations of lymphocyte influx from a blood vessel to the tissue compartment, it was investigated how contact frequency of tissue cells with lymphocytes varies with cell distance from the vessel. By introducing an abstract signal integration to the model, I implemented activation of stromal cells in tissue upon the contacts and how the probability to activate depends on the influx of lymphocytes.

In the context of interacting GCs, a measure for *in silico* comparison of immune responses was introduced, which was used to show that early GCs suppresses the responses of the later ones. In the same manner, the synchronous start of GC reactions appeared to generate more efficient immune responses than if GC reactions start sequentially with a delay.

In the study of T cell killing kinetics, I estimated the killing rate of T cells in the experimental system for several conditions. Using the data about target cell survival after different number of contacts with the T cells, I showed that the probability of the death depends on the previous contacts and dramatically increases after the third contact with a T cell.

1.5 Outlook

In this study I developed a framework which could be interesting to use for other systems and in the context of TLO development, especially if additional experimental data can be integrated. Although it still represents a rather simplistic view of the biological system, especially in the lack of known information about mechanisms governing TLO development in graft transplants, it may be useful for the estimation of therapeutic concentration of agents directed against receptors or chemokines participating in cell positioning in order to destabilize the system.

The GC interaction model provokes experimental investigation of mutual influence of GCs and could be tested in, for example, animal models of local immunization where an organism is sensitized to the antigen sequentially in different body parts and GC kinetics are then compared. Such experiments will help to validate the model of antibody feedback more precisely and directly estimate a contribution of antibody feedback in GC interactions and kinetics of affinity maturation.

The same framework used for 3D modelling of cell interactions in TLO can be applied to a system of effector T cells and infected target cells. The data on the probability of cell death depending on the contact number can be integrated into the model in order to estimate the contribution of multiple interactions with the T cells to the killing kinetics.

2

Secondary and tertiary tissue formation

2.1 Lymphoid tissue anatomy

Lymphocyte development, maturation and activation is performed in distinct anatomical tissues. There are two types of lymphoid tissue: primary (generative) and secondary (peripheral) organs [1].

Bone marrow and thymus represent the primary lymphoid tissue where generation and maturation of lymphocytes occur. Bone marrow is a source of all blood cells which are derived from hematopoetic stem cells and can differentiate to any lineage of the innate or adaptive immune system. Also, the bone marrow serves as a niche for antibody-producing B cells. The thymus is responsible for maturation of T lymphocytes. There, T lymphocytes, also called thymocytes, interact with thymic epithelial cells and are subjected to positive and negative selection. First, T cells must be able to interact with self-MHC complex, but cells with high affinity of interaction with dendritic cells are eliminated in order to avoid autoimmune responses.

Mature lymphocytes circulate between blood and secondary lymphoid organs such as lymph nodes and spleen, where they can get activated upon the contact with antigen.

Lymph nodes are collections of lymphoid tissue which are usually located at the junctions of large lymphatic vessels. Lymph nodes are oval-shaped anatomical structures covered with the lymph node capsula, which consists of connective tissue, fig. 2.1. The interior of the lymph node is divided into outer cortex and inner medulla. The cortex consists of B cell follicles without (primary follicles) and with developed germinal centres (secondary follicles). Germinal centres are anatomical structures located in lymph node follicles in which B cells are subjected to extensive proliferation, somatic hypermutations and selection. Upon the interaction between T follicular cells and B cells in GCs, memory B cells are generated which can boost the antibody response if the organism encounters the same antigen in the future. The interior part of the cortex, called paracortex, contains predominantly T cells and dendritic cells (DCs) and presentation of the antigen to T cells results in generation of memory T cells. The medulla is the inner part of lymph nodes and it serves as an exit point for lymphocytes.

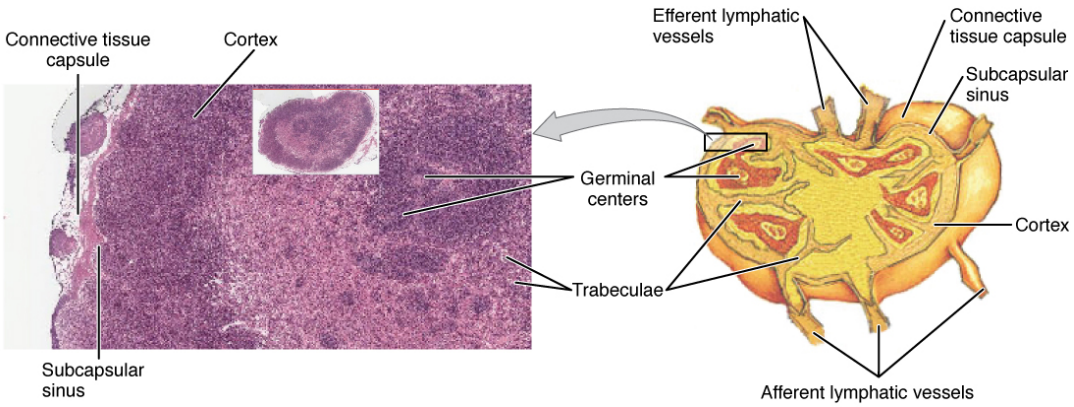

Source:https://upload.wikimedia.org/wikipedia/commons/c/c7/2207_Structure_and_Histology_of_a_Lymph_Node.jpg

Figure 2.1: Schematic representation of a lymph node.

Also it contains medullary cords, where antibody-secreting plasma cells reside. The lymph flows out of lymph nodes through medullary sinuses into efferent lymphatic vessels. Lymph nodes represent a specific environment where lymph is filtered and scanned for different antigens allowing to generate an efficient adaptive immune response. Every day, around 2 litres of lymph recirculates to the blood [1].

Spleen is a large organ of secondary lymphoid tissue which plays a major role in responses to antigen in bloodstream as well as participates in iron metabolism, thrombocyte storage and hematopoesis [161]. The spleen consists of red pulp, white pulp and the marginal zone in between. The red pulp includes half of the body monocytes [195] and is also populated with old red blood cells which are to be destroyed [161]. The blood enters the spleen via the splenic artery which constitutes approximately 5% of total cardiac output [69]. The splenic artery branches to trabecular arterias and, further, to central arteriols which are surrounded by the T cell-rich periarteriolar lymphoid sheath (PALS). Antigen, being trapped in the marginal zone, is transported by dendritic cells to PALS and presented to T cells. Marginal zone B cells are responsible for antigen transfer to the follicles. In the white pulp some of B cells are organized in primary follicles and where they surround clusters of follicular dendritic cells (FDCs) [69]. During the immune response, GCs are generated in the follicles similar to the responses in the lymph nodes.

Tertiary lymphoid organs (TLOs) represent organisation of lymphoid tissue due to chronic inflammatory conditions. Such structures of immune cells are observed in cancer, infection and autoimmune diseases and they vary in their form and cell content. The precise definition of TLO is still unclear and I discuss it in more details in this introduction later. Similar to the lymph nodes, TLOs consist of two distinct B and T cell zones and may include GCs which produce plasma cells with affinity to antigens in the locality of TLOs. Their function is usually considered in the context of disease and, depending on the conditions, TLO may be beneficial or detrimental. The formation of these structures is strongly

connected to stromal cells which may change their phenotype due to signals from immune cells and they create the microenvironment for immune cell homing. TLOs are considered as transient structures and after inflammation resolution, for example, viral infection clearance, they are supposed to dissolve as well.

There are other types of lymphoid organs such as mucosal- gut- and bronchus associated lymphoid tissue (MALT, GALT and BALT, respectively), which are referred to as SLOs but are less organized structures than lymph nodes or spleen and may be compared with TLOs as well.

2.2 SLO structure and development

Before we discuss the formation of TLOs, it is natural to give an overview of the main events and cells participating in SLO development and maintenance, since they share some structural similarities and TLO can be considered as an attempt to form SLO in non-predefined niche. From the structure and functioning of lymph nodes discussed in the previous section one can see that SLO has two major components, namely, stroma environment and immune cells. Their interactions are important for proper immune response, for example, antigen delivery and presentation events and, as a result, activation of different lymphocyte types. This is possible due to the specific environment created by stromal cells such as networks of follicular dendritic cells and fibroblastic reticular cells. They are responsible for immune cell positioning via chemokine secretion and providing survival and activation signals to the immune cells. Here, I will review in more details the role of different cell types participating in SLO development and structure maintenance.

Lymphatic tissue inducers cells (LTis) are responsible for the interaction with stromal cells to induce expression of chemokines for immune cell positioning. The origin and function of this type of cells is very well reviewed in [29, 115]. LTis are characterised by expression of $CD4^+CD3^-$ and their development is dependent on transcription factors RORγt, Id2, Ikaros, Tox and ligand-receptor pair RANKL-RANK [7, 53, 56, 72, 226]. LTis express chemokine receptors CXCR5 (for CXCL13 ligand) and CCR7 (for CCL21 and CCL19 ligands) and can be divided into 3 classes ($CXCR5^+CCR7^-$ at B follicle region, $CXCR5^+CCR7^+$ the boundary of B and T zones, $CXCR5^-CCR7^-$ at T zone stroma) [114]. Since LTis have CXCR5 receptor, they were shown to migrate to the lymph node environment which consists of CXCL13 secreting stromal cells [210].

LTis provide a signal to stromal cells through lymphotoxin receptor LTβR by LT$\alpha 1\beta 2$ molecule which activates NF-κB transcription factors resulting in expression of adhesion molecules and chemokines responsible for SLO homoeostasis, fig. 2.2. Another possible function of LTis is the maintenance of epithelial integrity due to their production of IL-22 [198]. TLis are attracted to the intestinal epithelium by CCL20 because of their expression of the CCR6 receptor and make clusters in cryptopatches. The

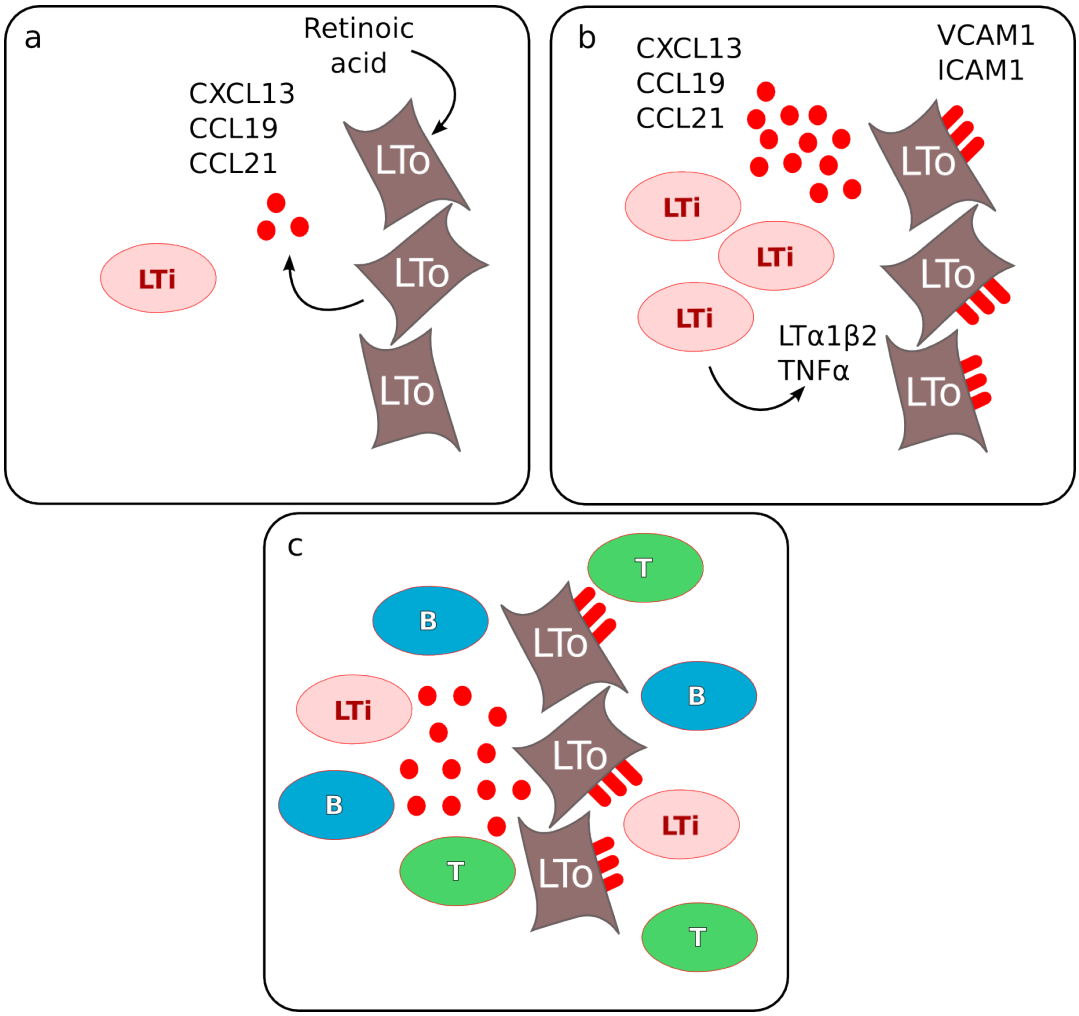

Figure 2.2: Interactions between stromal and immune cells during lymphoid tissue development. Retinoic acid produced by neural tissue induces chemokine secretion by stromal cells (a) what attracts LTis cells. Interaction via TNF and LT$\alpha 1\beta 2$ between LTis and stroma results in increase of chemokine expression and expression of adhesion molecules by stromal cells (b). Lymphocytes recruited by chemokines further contribute to LT$\alpha 1\beta 2$ signalling to the stromal cells (c).

cryptopatches give rise to isolated lymphoid follicles, where LTis cluster with dendritic cells and interact with B cells invoking T-cell independent IgA class switching [208].

In summary, LTis cells are important for SLO development and serve as activators of stromal cells inducing expression of chemokines and adhesion molecules which are important in SLO homoeostasis.

Lymphatic tissue organizers (LTo) are cells of mesenchymal origin. Much less is known about the development of this type of cells and about their precursors in comparison to the LTis. LTo are charachterised as VCAM^{high}ICAM^{high}MAdCam-1^{+} cells, the phenotype which stromal cells gain upon LT βR signalling. It was shown in *in vitro* experiments with mesenchymal stem cells that TNFα or LT$\alpha 1\beta 2$

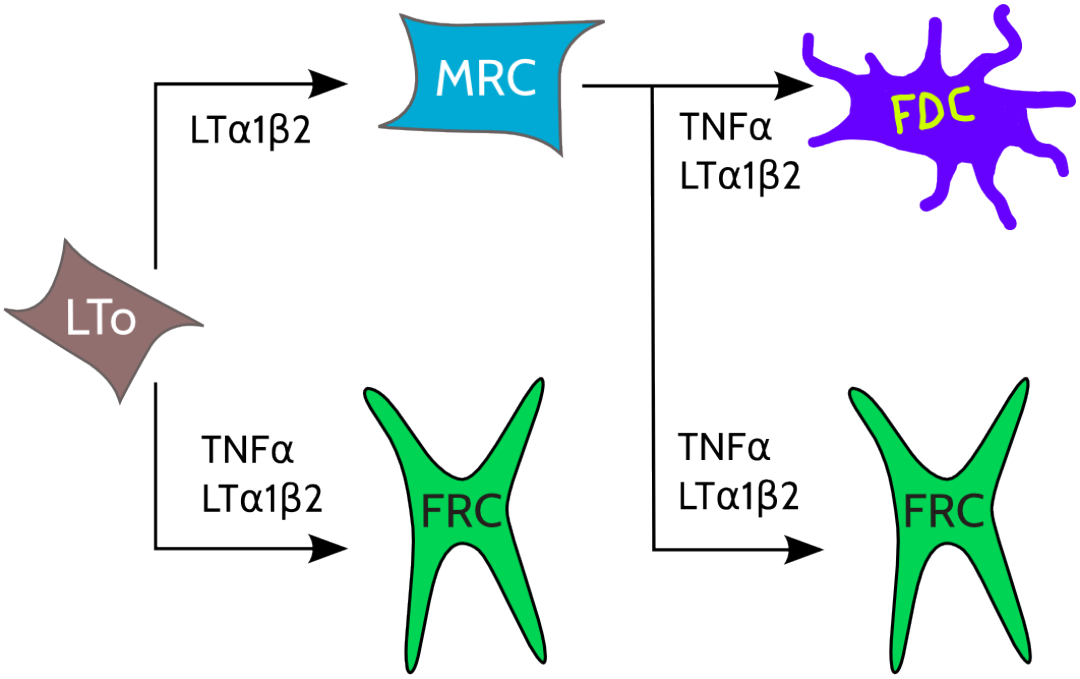

Figure 2.3: Model of stroma differentiation according to [182].

was sufficient to upregulate VCAM, ICAM or MAdCAM-1 [11]. LT-dependent signal is delivered by LTis cells, which are attracted to the chemokine CXCL13. The secretion of CXCL13 is initiated by the retinoic acid produced by the neuronal tissue [29], fig. 2.2.

LTo may differentiate to fibroblastic reticular cells (FRCs), FDCs, and, as later identified in [98], marginal reticular cells (MRCs), fig. 2.3. NKX2-5$^+$ and ISL1$^+$ cells were shown to be precursors of FDCs, FRCs and MRCs in spleen, but the origin of lymph node stromal cell remains unknown [35].

Fibroblastic reticular cells are typical fibroblast-like cells located in T cell areas. They govern cell migration by secretion of CCL19, CCL21 and also express IL-7 which is important for T cell survival [121, 131]. FRCs are responsible for construction of the conduit network, which is used for signal molecules and antigen transport into lymph node [65]. They are characterised by their surface markers PDPN$^+$PDGFRα^+CD31$^-$CD45$^-$ [65] and represent 20-50% of non-hematopoetic cells in lymph nodes [65]. In the spleen, FRC development depends on the LT interaction with B cells, which induce CCL21 and PDPN expression [154], although it is not necessary in case of lymph nodes. The differentiation to FRCs requires signalling via TNF-RI and LTβR, similar to FDCs, but interactions with CD4$^+$ T cells is necessary [97]. FRCs appear at the same time with MRCs and FDCs and share signalling pathways needed for their development. In [182] it is hypothesized that FRCs may originate from the same precursors as MRCs.

Podoplanin (PDPN), a molecule expressed at the FRC surface, is responsible for FRC network contractility and its inhibition results in loss of tension in the FRC network [4, 14]. Such a dense structure

allows for DCs and T cells migrating within to be in constant contact with FRCs. PDPN can also interact with CLEC2 (C-type lectin domain family 1 member b) on DCs, regulating their motility [3]. Interaction via PDPN-CLEC2 with platelets results in release of sphingosine-1-phosphate (S1P) [88]. S1P is responsible for the egress of immune cells from lymph nodes. It induces expression of adhesion molecules in HEV cells which changes HEV permeability [88].

Prosurvival signals provided by FRC by IL-7 to T and DCs cells are important for lymph node maintenance, and double deficiency in CXCL13 and IL-7 receptors results in the loss of lymph nodes [128], although CXCL13$^{-/-}$ lacks only certain types of lymph nodes [12]. FRCs participate in the regulation of lymph node remodelling due to damage and support survival of LTis cells [159].

FRCs may play immunosuppressive role to prevent damage of lymph nodes during acute reactions via production of nitrogen oxide which reduces proliferation of effector T cells [191]. Another way of T cell response inhibition is presentation of self antigens by FRCs resulting in tolerance induction by elimination of autoreactive T cell clones [66]. In certain types of lymph nodes FRC were shown to induce T regulatory cells [46].

FRCs are an important cell type for SLO maintenance and immune response regulation. They predominantly influence T cell responses and organize the environment for DCs and T cell interaction and survival.

Follicular dendritic cells are the stromal cells of B cell follicles, which are responsible for positioning and sustaining of B cells in germinal centres (GC) and primary follicles. FDCs secrete CXCL13, a ligand of the CXCR5 receptor on the B cell surface, present antigen-antibody complexes to B cells in GCs, and produce IL-6, inducing antibody secretion [61, 104, 106].

FDCs appear in the first week after birth and presence of B cells is necessary for differentiation of their precursors [48]. Recently it was found that perivascular progenitor cells may give rise for FDCs [111]. These cells express Mgfe8 and Pdgfrb and are able to gain an FDC phenotype *in vivo* and *in vitro*. The phenotype of FDCs and their precursors is described in table 2.1. Matured FDCs express at their surface adhesion molecules MAdCAM and VCAM, and can be distinguished from other stromal cells by expression of complement receptors CD35 and CD21 [86], which are used for antigen retention.

The differentiation of FDCs precursors depends on LT and TNF interactions [111]. Activation through TNF-RI and LTβR results in NF-κB signalling (reviewed in [182]). There are two distinct pathways, canonical and alternative, see fig. 2.4. The canonical pathway is activated by TNF signalling resulting in activation of IKK2. However, interaction through LTβR invokes both, canonical and alternative pathways, i.e. also activating IKK1. Knock-out studies show that a deficiency in the alternative pathway results in loss of FDCs, whereas the canonical pathway seems not to be crucial for FDC development.

	perivascular preFDC	marginal sinus preFDC	matureFDC
mural markers:			
PDGFRβ	+++	+	-
NG2	+++	-	-
FDC-associated markers:			
SDF1	++	n.d.	-
VCAM1	+	+	++
ICAM1	++	+	++
MAdCAM1	+/-	+	+
Mfge8	+	+	++
CXCL13	+	+	++
E-NPP2	++	+	++
IGFBP3	+	+	+
Periostin	+++	n.d.	+
Clusterin	+/-	+	+
BP-3	-	+	+
FcγRIIβ	-	+/-	+
CD21/35	-	-	+
TNFR1	+++	+	+
LTβR	+++	+	+
differentiation signals:			
LTis cells, B cells		LT$\alpha\beta$	
B cells			LT$\alpha\beta$, TNF

Table 2.1: Expression of markers during FDC maturation according to the model from [111].

FDCs participate in SLO maintenance and functioning. The homeostatic chemokine CXCL13 is responsible for the positioning of B and T follicular helper cells, which bear the CXCR5 receptor, fig.2.5. Disruption of the FDC network results in loss of spherical form by follicles, and cells become positioned in so-called 'bands' instead [217]. It is interesting that FDCs derived from lymph nodes are able to form B cell clusters *in vitro* in contrast to FDCs of spleen origin [86].

Another function of FDCs is antigen presentation. Earlier FDCs were thought to be a subset of DCs because of their appearance, but they were shown to be of mesenchymal origin. And although they present antigen at the surface as DCs do, antigen is presented using the complement receptor of the Fc receptor in the form of an immune complex, i.e. bound to antibody [8], while DCs use MHC (major histocompatibility complex) molecules for this. Moreover, in contrast to DCs which present processed antigen, i.e. in the form of peptide, FDCs do not process antigen before its presentation. The lifetime for such complexes is not measured yet, but it may be estimated from antigen decay rate and is in the order of years [200]. Such a long time probably could be explained by the process of antigen cycling: C3d-coated immune complexes bound to CR2 are transported to endosomes [85], keeping antigen from degradation. Opsonised intact complexes were still observed within FDCs after a period of 3 months [86].

Antigen may be delivered to FDCs by several ways depending on its size. Small antigens (less than 70kDa) are transported via conduit network and can be trapped directly by FDCs themselves [16, 183].

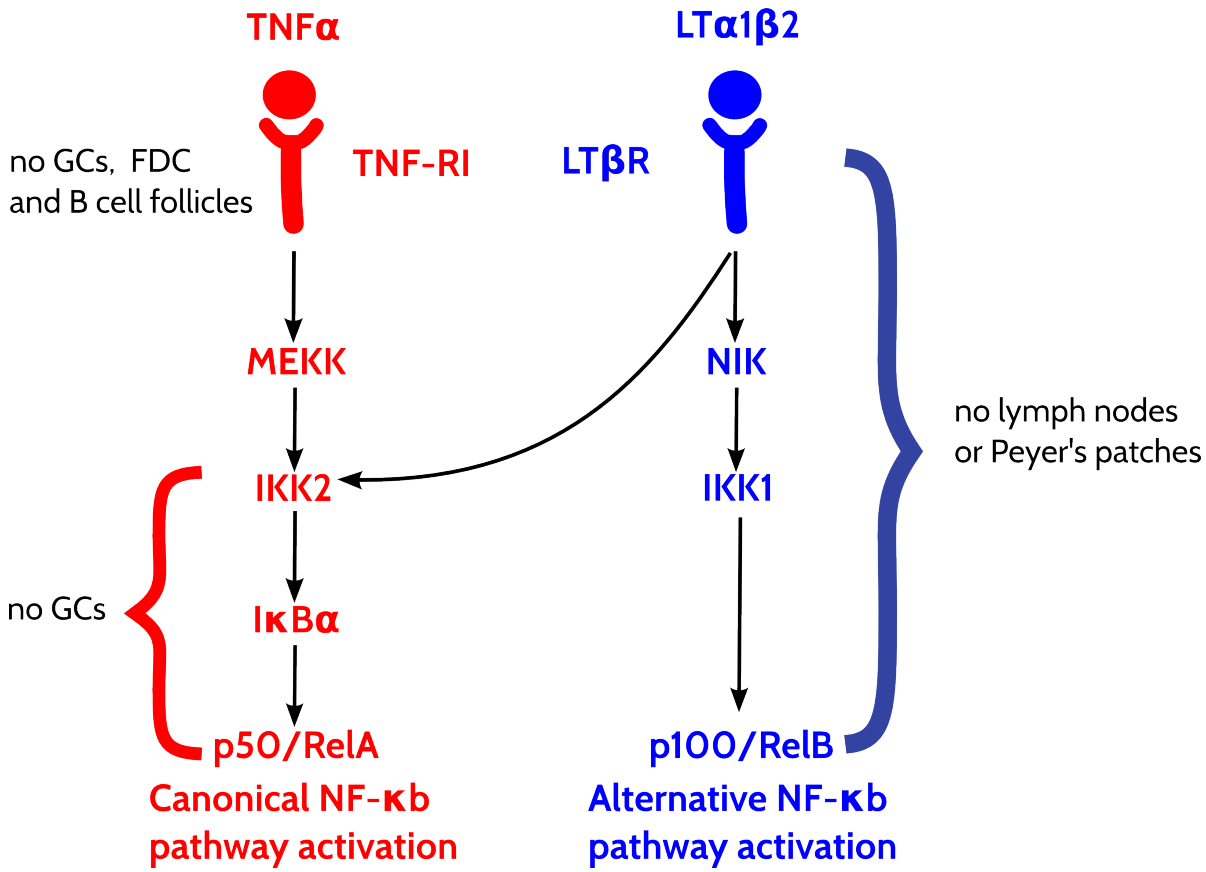

Figure 2.4: Activation of NF-κb alternative and canonical pathways and phenotype of mice deficient in different components of the cascades.

Activation of NF-κb alternative and canonical pathways and phenotype of mice deficient in different components of the cascades (as reviewed in [182]).

Bigger antigens are transported by other cells, namely, by SCS (subcupsular sinus) macrophages and lymph node-resident DCs, which allows to isolate FDCs from unprocessed antigen [77, 165]. These complexes are transported from DCs and SCS macrophages to naive B cells [165] and then they are transferred to FDCs, which was shown in co-culture *in vitro* experiments [85]. Antigen presenting function is crucial in germinal centres (GCs), anatomical structures inside of SLO, where B cells are selected in order to generate high affine antibodies. FDCs located in the so-called light zone of the GC are responsible for cognate interaction with B cells via B cell receptor (BCR) [213]. The germinal centre reaction is discussed in more details in chapter 4. Although antibody responses with affinity maturation were shown to exist even in the absence of FDCs [135], it required a high antigen load. If antigen doses are low, presentation via immune complexes at FDCs is needed for the response to occur [184]. Besides interaction via BCR, FDCs interact with B lymphocytes with adhesion molecules VCAM1 and ICAM1, which enhance signalling in B cells *in vitro* [33] and promote survival of GC B cells in co-culture experiments [103, 216]. Impaired expression of adhesion molecules by FDCs results in reduced

antibody affinity maturation in GCs [150, 176, 215, 216]. FDCs are capable to sense molecules of microbial origin not only in the form of immune complexes, but via pattern recognition receptor TLR4, which binds lipopolysacharides. Lack of this receptor in FDC results in reduced affinity maturation [70].

FDCs express molecules promoting follicular and GC B cell survival. BAFF expression by FDCs was shown to be important for GC sustaining, and its deficiency leads to GC ablation [174]. In addition, FDCs may influence B cell survival via signalling through Wnt, Sonic hedgehog (SHH) and Notch cascades. This was shown *in vitro* for Wnt and Notch [118, 228] and hypothesized for SHH in [6] since B cells and FDCs express SHH receptors and SHH is expressed by FDCs.

Another role of FDCs in GC is connected to marking apoptotic GC B cells, which accumulate during GC reaction due to negative selection. It is very unfavourable for self-molecules to be released in the area of the GC reaction in order to avoid generation of self-specific B cell clones, which is why there is an efficient mechanism for removal of apoptotic material. FDCs secrete Mfge8 [109], a molecule that interacts with phosphatidylserine which is exposed on the surface of apoptotic cell [83]. Tingible body macrophages (TBM) recognize Mfge8 and engulf such cells [82].

In conclusion, FDCs are important players of lymphoid tissue which participate in its homoeostasis and participate in the adaptive immune response in GCs by providing survival signals to B cells and supporting elimination of apoptotic lymphocytes.

Marginal reticular cells, the stromal cells adjacent to subcapsular synus, are less studied stromal cell phenotype. It is still not shown that LTo are precursors of MRC, but comparison of different expressed markers points to this possibility [98, 182]. These cells express VCAM-1, ICAM-1, BP3, RANKL, CXCL13, MAdCAM-1, where expression of the last two molecules depends on LT interactions, which was shown in experiments with blocking of LTβR. However, contacts with B or T lymphocytes do not seem to be necessary for MRC maturation [98]. In [182] it was concluded that MRC and FDC share common differentiation pathways based on the phenotype of knock out animals ($p52^{-/-}$, $RelB^{-/-}$), where deficient expression of CXCL13 was observed [31, 68, 168]. In comparison to MRCs, the maturation of FDCs requires stimulus through TNF-RI in addition to LTβR, and MRCs may be considered as FDC precursors, since MRCs were shown to be responsible for FDCs generation in lymph nodes [227]. It is interesting to note that MRCs were not found at the sites of ectopic lymphoid tissue which limits their functions to SLOs [26, 98].

LTis and LTo are central players in secondary lymphoid organ development, where LTo are responsible for expression of molecules crucial for lymphocyte homing and LTis are responsible for the activation of stroma and seem to be a limiting factor [137].

Vascular cells organize molecular and cellular transport. There are two types of lymphatics: lymphatic vessels (LVs) and capillaries. Capillaries represent the smallest vessels which have highly permeable blind ends. Interstitial fluid enters the capillary due to interstitial pressure and is transported to

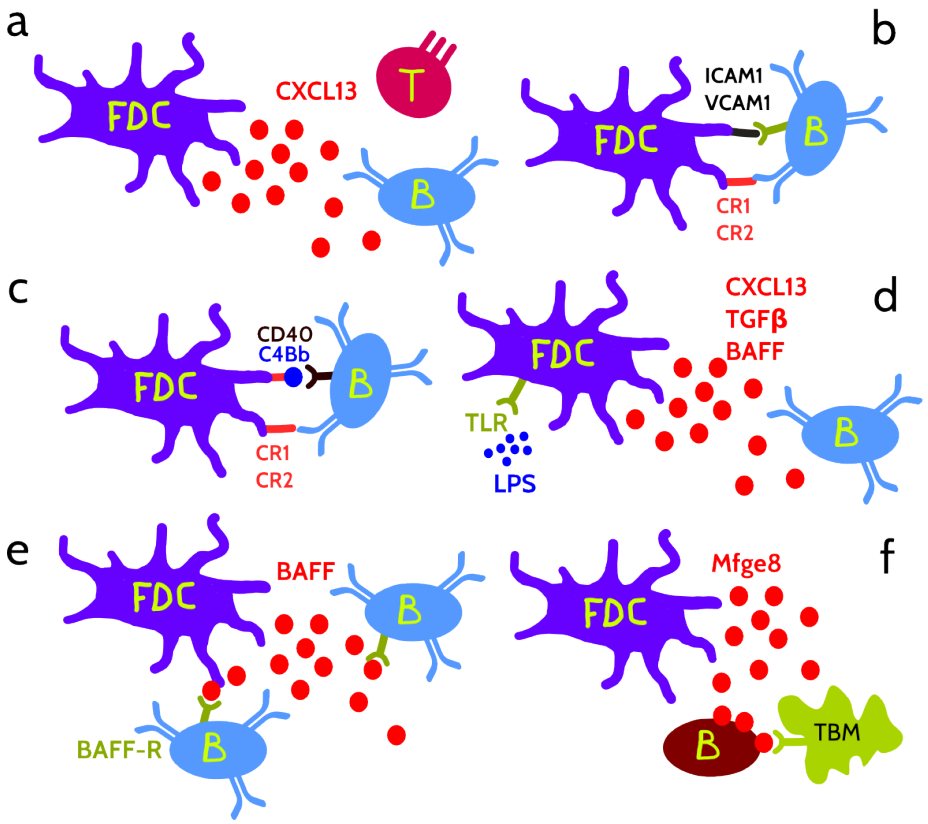

Figure 2.5: FDC functions: positioning of GC and follicular B cells and T follicular cells via chemokine secretion (a); immunological synapse formation with B cells using adhesion molecules VCAM1 and ICAM1 (b); antigen presentation to GC B cells couples with activation of CD40 (c); innate sensing of bacterial lipopolysaccharides via Toll-like receptor resulting in upregulation of factors responsible for B cell survival, positioning and antibody class-switching (d); pro-survival signalling via BAFF secretion to B cells (e); marking of apoptotic B cells with Mgfe8 to induce their clearance by tingible body macrophages (TBM) (f). [6]

LVs, which are larger and have smooth muscle walls. These collecting LVs deliver fluid, or lymph, to the right lymphatic duct and then afferent LVs bring it to the lymph nodes. Efferent LVs which go out of lymph nodes may serve as afferent ones for another lymph node or may return lymph to the lymphatic duct where it enters the blood.

LVs originate from the cardinal venule and separate from blood endothelial vessels after PDPN-CLEC2 interaction with platelets [160]. LVs form a dynamic network which can be subjected to lymphangiogenesis during inflammation in order to regulate lymph circulation and to avoid excessive swelling [92]. Transport function of LVs is important for the adaptive immune response, because they are responsible for antigen delivery to lymph nodes in soluble form via lymph or by antigen-presenting cells such as DCs and macrophages [29, 178]. Efferent (outgoing) LV cells express S1P ligand which regulates cell egress from the lymph node and sustains homoeostasis of lymph nodes [164]. Similar to

FRCs, LVs contribute to peripheral tolerance by persistently expressing and presenting tissue-restricted antigens, but the exact mechanism is still unknown [67].

Another type of vasculature are high endothelial venules (HEV). Their function is to organize the entrance of lymphocytes into lymph nodes from the blood. They express PNAd, a leukocyte adhesion molecule, which slows leukocyte motion down and allows them to sense and follow chemokine gradients generated by the lymph node environment [194]. As for other cell types supporting SLO structure, HEV need LTβR interaction for their development and sustainment [27, 158].

Summary on SLO development. There are two important cell types necessary for SLO development: LTis and LTo cells. Activation of CXCL13 secretion by LTo may be stimulated by retinoic acid produced by neural tissue. LTis are attracted to LTo cells due to expression of CXCR5 (receptor for CXCL13), and can interact via LT$\alpha\beta$ with LTo which might result in signalling via NFκB cascade and leads to upregulation of CXCL13, CCL19, CCL21 needed for lymphocyte positioning and positive feedback loop in CXCL13 expression, fig. 2.6. Interaction of LTo with immune cells induces their differentiation into different stromal cell subpopulations such as FRCs and FDCs, which form network environments for immune cell communication and perform other maintenance functions reviewed above. Interaction in LT-dependent manner with immune cells regulates vascular endothelial growth in HEV, which are responsible for lymphocyte trafficking. Such complex interaction between stromal and immune cells allows to develop and maintain SLO organisation and to provide an environment for effective immune responses.

2.3 Tertiary lymphoid tissue and chronic inflammation

SLOs represent an environment with a structure specialized for immune cell homing and the immune response establishment. However, during conditions of chronic inflammation such as infection or transplantation, so-called tertiary lymphoid organs may form. Since such structures do not have a predefined position and environment formed during embryogenesis, and because they are observed at different stages of their development, a definition is needed in order to distinguish immune cell infiltrate from matured TLO. A good review on TLO development can be found in [153], and in [153] an immune cell cluster is defined as TLO if

- it has two adjacent but anatomically distinct T an B cell compartments
- FRCs and PNAd$^+$MECA79$^+$ HEV are present in the T cell compartment
- stromal cell with FDC phenotype are found
- there are formed GCs populated with AID$^+$ B cells

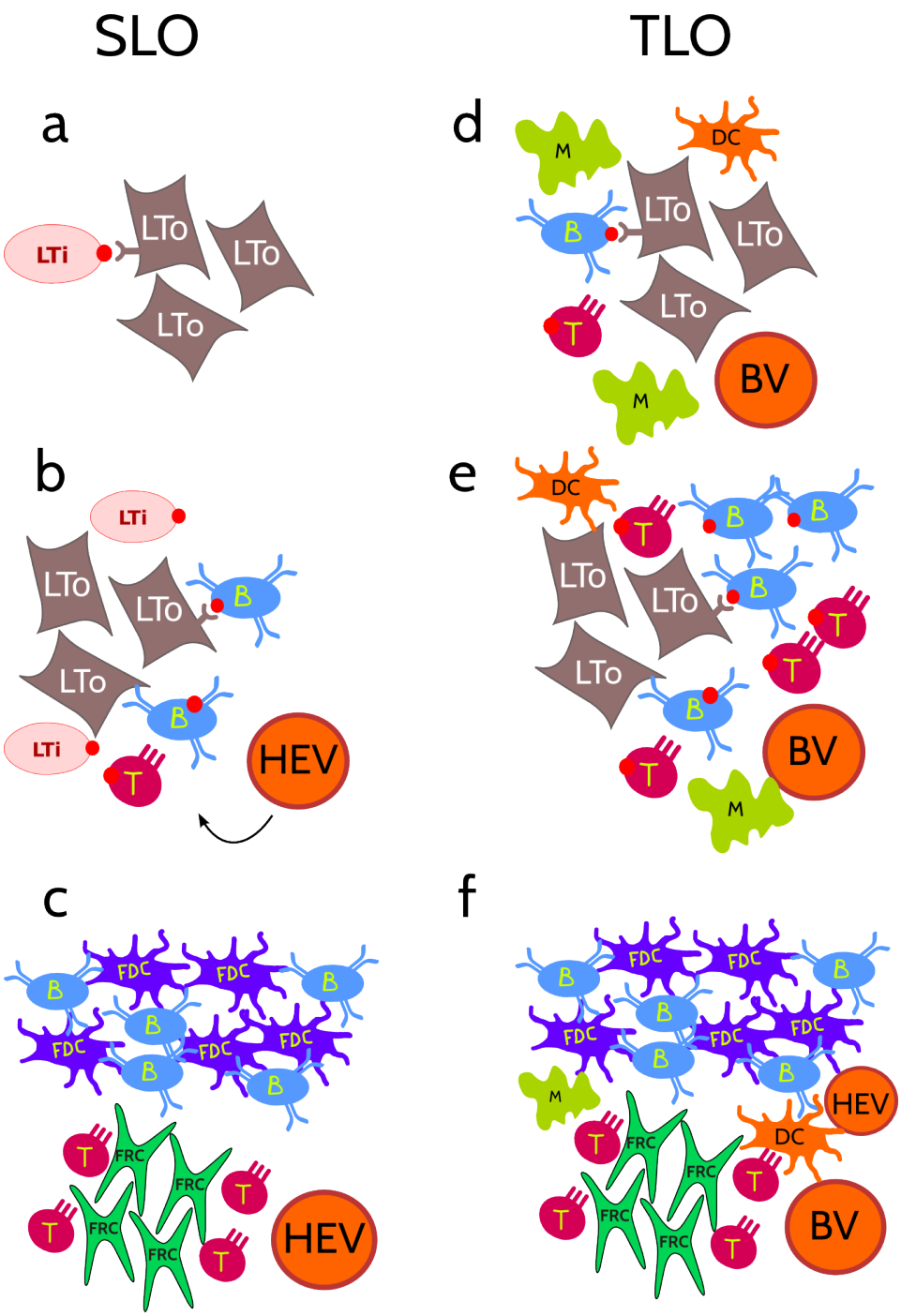

Figure 2.6: Model of SLO and TLO development. At the early stage of SLO formation, interaction between LTis and LTo results in chemokine and adhesion molecule expression by LTo (a); lymphocytes recruited via developed HEV contribute to signalling to LTo cells (b); LTo cells differentiate to FDCs and FRCs which govern lymphocyte migration via chemokine production, B and T cell compartments appear(c). TLO development starts from inflammatory condition, where immune cells (DCs, T and B lymphocytes, macrophages (M)) are recruited via inflamed blood vessel (BV) (d); in chronic inflammation lymphocytes play a role of LTis by persistently delivering LT$\alpha 1\beta 2$ signal (red dotes) to stromal cells (e); stromal cells acquire FDC and FRC phenotype, endothelial cells get HEV-like phenotype; chemokines and other factors secreted by stromal cells support lymphocyte survival and compartmentalisation (f).

- class-switching is shown to happen in GC B cells.

Development of TLO shares the same signalling pathways as SLO. Lymphotoxin-dependent interactions are obligatory for lymphoid organogenesis formation, since mice deficient in LTα lacks any SLOs. Transgene expression of LTα in kidney and pancreas results in TLO formation in these tissues where not only organized T and B cell clusters and the ability to develop specific immune responce were observed, but also vessels with morphology of HEV were found [110]. The difference from SLO is that TLO do not have predefined regions where activation of stromal cells is orchestrated by an initial signal from neural tissue and with the help of LTis cells interacting with stroma via LT. In case of chronic inflammation, other cell types expressing LT$\alpha 1\beta 2$, such as B cells, NK cells or T lymphocytes are believed to perform LTis function [10]. Although the importance of LT-interactions was reported in many conditions, lymphoid neogenesis may be observed even in LTa$^{-/-}$ mice. In an influenza infection model, CXCL13 and CCL21 chemokine production and iBALT formation were observed even in absence of TNF or LT-dependent stimulation [148]. A possible explanation may be that lymphoid tissue neogenesis can be activated via Toll-like receptors [10].

In TLOs, similar to SLOs, chemokines govern cell migration and their overexpression in different model systems leads to lymphoid neogenesis. For example, lymph node-like structures were found if expression of CCL21 in pancreas was transgenically induced [39]. However, it should be pointed that it was not true for skin, hence it needs some tissue specific conditions. Overexpression of CXCL13 in pancreas induced TLO with T and B cell zones and HEV [130]. In this study, TLO development did not happen if LT$\alpha\beta$ was blocked. Two other important chemokines, CCL21 and CCL19, responsible for T cell positioning, did not induce TLO development upon being ectopically expressed, although lymphocyte clustering was observed in this set up [129]. Relevance of SLO homeostatic chemokines for TLO development is supported by analysis of their expression in different disease conditions. For example, in rheumatoid arthritis, CXCL13 and CCL21 were associated with formation of organized TLO-like cell aggregates [134]. Similarly, in autoimmune thyroid diseases, CXCL12, CXCL13 and CCL21 levels were higher in tissue specimens containing ectopic lymphoid structures. Moreover, expression of these chemokines or their receptors is essential for ectopic lymphoid tissue formation. Loss of CCL21 and CCL19 resulted in impaired iBALT formation [179], and deficiency in receptor CCR7 or CXCR5 expression also disturbed development and organisation of TLO in chronic antigen-induced arthritis mice [221]. Expression of the cytokine IL-7 seems to contribute to neogenesis as well. This molecule is important for T cell homeoestasis as discussed earlier and its overexpression results in additional lymph node development [153]. In rheumatoid arthritis patients expression of IL-7 is correlated with LTβ expression in synovial tissue [203].

The stroma compartment is important for lymphoid organ maintenance and TLO were shown to include developed reticular cell network and conduits [120]. The ability of stromal cell from certain

tissue to gain a phenotype of LTo cells probably defines sites where TLO may be observed. For example, meninges are fibroblast-rich tissue, and in patients with multiple sclerosis, fully developed B cell follicles were observed inside this tissue, but never in white-matter lesions in spite of the presence of immune infiltrate [189]. The ability of different cells types to gain an LTo phenotype was shown in several works. Aorta smooth muscle cells expressed adhesion molecules VCAM1, ICAM1 and chemokines such as CXCL13 upon LTβ and TNFR1 signalling [126]. In another study [111], perivascular cells were shown to give rise to FDCs upon LT and TNF-dependent stimulation, which means that FDC precursors are ubiquitous in the organism. But not only the location of chronic inflammation is important for TLO development. It was shown that different types of infection results in different TLO structures. Mice infected with MVA (Modified Vaccinia Ankara) developed in their lungs iBALT, containing stromal cells producing CXCL12 and FDCs in B cell follicles [63]. In contrast, *P. aeruginosa* infection did not lead to FDC development, although iBALT containing CXCL12$^+$ cells were observed [64].

A positive feedback generated during stromal cell-lymphocyte interactions by secretion of CXCL13 attracting B cells and support of this stroma phenotype by lymphotoxin signalling makes it difficult to dissect the role of immune and stromal cells in TLO organisation. However, it is interesting to note that depletion of B cells via anti-CD20 therapy did not result in improvement in Sjögren syndrom, and associated parotid lymphoma and BAFF overexpression were observed over the course of the disease [171]. That implies an active contribution of stroma to chronic inflammation condition, hence stromal cells may be considered as therapeutic targets.

Another cell type which was shown to contribute to TLO development are DCs, probably due to their LTβ expression [73, 75]. Injection of DCs results in iBALT neogenesis, and DCs depletion reduced the number of iBALT associated with influenza infection [75]. A similar effect was observed after DCs depletion in mice infected with MVA, where iBALT size was reduced [80].

Summary of TLO development. TLO development has similarities to SLO development in terms of events and cell types participating in its organization and maintenance, although the precise mechanism is still unknown and may vary depending on the tissue and inflammation type. Lymphocytes recruited to the chronically inflamed region may play the role of LTis cells and local stromal cells perform LTo function, where the same signalling pathways via lymphotoxin seem to be used, fig. 2.6. The same chemokines necessary for SLO homoeostasis were shown to be involved in TLO formation. Cytokines such as IL-7 may also contribute to neogenesis. TLOs are considered as transient structures [167] in contrast to SLOs and their stability is an interesting question for research.

2.4 TLO in disease

As discussed in the previous section, chronic inflammation may lead to TLO formation. Depending on the conditions, the presence of TLO may have either positive or negative impact on the inflammation

outcome.

An example of a beneficial role is lymphoid neogenesis during infection, where TLOs were shown to play a protective role. Mice infected with influenza virus develop TLOs in lungs where B cells differentiate to plasma cells specific to viral proteins [75]. Moreover, these structures are able to protect the organism from the influenza infection even if SLOs are absent [147]. iBALT in lungs as well as ectopic lymphoid structures in gut can attract B cells which produce IgA antibodies specific to influenza or interstitial infections [153]. Spatial organisation of immune cells at the inflammatory sites via chemokines produced in lungs is important for control of *M. tuberculosis* growth [102].

Although TLO may be associated with positive outcomes during chronic infections, their presence in autoimmune disease is related to its severity. The molecules involved in TLO formation which were discussed above, such as CXCL13, CCL21, CCL19 and LTα/β, were detected at sites of chronic inflammation and the level of their expression is correlated with the degree of TLOs organisation [29]. Since matured TLOs may include GCs in their structures, there is a risk of autoimmune B cell clone selection during germinal centre reaction due to the high availability of disease specific antigen, for example, nicotinic acetylcholine receptor in the case of myasthenia gravis or SBB/La (Sjögren syndrome antigen B, autoantigen La) in the case of Sjögren syndrome [10]. Tightly regulated SLOs have mechanisms which prevent entry of autoreactive B cells to GCs due to downregulation of CXCR5, a receptor for CXCL13 [60]. TLOs lack this function and in rheumatoid arthritis, Sjögren syndrome and other autoimmune diseases, high-affinity autoreactive B cell clones were observed [167]. B cells in GCs from chronic inflammation sites were shown to be subject to somatic hypermutations in patients with rheumatoid arthritis and Sj̈orgen syndrom. Impaired GC regulation may lead to aberrant clonal selection and neoplasia [29]. Lymphoma were observed predominantly in TLO but not SLOs during inflammation and, for example, they can develop in *H.pylori* gastritis and Sjögren syndrome [20, 225].

Chronic infiltration by immune cells is also observed in cancer. However not every tumour type may lead to TLO development. It is likely to depend on the expression of certain molecules, which are also involved in TLO development, such as LT$\alpha\beta$, TNF, IL-1β, IL-6 [167]. Presence of LTO may be associated with improvement. For example, TLOs are correlated with higher survival rate in patients with hepatocellular carcinoma and with prolongation of metastasis free-survival in case of breast cancer (reviewed in [192]). Although in some cases patients with developed immune response against a tumour have a better prognosis and expression of such chemokines as CXCL13 and CCL19 was shown to be beneficial [167], tumour infiltration by immune cells may invoke angiogenesis due to activation of complement system or inhibit immune responses because of the recruitment of T regulatory cells. Hence contribution of immune cells to cancer prognosis remains controversial [73, 180]. It is interesting to mention the ability of B cells from tumour-associated TLOs to produce tumour specific antibodies not only of IgG, but of IgA class as well [74], resembling T cell independent IgA-class switching in gut. Antibody specificity may be connected with positive or negative outcomes depending on the antigen.

For example, antibodies to XAGE1 and MUC1 are correlated with better survival what is not the case for p53 [76, 181].

In transplantation, chronic inflammation and high alloantigen availability may promote immune response against grafts. During chronic rejection, the inflammation is shifted towards the adaptive immune response which may be accompanied by a gradual organisation of lymphocytes into TLOs [202]. Almost all human grafts (including kidney, lungs, heart), which were explanted due to their failure, harboured TLOs [201]. The extent of TLO contribution to graft failure is unclear, partially due to design of the respective studies, because most of them are based on biopsies from already explanted transplants. A tissue sample obtained during the biopsy represents only approximately 1/10000 part of the organ in the case of a renal graft [201]. Hence it has its own limitations. However, characterisation of gene expression in TLOs from chronically rejected kidney grafts showed that graft life expectancy depends on how functional TLOs are [202]. Moreover, the repertoires of allospecific antibodies generated by cells from TLOs and SLOs had minimal overlap, which means that the local immune response is separated from SLO-mediated.

TLOs may be associated not only with rejection but with beneficial outcomes as well (recently reviewed in [91]). A tolerogenic role of TLOs was shown for lung transplants where a decrease in BALT number was correlated with rejection, perhaps, because BALTs may contribute to the defence against infection according to [90]. It seems that TLO which are rich in T regulatory cells may result in immunosuppression as it was shown in cancer and renal transplant patients [91].

The contribution of TLO to disease outcome varies among tissues and disease pathology. Lack of direct evidence for the TLO contribution makes it difficult to conclude when TLO development is desired or detrimental for the patient state.

3

Modelling of tertiary lymphoid organs

3.1 Background

TLO were shown to develop at chronic inflammation sites as discussed in the previous section. These structures may contribute to disease outcome, which is why the problem of their formation and maintenance is very important for clinical implications. Although the whole complex mechanism underlying lymphoid neogenesis is not known and seems to vary among different inflammatory conditions, I aim to investigate B cell clustering in the context of renal graft transplants using mathematical modelling. The presented model is rather general and can be considered as a framework which implements cell migration, cell-cell interactions, chemokine diffusion and receptor dynamics at the cell surface, hence it can be further applied for similar systems where cell clustering is observed and governed by chemokine gradients.

B cells from TLOs in the context of cancer or chronic graft rejection were shown to produce antibodies *in situ* which are specific to tumour antigen or to the donor HLA [73, 167]. In the case of cancer, B cell presence may be correlated with worse outcome [52] in ovarian carcinoma. On the other hand, B cells together with DCs may be involved in activation of $CD4^+$ T cells and high density of B cells correlates with increased survival [74]. And although in the case of cancer, the ability of B cells to present antigen can be considered as beneficial, in the context of transplantation this is undesired. The role of TLOs in transplant rejection is controversial and in primate studies their presence was shown to be not predictive for the outcome, but this was concluded only for early rejection [96]. In the same studies, TLO were more often found in samples with interstitial fibrosis and tubular atrophy, which means that TLOs may have a role in graft damage.

B cell clusters may contribute to the pathogenesis not only by producing donor-specific antibodies after germinal centre formation. The ability of B cells to play the role of antigen-presenting cells may foster T cell responses, which was demonstrated in [151] where skin grafts were rejected in mice lacking any SLOs if they harboured TLOs and generation of effector and memory T cells by TLOs was proven. Another contribution of B cells to the immune response may be the production of cytokines

which modulate $CD4^+$ T cell responses. Hence, B cell clustering seems to lead to worse clinical outcomes, although there is no direct evidence for it in the case of chronic graft rejection [201]. On the other hand, there is evidence for regulatory function of B cells in transplantation as well, for example, anti-CD20 treatment of naive patients enhanced acute cellular rejection and peripheral B cell numbers were increased in patients with long-term graft functioning [42, 162, 201]. Most of the results show a correlation between outcome and B cell presence, and must be treated carefully since the real confounding factor of graft failure or adaptation could be different. Probably B cell presence may be either beneficial or negative depending on additional conditions.

Stability of immune cell clusters formation is an interesting topic which may have clinical implications. Since cell movement and differentiation is governed by molecule interaction, disturbance of this interaction may lead to cluster resolution. For example, knocking out the CXCR5 gene in a mouse model of rheumatoid arthritis reduced joint damage [221] and neutralizing CXCL13 with antibodies results in TLO desorganisation in NOD mice [87]. Here, I attempt to model chemokine gradient generation and its sensing by lymphocytes and to investigate how model parameters influence CXCL13 gradient and lymphocyte sensitivity to it.

In order to describe such a complex system, I used an agent-based approach, i.e. every cell is treated as an individual instance moving in space and changing its behaviour according to pre-set rules. To efficiently track cell collisions, I implemented a collision detector algorithm, reviewed in section 3.2.1. Since the number of secreted molecules in the system is very large, molecular interactions are easier to model using a diffusion equation than via agent-based modelling. Having bound to a receptor, the chemokine-receptor complex can be internalized and I included such dynamics in the model as well in order to see what impact on the system state complex internalisation may have.

As reviewed earlier, the precise mechanisms of TLO formation are still unknown and I use simplified assumptions about the biology of the system. I assume that B cells enter the tissue via blood vessels and perform persistent random movement in the absence of chemokine gradients. In [111], it was hypothesized that B cells may be responsible for stroma activation since they can provide signalling via lymphotoxin receptor. This assumption is implemented in the model in the form of a phenomenologically described signal which is integrated by stromal cells upon every contact with B lymphocyte. Having reached a certain threshold, stromal cell start to secrete CXCL13. B cells which are able to sense the gradient move towards the chemokine source. Simulation in different parameters ranges will show how relevant each parameter is for the cluster stabilisation and in which condition cluster formation is more likely.

3.2 Framework for TLO modelling

3.2.1 Collision detection

Agent-based modelling includes the simulation of physical interaction between cells, which demands efficient tracking of cell collisions. Collision detection is one of fundamental problems in computer science, robotics, game development, physical simulations and computer animation. Collision detection can be utilized for prognosis of future interactions, for example, for obstacle avoidance in robotics or ray-tracing in animation, or it can be used for identifying already happened collisions in a system, e.g. finding all neighbouring molecules inside the interaction radius. Depending on the system type and the application purpose, the following two variations of collision detection algorithms are used:

Continuous collision detection aims to identify collisions *a priori* by modelling paths of agents and finding their intersections in advance, before trajectories of the agents are updated. It allows to compute the exact time of contacts, but in case of complex physics of the problem it will result in computationally expensive calculations.

Discrete collision detection identifies contact events *a posteriori*, i.e. after volumes of the objects have penetrated each other. This method is much simpler in implementation and in computational effort but does not provide exact time points of collisions.

The choice of the algorithm depends on the size of the time step used for simulation and on the speed of object movement. If the objects are moving very fast, an *a posteriori* algorithm may miss the collision event, because in this case the objects may never overlap in the simulation due to large time steps, when the object displacement is larger than the object size. The drawback of *a priori* algorithms is their dependence on the physics of the problem and higher dimensionality of the computational problem because one needs to consider the time component in order to predict future collisions. Since the aim of the developed framework does not include detailed mechanistic implementation and exact solution of physics underlying cell contacts, I decided to use an *a posteriori* algorithm to gain benefits of computational performance. In the simulations, cell positions were updated with the time step of 0.1 min. For a cell speed of 10 μm/min and cell size of ≈ 10 μm, cell penetration will not exceed 2 μm, or 20% of its diameter, in the worst case.

Overview of *a posteriori* collision detection algorithms

The form of the objects may be very complex. In order to reduce computational costs, the first step for a collision detection is to exclude objects pairs which do not overlap. This step is called *broad-phase* collision detection. After this step, during the *narrow phase*, the rest of the objects are tested for exact

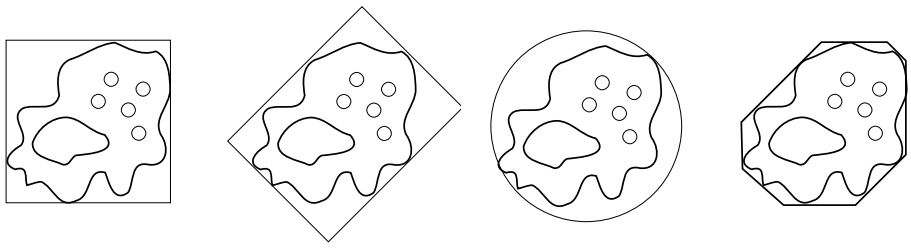

a b c d

Figure 3.1: Methods of object geometry representation for broad-phase collision detection: (a) axis-aligned bounding box; (b) oriented bounding box; (c) bounding circle; (d)k-discrete oriented polytope ($k = 8$).

collisions with respect to their geometry. In the simulations, I assume cells to be of spherical form, hence the exact test for collision will be straightforward as

$$\text{Collision status}(r_1, r_2) = \begin{cases} \text{colliding, if} & \frac{\|\vec{r}_1 - \vec{r}_2\|}{\|r_1\| + \|r_2\|} < 1 \\ \text{not colliding, otherwise,} & \end{cases} \tag{3.1}$$

where $\vec{r}_1, \vec{r}_2$ are the radius vectors of two cells being checked for collision and $\|\cdot\|$ is the euclidean norm.

To simplify detection of object pairs during the broad phase of the algorithm, different abstractions of the object geometry are used. The simplest representation is axis-aligned bounding boxes (AABB), which consist of a minimal cuboid constructed for the object. There is a variety of other methods including bounding spheres, polytopes and oriented bounding boxes, but because of the spherical form of the cells assumed in the model, the AABB method was used for broad-phase collision detection.

The simplest way of collision candidate detection is the naive approach checking all possible object pairs, hence it has complexity of $O(n^2)$, where n is the object number. However, there are more efficient algorithms, which are shortly reviewed below.

Spatial partitioning algorithms. One approach to reduce the number of collision tests is to divide the simulation space into distinct volumes and to assume that all objects located inside of the same volume are candidates for collision and they will be investigated during the narrow phase of collision detection later. At every simulation time step the partitioning structure is to be reconstructed as in case of kd-trees [24] and octrees [17] or objects are sorted among grid cells if regular grids [230] or hash tables [145] are used. The advantage of spatial partitioning is its very simple parallelization, since the problem is divided into a high number of similar subproblems. One can choose a very small cell size. In this case, in every cell can be at most only one object and neighbour check is very simple. On the other hand, there exists an optimal cell size, since the number of subproblems increases quadratically with the decrease of cell side length. Hence, it is obvious that the partitioning algorithm may lack performance if the objects are very diverse in size.

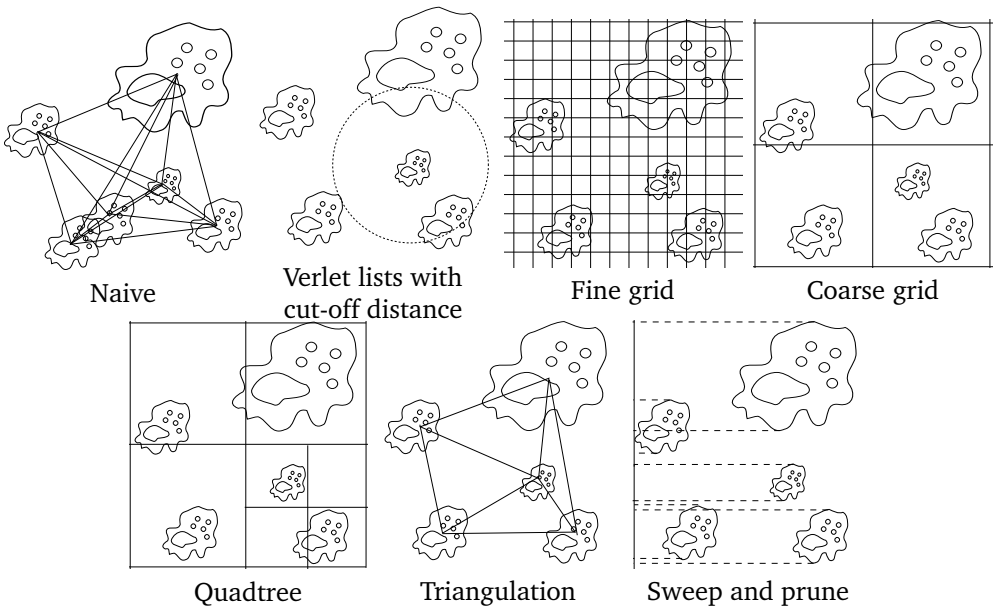

Figure 3.2: Overview of *a posteriori* collision detection algorithms.

If the number of dimensions is d then the number of neighbouring cells is $3^d - 1$. Having a grid with m cells per every dimension, the average object number per cell will be $n_c = n/m^d$ and the number of distances to check is [149]

$$p = \left((3^d - 1)\frac{n_c}{2} + \frac{n_c(n_c - 1)}{2} \right) m^d, \tag{3.2}$$

where we assume that every pair is checked only once, hence only half of the neighbouring cells is considered every time.

Verlet lists. A similar approach is to define a cut-off distance for particles to be called neighbours and to construct a list of this neighbourhood which is called the Verlet list [212]. In this case, the cut-off distance R_{cut} is chosen in such a way that one can use the same list for n_{step} simulation steps, i.e.

$$R_{\text{cut}} = R_{\text{inter}} + n_{\text{step}} d, \tag{3.3}$$

where R_{inter} is the interaction distance between particles and d is the maximum displacement of the objects during one simulation step. In our case, R_{inter} is the sum of cell radia. For N objects, the complexity of list construction is $O(N^2)$. The collision test for every simulation steps will cost $O(N n_{\text{step}}^2)$. This means that the value of n may be optimised to increase performance.

Triangulation An elegant approach is the construction of a Delaunay triangulation graph of neighbours. In agent-based simulations, system states at two subsequent time steps are very much alike, because cells do not move for long distances during one time step. This feature is called *temporal coherence* of the states. The dynamic triangulation algorithm exploits this feature, because it uses previous

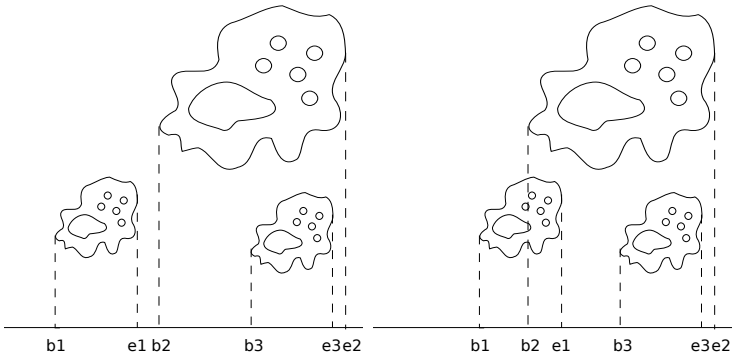

Figure 3.3: Update of boundary list. 'b' denotes for the projection beginning and 'e' denotes for the ending respectively.

states for new graph construction which improves efficiency of collision detection [186]. In addition, a Voronoi tessellation, the dual set of points for the Delaunay triangulation, allows to estimate cell contact surfaces.

However, this algorithm is very sensitive to rounding errors and demands the implementation of high-precision computations.

Sweep-and-prune algorithm. The specificity of our model system is its inhomogeneity, since cells may form clusters. In case of the partitioning algorithms, in some grid cells there will be many objects but some will be almost empty. This will reduce efficiency of the algorithm because its main idea is to distribute the problem among several subproblems. The sweep-and-prune algorithm manipulates with relative order of objects along the axes and is less sensitive to such objections. Also, the sweep-and-prune algorithm allows to exploit temporal coherence, since it uses data structures generated at a previous time step.

The basic idea of the sweep-and-prune algorithm is the projection of the object's AABBs on one or several axes [45]. In this case, one works with intervals corresponding to AABB edges. For detecting the collision, only the relative position of the object to others is important, i.e. there is no need to define any additional abstraction in space like grid or octree.

The first step of the algorithm is the construction of lists of boundaries for every axis, which are generated based on the object's AABBs. For the 3-dimensional case, we have 3 lists of length $2n$, where n is the object number, because for every object there is a beginning and an ending projection point. All boundaries are sorted with respect to the coordinate and one can easily detect intersections between object projection in this case. Objects are considered as candidates for collision if their projections are intersecting at all three axes. The candidate pairs are tested with the narrow-phase collision detection algorithm, since intersection of AABBs does not obligatory mean objects collision, for example, it can take place for non-convex objects. In our case we use the rule from eq. 3.1 for the narrow-phase step.

Variable	Meaning
n	total AABBs
k	dimensions
m	migrations (insertions + removals)
u	updates (moving AABBs)
s	swaps
o	AABB pairs overlapping
e	changes in o

Table 3.1: Definitions of variables used for estimation of the sweep-and-prune algorithm complexity.

During simulation, the objects change their positions, hence, the collision status must be updated accordingly. At every time step, AABBs boundaries are updated and sorted in the lists. Since time steps are small enough, that objects do not move for a large distances, the boundary list will be almost sorted after coordinate update. I used the insertion sorting algorithm, because it was shown to be efficient for this kind of lists and using this time coherence between two system states allows to reduce computational complexity from $\mathcal{O}(n \log n)$ to $\mathcal{O}(n)$, where $\mathcal{O}(.)$ stands for the big O notation [19, 45]. During the sorting procedure, collision status is updated according to the following rules:

- If two left boundaries passed each other, the projections continue to be overlapping
- If two right boundaries passed each other, the projections continue to overlap as well
- If the left boundary and the following right boundary have exchanged, the projections do not overlap any more at the axis and collision between these two objects should be removed
- If the right boundary and a following left boundary has exchanged, a new collision at the axis appears; if the object's projections overlap at all three axes, a new colliding pair is to be added.

The complexity may be further estimated if one includes into consideration migration events (insertions and removals), the number of swaps, AABB coordinates updates, updates of collision status etc., the total complexity of the collision detection workflow is $\mathcal{O}(uk+sk+e+mnk+o)$ [206]. For the definition of the equation terms, see table 3.1. Further, following [206] one may estimate the number of swaps depending on the object density. Let us consider two cubic environments E and E' in k dimensions having side lengths l_E and $l_{E'}$ and the same object volumetric density V. Hence

$$V = \frac{nc}{l_E^k} = \frac{fnc}{l_{E'}^k}, \tag{3.4}$$

considering that there are n objects in E and fn in E'. From this, the side ratio $l_{E'}/l_E = \sqrt[k]{f}$ can be found. With the increase of the object number by a factor of f, the number of swaps is increased by factor of $f^{1-1/k}$. In this case, the swap number is estimated as $s = ukn^{1-1/k}$. Finally, the complexity of sweep and prune collision detection will be $\mathcal{O}(uk^2n^{1-1/k} + mnk + e + o)$.

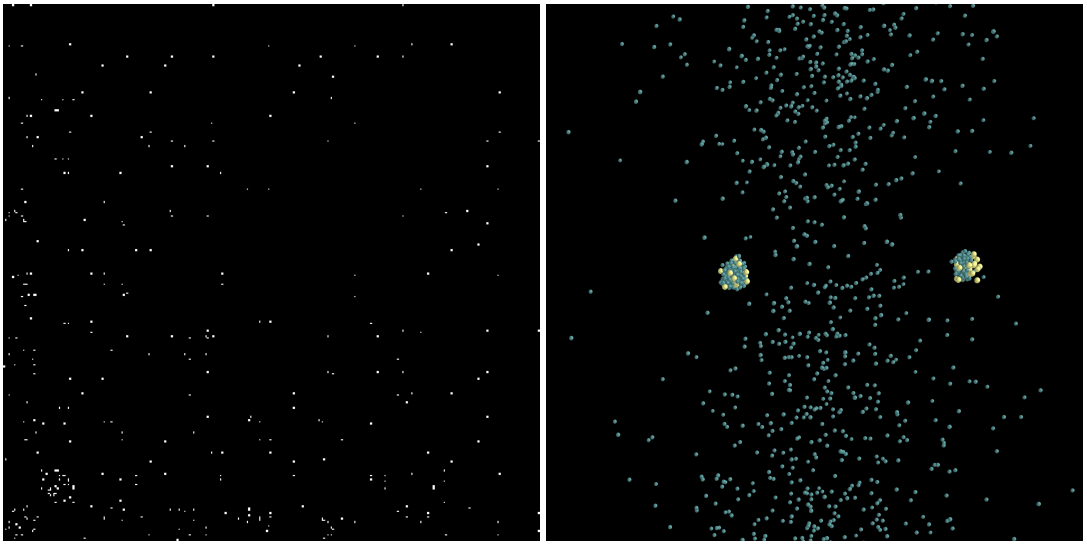

a b

Figure 3.4: a: The collision matrix for a system with two cell clusters. The black space corresponds to non-colliding pairs and white points are potential collisions. Since the matrix is very sparse, only a 300x300 submatrix is plotted. b: Rendering of the system with two clusters of B cells (blue) aggregated around stromal cells (yellow) (using the Mayavi software [175]).

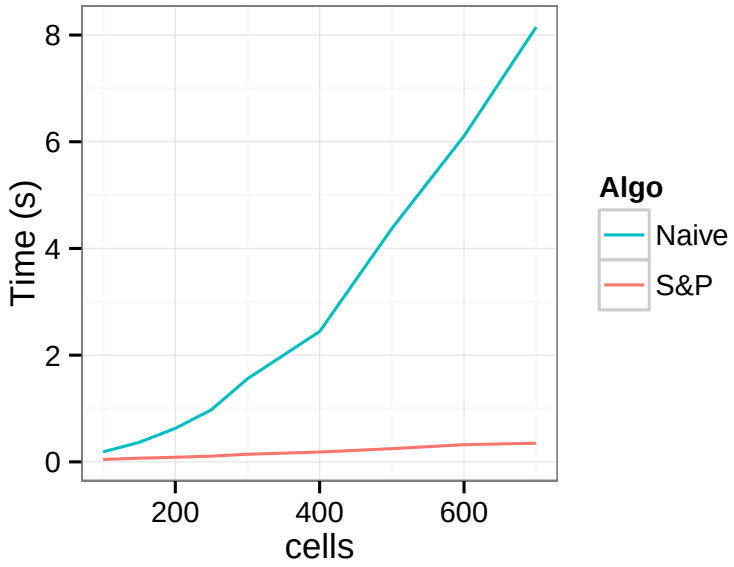

Figure 3.5: Comparison of sweep and prune algorithm versus the naive approach in simulation of cell movement for different cell numbers. Only collision detection and cell movement were simulated, i.e. no diffusion or other complex cell behaviour from the model was used.

The number of colliding object pairs is very low in comparison to the number of all possible pair combinations, and the collision matrix for our system is very sparse, see fig. 3.4. The sweep-and-prune algorithm allows us to avoid redundant collision testing, which dramatically increases the performance of the collision detection in the framework. For comparison with the naive approach see fig. 3.5. The simulation included only simple B cell movement without chemosensing. The size of the simulation box was 1000μm x1000μm x1000μm and the simulating time corresponds to 100min.

3.2.2 Chemokine diffusion

Long range interaction between stroma and immune cells depends on the spatial distribution of chemokine molecules and can be described with the diffusion equation:

$$\dot{c}(\mathbf{x},t) = D \triangle c(\mathbf{x},t) - \kappa \cdot c(\mathbf{x},t) + r(\mathbf{x},t,c(\mathbf{x},t)) + q(\mathbf{x}), \tag{3.5}$$

where

- t is the time,
- $\mathbf{x}$ is the position in the space,
- $\triangle$ stands for the Laplace operator, $\triangle c = \frac{\partial^2 c}{\partial x^2} + \frac{\partial^2 c}{\partial y^2} + \frac{\partial^2 c}{\partial z^2}$
- $c(\mathbf{x},t)$ is the chemokine concentration,
- κ is the chemokine decay rate due to degradation,
- D is the diffusion coefficient for the chemokine,
- $r(\mathbf{x},t)$ is the term describing receptor dynamics and chemokine internalization by the immune cells. In more details, receptor dynamics is discussed in the subsection 3.2.3;
- $q(\mathbf{x})$ is the secretion of the chemokine by stromal cells.

Following [218], the diffusion coefficient was estimated with the empirical formula [116, 199]

$$D = \frac{A}{\mathrm{MW}^{1/3}} = 7.3 \cdot 10^3 \mu\mathrm{m}^2/\mathrm{min}, \tag{3.6}$$

where $A = 2.82 \cdot 10^{-5}\,\mathrm{cm}^{-2}/\mathrm{s(g/mol)}^{1/3}$, $\mathrm{MW} = 12664$ g/mol is the molecular weight of CXCL13.

To solve the equation numerically I applied the splitting approach, which is widely used to simplify the treatment of complex problems by sequentially solving simpler subproblems [112, 127, 193]. In our case, the right hand side of the equation is represented as superposition of spatial term and the

term for the chemical reaction. The numerical scheme can be split in sequential solving of the diffusion step and reaction step:

$$\dot{c_1}(\mathbf{x},t) = D \triangle c_1(\mathbf{x},t) \tag{3.7}$$

$$\dot{c_2}(\mathbf{x},t) = -\kappa \cdot c_2(\mathbf{x},t) + r(\mathbf{x},t,c_2(\mathbf{x},t)) + q(\mathbf{x}) \tag{3.8}$$

In this case, the equation for c_1 is solved up to the next time point t_{n+1} using the chemokine distribution $c(\mathbf{x},t_{\mathrm{n}})$ at the time step t_{n} as the initial condition. Its solution $c_1(\mathbf{x},t_{\mathrm{n+1}})$ is used as the initial condition for the equation describing the reaction step $c_2(\mathbf{x},t_{\mathrm{n}}) = c_1(\mathbf{x},t_{\mathrm{n+1}})$. The chemokine distribution at the time step $t_{\mathrm{n+1}}$ is defined as $c(\mathbf{x},t_{\mathrm{n+1}}) = c_2(\mathbf{x},t_{\mathrm{n+1}})$.

For solving the diffusion equation I used the forward-time central-space (FTCS) explicit scheme and the implicit Crank-Nicolson scheme. This are the so-called finite difference schemes, because the solution is approximated by values arranged on the regular rectangular grid.

For a diffusion equation

$$\frac{\partial c}{\partial t} = D\left(\frac{\partial^2 c}{\partial x^2} + \frac{\partial^2 c}{\partial y^2} + \frac{\partial^2 c}{\partial z^2}\right) \tag{3.9}$$

the FTCS scheme reads as

$$\begin{aligned}\frac{c^{n+1}_{i,j,k} - c^n_{i,j,k}}{\tau} =& D\frac{c^n_{i+1,j,k} - 2c^n_{i,j,k} + c^n_{i-1,j,k}}{h^2_{\mathrm{x}}} + \\ & D\frac{c^n_{i,j+1,k} - 2c^n_{i,j,k} + c^n_{i,j-1,k}}{h^2_{\mathrm{y}}} + D\frac{c^n_{i,j,k+1} - 2c^n_{i,j,k} + c^n_{i,j,k-1}}{h^2_{\mathrm{z}}},\end{aligned} \tag{3.10}$$

where h_* is the discretization step in space, τ is the time step, i,j,k are the indexes of grid points for x, y and z axis, respectively. This scheme is conditionally stable, i.e. it is stable if and only if the following Courant condition is satisfied:

$$\frac{D\tau}{2}(1/h_x^2 + 1/h_y^2 + 1/h_z^2) < 1. \tag{3.11}$$

The FTCS scheme is very easy to implement but may demand very small time steps because of the stability condition. That is why an implementation of the Crank-Nicolson scheme was used, which is derived as a half-sum of forward and backward Euler method:

$$\begin{aligned}\frac{c^{n+1}_{i,j,k} - c^n_{i,j,k}}{\tau} = \frac{D}{2}\Bigg(&\frac{c^n_{i+1,j,k} - 2c^n_{i,j,k} + c^n_{i-1,j,k}}{h^2_{\mathrm{x}}} + \frac{c^{n+1}_{i+1,j,k} - 2c^{n+1}_{i,j,k} + c^{n+1}_{i-1,j,k}}{h^2_{\mathrm{x}}} + \\ &\frac{c^n_{i,j+1,k} - 2c^n_{i,j,k} + c^n_{i,j-1,k}}{h^2_{\mathrm{y}}} + \frac{c^{n+1}_{i,j+1,k} - 2c^{n+1}_{i,j,k} + c^{n+1}_{i,j-1,k}}{h^2_{\mathrm{y}}} + \\ &\frac{c^n_{i,j,k+1} - 2c^n_{i,j,k} + c^n_{i,j,k-1}}{h^2_{\mathrm{z}}} + \frac{c^{n+1}_{i,j,k+1} - 2c^{n+1}_{i,j,k} + c^{n+1}_{i,j,k-1}}{h^2_{\mathrm{z}}}\Bigg).\end{aligned} \tag{3.12}$$

Since this scheme is implicit, it demands solving of a system of linear algebraic equations. I used an implementation of the biconjugate gradient method and the Crank-Nicolson scheme from [187]. The implicit scheme is unconditionally stable, it means it is numerically stable at any time and space

discretization step sizes. Although the implicit scheme allows making large time steps, in our case it appeared that the explicit scheme is faster at time steps in its stability region, hence throughout the work I used only the FTCS-scheme.

For boundary conditions, I used Dirichlet conditions at x and y axis with 0 concentration. In the simulations I consider a cylindrical blood vessel positioned in the center of the simulation box with the size of $L_x \times L_y \times L_z$. I assume that the vessel length is much longer than L_z and use periodic boundary conditions along Z axis, i.e. concentration at up and down are always equal:

$$c|_{x=0} = 0, c|_{x=L_x} = 0 \tag{3.13}$$

$$c|_{y=0} = 0, c|_{y=L_y} = 0 \tag{3.14}$$

$$c|_{z=0} = c|_{z=L_z}. \tag{3.15}$$

The reaction rate v of the proteolytic degradation can be described with Michaelis-Menten kinetics

$$v = \frac{k_{\text{cat}} cE}{K_m + c}, \tag{3.16}$$

where E is enzyme concentration, k_{cat} is the catalytic rate constant, K_m is the Michaelis constant. Assuming chemokine concentration to be small, the reaction rate can be simplified to

$$v = \frac{k_{\text{cat}} cE}{K_m} = \kappa c. \tag{3.17}$$

The degradation rate of CXCL13 in tissue is not known but there are available data about proteolysis of other chemokines. In [37, 218] where chemokine gradients were modelled, degradation kinetics were based on the analysis of [23, 113, 170, 205, 229], and κ was estimated to be in the range of $10^{-5} - 5 \cdot 10^{-3}\text{s}^{-1}$. Given eq. 3.17, the degradation step during the simulation is described with the exact solution of first-order kinetics

$$c_{n+1} = c^*_{n+1} e^{-\kappa\tau}, \tag{3.18}$$

where c^*_{n+1} is the concentration calculated after diffusion step and κ is the degradation rate.

Chemokine secretion is modelled as a point source at the closest grid point in respect to the stromal cell

$$q(x_{\text{i}}, y_{\text{j}}, z_{\text{k}}) = \frac{q}{V}, \tag{3.19}$$

where $V = h_{\text{x}} h_{\text{y}} h_{\text{z}}$ is the volume of a grid cell, i, j and k are the X, Y and Z axis indexes of the grid point and q is the secretion rate by a single cell.

The secretion rates of other chemokines were used as estimation for q in the simulations. In [218], the CXCL12 secretion rate range was estimated as 0.01-1 pg/hr/cell (or $8 \cdot 10^{3-5}$ molecules/cell/min) based on [41, 94, 117, 185]. Also a measurement of CXCl13 secretion rate by macrophages was reported in [32], where primed cells were able to secrete the chemokine at rate of 11 molecule/min.

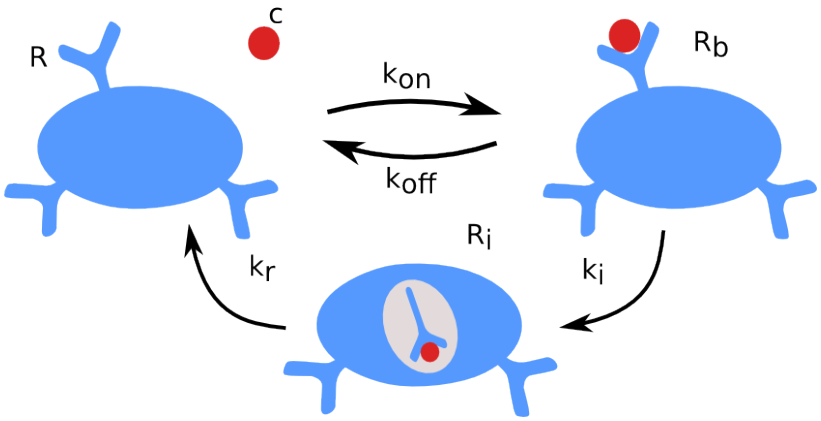

Figure 3.6: A scheme of receptor dynamics. Chemokine forms a complex with a receptor which is internalised by the cell. The free receptor is recycled to the cell surface.

In experiments with microfluidic device for the generation of CXCL12 gradient, the transduced breast cancer cells were secreting the chemokine at rate of 15-25 molecules/cell/s (900-1500 molecules/cell/min) [36] and this range was used later in computational modelling of the gradients in a similar set-up in [37]. Based on these estimations, the CXCL13 secretion rate is assumed to be in the range $10^3 - 10^5$molecules/cell/min.

3.2.3 Receptor dynamics

Chemokines are sensed by cells via receptors at their surface. Upon binding, ligand-receptor pairs are being internalised by the cell and the receptor is recycled back to the surface later. I do not include phosphorylation of the receptor [119] into the model or, for example, its interactions with β-arrestin [37] and describe the kinetics of chemokine-receptor complexes phenomenologically without underlying mechanism implementation, fig. 3.6.

The internalisation process changes the chemokine concentration at the lymphocyte location. The receptor dynamics can be described by the system of ordinary differential equations which has to be coupled with the chemokine dynamics:

$$\dot{R} = -k_{\text{on}} R c + k_{\text{off}} R_{\text{b}} + k_{\text{r}} R_{\text{i}} \tag{3.20}$$

$$\dot{R}_{\text{b}} = k_{\text{on}} R c - k_{\text{off}} R_{\text{b}} - k_{\text{i}} R_{\text{b}} \tag{3.21}$$

$$\dot{R}_{\text{i}} = k_{\text{i}} R_{\text{b}} - k_{\text{r}} R_{\text{i}} \tag{3.22}$$

$$\dot{c} = -k_{\text{on}} R c + k_{\text{off}} R_{\text{b}}, \tag{3.23}$$

where

- k_{on} and k_{off} are rates of binding and unbinding of chemokine to receptors,

- k_{i} is rate of receptor-chemokine complex internalization,
- k_{r} is rate of receptor recycling to the cell surface;
- R is the number of free surface receptors,
- c is the concentration of the chemokine,
- R_{b} is the number of receptor-chemokine complexes (bound receptors),
- R_{i} is the number of internalized receptors.

Instead of absolute receptor numbers, I use concentrations calculated as receptor number divided by the grid cell volume V, in order to comply with dimensions in the kinetic equation. The total number of receptors is assumed to be constant within the simulation time: $R_{\text{total}} = R + R_{\mathrm{b}} + R_{\mathrm{i}}$. Hence, the system can be simplified to

$$\dot{R} = -k_{\text{on}} R c + k_{\text{off}}(R_{\text{total}} - R - R_{\mathrm{i}}) + k_{\mathrm{r}} R_{\mathrm{i}} \tag{3.24}$$

$$\dot{R}_{\mathrm{i}} = k_{\mathrm{i}}(R_{\text{total}} - R - R_{\mathrm{i}}) - k_{\mathrm{r}} R_{\mathrm{i}} \tag{3.25}$$

$$\dot{c} = -k_{\text{on}} R c + k_{\text{off}}(R_{\text{total}} - R - R_{\mathrm{i}}). \tag{3.26}$$

To solve these equations I used an implicit Euler scheme, because it is stable and can be used for stiff systems where the processes have different kinetic rates [30]. In our case, the system is stiff due to a fast binding of chemokine to receptors and a slower reaction of receptor internalization. In case of a single B cell, the implicit scheme may be treated analytically and it was decided to follow the splitting technique as mentioned above and to solve the receptor dynamics equations sequentially for cells located at the same grid point. The implicit Euler scheme yields the system

$$\frac{R_{\mathrm{n+1}} - R_n}{\tau} = -k_{\text{on}} R_{\mathrm{n+1}} c + k_{\text{off}}(R_{\text{total}} - R_{\mathrm{n+1}} - R_{\mathrm{i,n+1}}) + k_{\mathrm{r}} R_{\mathrm{i,n+1}} \tag{3.27}$$

$$\frac{R_{\mathrm{i,n+1}} - R_{\mathrm{i,n}}}{\tau} = k_{\mathrm{i}}(R_{\text{total}} - R_{\mathrm{n+1}} - R_{\mathrm{i,n+1}}) - k_{\mathrm{r}} R_{\mathrm{i,n+1}} \tag{3.28}$$

$$\frac{c_{\mathrm{n+1}} - c_n}{\tau} = -k_{\text{on}} R_{\mathrm{n+1}} c_{\mathrm{n+1}} + k_{\text{off}}(R_{\text{total}} - R_{\mathrm{n+1}} - R_{\mathrm{i,n+1}}) \tag{3.29}$$

with the exact solution

$$R_{\mathrm{n+1}} = \frac{-B + \sqrt{B^2 - 4AC)}}{2A} \tag{3.30}$$

$$R_{\mathrm{i,n+1}} = \alpha_2 - \alpha_3 R_{\mathrm{n+1}} \tag{3.31}$$

$$c_{\mathrm{n+1}} = (R_{\mathrm{n+1}} - \tau k_{\mathrm{r}} R_{\mathrm{i,n+1}}) + \alpha_1, \tag{3.32}$$

where

$$\alpha_1 = (c_n - R_n), \alpha_2 = \frac{R_{\text{i,n}} + \tau k_{\text{i}} R_{\text{total}}}{1 + \tau(k_{\text{i}} + k_{\text{r}})}, \alpha_3 = \frac{\tau k_{\text{i}}}{1 + \tau(k_{\text{i}} + k_{\text{r}})} \tag{3.33}$$

$$A = k_{\text{on}}\tau(1 + \alpha_3 \tau k_{\text{r}}) \tag{3.34}$$

$$B = 1 + \tau k_{\text{off}} + \alpha_3 \tau(k_{\text{r}} - k_{\text{off}}) + k_{\text{on}}\tau(\alpha_1 - \tau k_{\text{r}} \alpha_2) \tag{3.35}$$

$$C = -\tau k_{\text{off}} R_{\text{total}} - \tau(k_{\text{r}} - k_{\text{off}})\alpha_2 - R_0 \tag{3.36}$$

For the parameters values in the model, I use estimations for similar receptors in experiments with T cells and cancer cell lines. The only available parameter values for the CXCL13-CXCR5 pair are k_{on} and k_{off} rates which were are measured in [21], $k_{\text{on}} = 7.7 \cdot 10^4\,\text{M}^{-1}\text{s}^{-1}$ and $k_{\text{off}} = 3.5 \cdot 10^{-3}\text{s}^{-1}$. For CXCR5, there are no available data about internalization and recycling dynamics, and data for CXCR4 are used as an estimation instead [36, 44]. The internalization rate is $k_{\text{i}} = 4.7 \cdot 10^{-3}\text{s}^{-1}$ and the recycling rate is $k_{\text{r}} = 6.9 \cdot 10^{-5}\text{s}^{-1}$.

The density of CCR7 receptors in T cells is estimated as $2 \cdot 10^4$ receptors/cell [224]. In case of transfected cancer cell lines in [37] the density of CXCR4 is $7.1 \cdot 10^5$ and for CXCR7 it is $2 \cdot 10^6$ receptors/cell. The same work refers to a previously measured receptor density interval for cancer cells as $10^3 - 10^5$ [89, 156]. Based on these results, we will perform simulations assuming the receptor number to be in the range of $10^3 - 10^6$ per cell.

3.2.4 Cell migration

Cell movement is governed by a signal which they get from the chemokine receptors. Chemokines are secreted in order to position cells within certain regions. As discussed in sec. 2.2, secretion of CXCL13 by stromal cells, which are differentiated into FDCs, attracts CXCR5$^+$ B lymphocytes.

Directed migration of cells depends on their ability to get polarized along with the direction of chemokine concentration gradient. I assume that a B cell defines its direction based on the difference of receptor-chemokine complexes at two opposing sides [119]. Since the receptor binding is the fastest process in the system, we may consider the reaction in equilibrium, i.e.

$$k_{\text{on}} c R = k_{\text{off}} R_{\text{b}}. \tag{3.37}$$

Assume that the total surface receptor numbers at opposite cell sides are equal $R^- + R_{\text{b}}^- = R^+ + R_{\text{b}}^+ = R_{\text{surface}}/2$, where $R^+ + R^- = R$, $R_{\text{b}}^+ + R_{\text{b}}^- = R_{\text{b}}$. For a small concentration difference $\triangle c$, the difference in bound receptors is estimated as

$$\triangle R_{\text{b}} = \frac{R_{\text{surface}} \triangle c}{2(K_{\text{d}} + c)}, \tag{3.38}$$

where K_{d} is the dissociation constant for the chemokine, $\triangle c = |\nabla c| d$ is the difference in chemokine concentration at the opposite cell sides, d is the diameter of the cell, ∇c stands for the chemokine

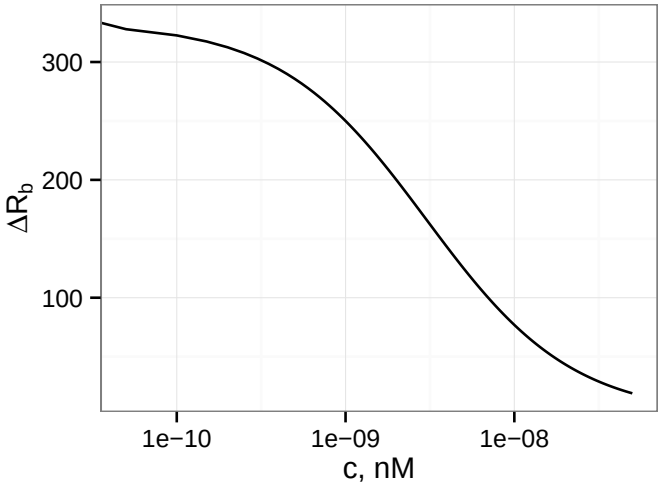

Figure 3.7: Difference in bound receptor numbers depending on concentration according to the eq. 3.38. The chemokine concentration difference $\triangle c$ is set to be constant.

gradient. The difference in bound receptors depends not only on the steepness of the gradient but on the absolute chemokine concentration as well. An example of such a dependency is shown at fig. 3.7. A cell performs persistent random walk if the difference $\triangle R_\mathrm{b}$ is too low and it moves along with the chemokine gradient otherwise. I use the threshold number $\triangle R_\mathrm{b} > 10$ which is justified by estimation of fluctuations in bound receptors [207] and is used in [119, 218] for modelling of cell polarization in the presence of the chemokine gradient.

According to [143], a B cell has a persistence time $t_\mathrm{persist} = 1.24$ min, after which it changes its direction according to the chemokine field. I use the speed value estimated from two-photon imaging of B lymphocytes $v_B = 6.4$ μm/min [143], if not otherwise specified.

The detailed modelling of physical interactions is beyond the scope of this work. If two cells collide, their interaction is simplified with an elastic repulsion force

$$F = \max(F_0, k\|\vec{r}_1 - \vec{r}_2\|) \cdot \frac{\vec{r}_1 - \vec{r}_2}{\|\vec{r}_1 - \vec{r}_2\|}, \tag{3.39}$$

where F_0 is the maximal force magnitude, which is introduced in order to prevent high speed jumps of the cells. I neglect cell acceleration in computation of cell movement, assuming that the viscosity of the medium in the tissue is high enough, and cell speed is constant during a time step. Hence, cell velocity can be found from Stock's law

$$\vec{v} = \vec{F}/\gamma \tag{3.40}$$

To put aside detailed physics of cell contacts, we may use arbitrary force units which can be mapped to cell velocity then. In this case $\gamma = 1\,\mu\mathrm{m}/(\mathrm{min}\cdot\ \mathrm{a.u.})$ and $k = 10\,\mathrm{a.u.}/\mu\mathrm{um}$, where a.u. stands for

arbitrary units. Active cell migration of B lymphocytes is implemented as

$$\vec{F} = \gamma v_{\text{B}} \vec{p}, \tag{3.41}$$

where $\vec{p}$ is the direction of B cell polarization. Inside the blood vessel cells are subjected to an additional force which pushes them away from the vessel in the X-Y plane (the vessel is directed along the Z axis):

$$F_{\text{vessel}} = 1\text{a.u.} \cdot \frac{\vec{r} - (r, e_z)e_z}{\|\vec{r} - (r, e_z)e_z\|} \tag{3.42}$$

3.2.5 Stromal cell activation

Stromal cells change their phenotype due to interaction with B cells, which migrate inside the tissue. In our model, stromal cell are represented as static spheres, which are distributed with the constant density in the simulation space. There are no available data about the stromal cell size in the condition of chronic inflammation. Being differentiated into FDCs, they may have a complex morphology characterised by dendrites with the length of 15-20μm [196]. Without loss of generality, I assume that stromal cell have a diameter of $d_{\text{stroma}} = 15\mu$m. This parameter can be adjusted in the future if the data about stroma morphology are available.

I assume that the structure of the stroma environment is not tight due to edema [49], a process of accumulation of liquid during chronic inflammation. As with the stromal cell diameter, the density of this cells is not known as well. Stromal cells are positioned with density which corresponds to rectangular packing of cells with the interval of $2d_{\text{stroma}}$, i.e.

$$d_{\text{stroma}} = \frac{1}{(30\mu\text{m})^3} = 3.7 \cdot 10^{-5} \mu\text{m}^{-3} \tag{3.43}$$

If a B cell gets in contact with any stromal cell, it stops moving for the interaction time $t_{\text{inter}} = 1$min. After this time period, the B cell reverts its direction and continues migration.

Since there is no known mechanism of stroma activation, I implemented a phenomenological model based on the signal integration model for T cell activation [173]. I define the signal as cumulative time of interaction and after every contact, the value increases with t_{inter}. A cell has a limited memory for a contact, and contribution of every interaction decays exponentially with time. If the signal achieves the threshold value θ, the stromal cell is assumed to differentiate into an FDC phenotype and it starts to secrete CXCL13. This process is supposed to a have a limited memory, i.e. cell contacts which happen long time ago do not contribute to stromal cell fate decision. I illustrate this kind of process in the next section where I introduce the decay rate d, which is an arbitrary value, as well as the signal threshold.

3.2.6 Implementation

There is a big variety of paradigms for computer program development. The object-oriented approach is one of the most popular for agent-based simulations. It can be explained by the sim-

plicity of translation of the model into programming language code, since the main term is the object itself. For example, in our case, to describe B cells we would need to introduce a class

```
struct BCell {
  size_t id;
  const double radius;
  const double maxSpeed;
  const double receptorTotal;
  double nextTurningTime;
  Vector direction;
  Vector position;
  Vector velocity;
  double receptor;
  double internalizedReceptor;
};
```

Listing 3.1: OOP B cell class

Every object of this class has information about cell position, direction, velocity etc. Although it is much easier to map the model to the code, this approach has its drawback in cache utilization. For example, if we have a vector of B cell objects and we would like to update coordinates of the cells, there will be a lot of cache misses due to data layout in memory, since data from one object in this case will be packed together.

An alternative approach for the code design is so-called data-oriented programming [125]. The main idea of it is to abstract from objects to data and to consider the program as processing of a data flow. The agents are divided in simpler components which can be processed with small functions using less data. In this case, instead of vector of structures we deal with structure of vectors:

```
struct BCells {
  Movables *    movables;
  CollidableSpheres * collidables;
  const double radius;
  const double maxSpeed;
  const double receptorTotal;
  std::vector<size_t> IDs;
  std::vector<double> nextTurningTime;
  std::vector<Vector> directions;
  std::vector<double> receptor;
  std::vector<double> internalizedReceptor;
};
struct CollidableSpheres {
  std::vector<size_t> IDs;
  std::vector<CellTypes> cellTypes;
  std::vector<Vector> positions;
  std::vector<double> radius;
};
```

Listing 3.2: DOD B cell class

The class of B cells is linked to components for collidable objects and for movable objects and it delegates storing of information about position and velocity to these two classes and includes only B cell specific data. If one needs to update the position of all cells given their velocities, it can be done by a very simple function which takes a vector of velocities and cell positions, allowing for more efficient cache-utilization, since all position data are closely packed now. This approach is structurally very similar to relational databases, because structures of vectors can be seen as data tables now with unique id keys to connect information of the same B cell. Another useful advantage of this approach is that the set of functions performing actions on vectors are simple to parallelize.

Symbol	Meaning	Value	Range*	Units	Reference
q	CXCL13 secretion rate	varying	$10 - 10^5$	molecules/(cell · min)	[32, 36, 37, 41, 94, 117, 185, 218]
R_{tot}	surface receptor number	varying	$10^3 - 10^6$	#	[37, 89, 156, 224]
κ	CXCL13 degradation rate	10^{-5}	$10^{-5} - 10^{-3}$	s^{-1}	[18, 23, 113, 170, 205, 218, 229]
v_B	B cell speed	exp	6.4-8.3	μm/min	[43, 143]
t_{persist}	persistence time for B cell	exp	1.24	min	[143]
r_B	B cell radius	exp	5.5	μm	[71]
d_S	stromal cell density	assum	$3.6 \cdot 10^{-5}$	μm^{-3}	
r_S	stromal cell radius	assum	7.5	μm	
t_{inter}	interaction time	assum	1	min	
θ	activation threshold	varying	10-20		
d	signal decay	varying	0.01-0.05	min^{-1}	
$\triangle R_b$	threshold of bound receptor difference	estimated	10	#	[119, 207, 218]
k_{on}	receptor-CXCL13 binding rate	exp	$7.7 \cdot 10^4$	$M^{-1}s^{-1}$	[21]
k_{off}	receptor-CXCL13 dissociation rate	exp	$3.5 \cdot 10^{-3}$	s^{-1}	[21]
K_{d}	dissociation constant	exp	$5.05 \cdot 10^{-8}$	M	[21]
k_{i}	internalization rate	exp	$4.7 \cdot 10^{-3}$	s^{-1}	[44]
k_{r}	receptor recycling rate	exp	$6.9 \cdot 10^{-5}$	s^{-1}	[44]
r_V	vessel radius	assum	60	μm	ca. 10 cells

Table 3.2: Model parameters.

3.3 Simulations

3.3.1 Stochastic modelling of signal integration for a single stromal cell

According to our assumptions, interactions between B cells and stromal cells play the key role in activation of stromal cells. We expect that rare contacts are not able to induce stroma differentiation, otherwise any contact with lymphocytes would result in TLO development and these structures would be observed ubiquitously in a healthy organism. Frequency of contacts is directly related to B cell concentration, which is a measurable value. Moreover, immunosuppresive therapy with Rituximab is directed exactly to control the B cell numbers. To investigate how stroma activation could depend on the B cell number, I constructed a simplistic stochastic model of signal integration. A similar proposition was made for T cell activation via temporal signal integration [173]. In this model, I consider a stromal cell which is located in a volume filled with randomly moving B cells. Due to random collisions, a stromal cell will get in a contact with B cells and get an activation signal α. I consider here that stroma cells have limited memory, i.e. signal decay is modelled as

$$\dot{S} = b(t) - dS, \tag{3.44}$$

where d is a decay parameter and $b(t)$ is the signal from a B cell. For simplicity, I assume that after every interaction S increases as α, and for given interaction times $\tau_1, \tau_2 \dots \tau_n$ the equation reads

$$\dot{S} = \alpha \sum_{i=1}^{n} \delta(t - \tau_i) - dS, \tag{3.45}$$

where $\delta(t)$ is the Dirac delta function. Having zero signal in the beginning, the solution is

$$S(t) = \left(\alpha \sum_{i=1}^{n} [t \geq \tau_i] e^{d\tau_i} \right) e^{-dt}, \tag{3.46}$$

where the indicator function is defined as

$$[t \geq \tau] = \begin{cases} 1, t \geq \tau \\ 0, t < \tau \end{cases} \tag{3.47}$$

It is straightforward to treat equation 3.44 if the times of interaction are given, but in reality $b(t)$ is a Poisson random process and the equation 3.44 becomes a stochastic-differential equation. To describe our system evolution in time, I perform numerical simulations, see fig. 3.8. The contact times are generated from a Poisson distribution by algorithm 3.1, p. 41, and the signal S can be computed according to eq. 3.46 for the period of time $[0, T]$. Since in the model, a stromal cell gets activated when a certain threshold value of a signal θ is achieved, it is interesting to characterise the expected time of activation and at which frequency of contacts the signal will be above the threshold for most of the time. Hence, I defined two measures of interest here:

- first passage time, the time needed to reach the threshold value θ starting from zero signal $S(0) = 0$

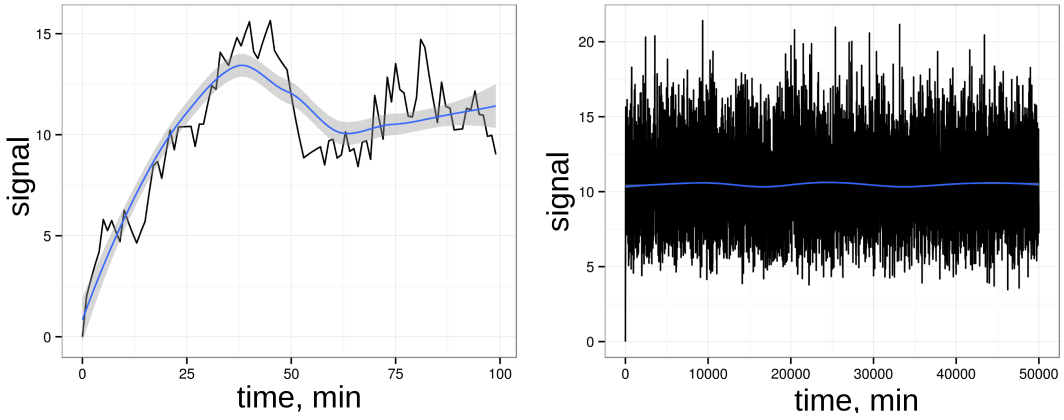

Figure 3.8: Example of stromal cell signal simulation for the frequency of 1 interaction per minute and decay rate $d = 0.1\text{min}^{-1}$.

Algorithm 3.1: Algorithm for generation of Poisson events.

```
/* For a given time interval [0,T] and frequency f:
generate event number                                   */
N ⟵ Poisson(fT)
/* generate times of events:                            */
for i ∈ 1..N do
    T_i ⟵ Uniform(0, T)
sort event times T_1, T_2 ··· T_N → τ_1, τ_2 ··· τ_N
```

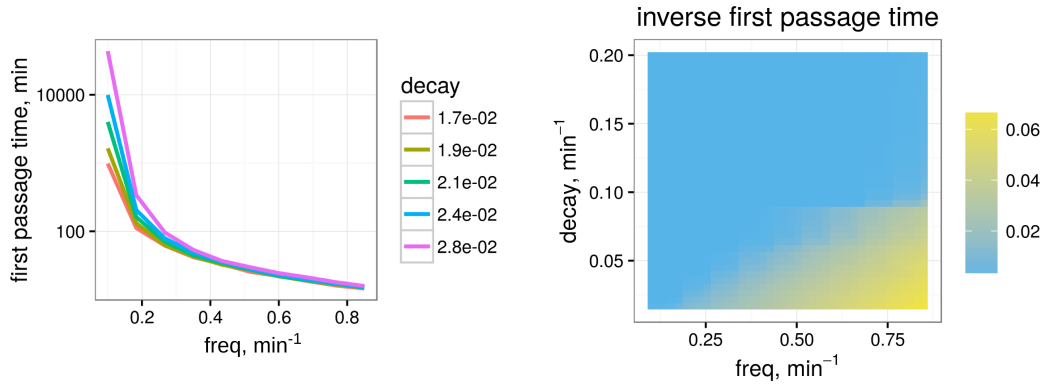

Figure 3.9: Dependency of first passage time for a threshold value of $\theta = 10$ (left) and for varying signal decay and cell contact frequency values (right).

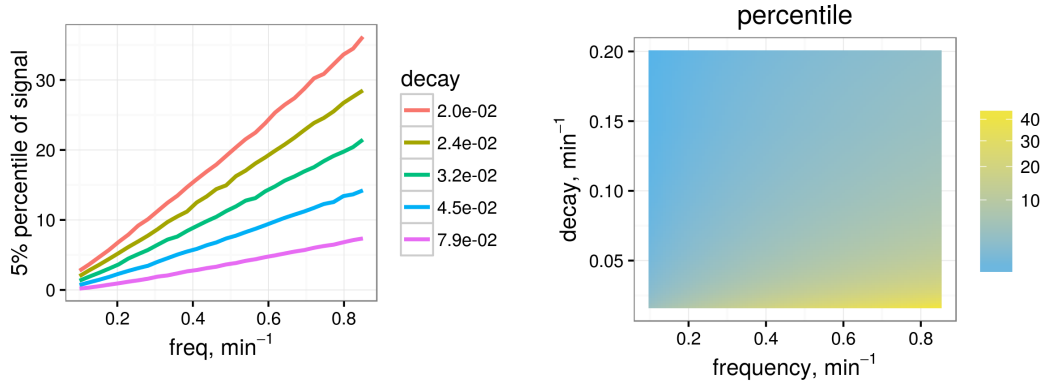

Figure 3.10: Dependency of signal 5% percentile for varying signal decay (left) and cell contact frequency values (right).

- 5% percentile of the signal distribution during the time, i.e. a signal value $S_{0.05}$ such that

$$\frac{\int_0^T [S(t) < S_{0.05}]dt}{T} = 0.05, \tag{3.48}$$

where [.] is the indicator function.

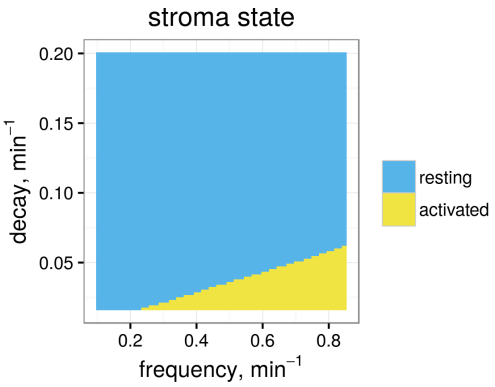

Figure 3.11: Phase diagram for stromal cell activation for a signal threshold of $\theta = 10$.

As fig. 3.9 shows, the first passage time dramatically decreases as the frequency of contacts increases. This means that the contact frequency is a crucial parameter of the system and that the lymphocyte concentration in the stroma area defines the activation time. Since immunosuppresive therapy helps to decrease lymphocyte numbers, this simulation suggests that a moderate decrease in lymphocyte concentration may lead to a higher order increase in the expected first passage time, hence, a longer expected time for stroma activation.

A complement measure, the 5% percentile $S_{0.05}$ (see fig. 3.10) shows a linear dependency of $S_{0.05}$ on the contact frequency. Unfortunately, there are no available experimental data on stroma activation, and although this model is rather abstract, one may see that at a certain signal decay rate and contact frequency, the signal S will be above the threshold θ for 95% of time, i.e. $S_{0.05} > \theta$, see fig. 3.11. One may associate this regime with a stable activation of stroma, which may result in development of lymphocyte clustering due to continuous chemokine secretion.

Conclusion

- The stochastic model with decay for stromal cell signal integration illustrates that contact frequency may be a very good controller for first passage time, i.e. for stroma activation.
- The system parameters, signal decay rate d and contact frequency f, define regions in which stroma remains activated most of the time and where the signal is above the threshold (resting).

3.3.2 Contact frequency in perivascular space

In order to test our collision detection algorithm and to investigate how the position of a stromal cell in tissue influences the contact frequency with lymphocytes, I performed simulations for a case of cell influx from a blood vessel into the tissue. If migrating cells leave the perivascular area they are deleted

from the simulation, if a cell reaches upper or bottom bound I apply periodic boundary conditions, i.e. the cell appears from the opposite side. In this case, cell migration without chemotaxis is similar to molecule diffusion, hence this problem can be compared with the solution of the diffusion equation for a cylinder [34]:

$$B(r) = \frac{(B_2 - B_1)\log r + B_1 \log r_2 - B_2 \log r_1}{\log r_2 - \log r_1}, \tag{3.49}$$

where B_1 and B_2 are concentrations of lymphocytes at the inner radius r_1 and at the outer one r_2. In case of zero Dirichlet boundary conditions (i.e. all cells reaching the outer boundary are deleted), the equation is simplified to

$$B(r) = \frac{B_1 \log(r_2/r)}{\log(r_2/r_1)}. \tag{3.50}$$

Since contact frequency of stromal cells with lymphocytes is proportional to the concentration of the latter (for a given stromal cell density), the dependency of the contact frequency $f(r)$ on the distance from the vessel centre r will look linear in logarithmic scale for r.

I constructed a system of stromal cells surrounding a blood vessel of diameter equal to 10 lymphocytes sizes (as it was suggested after biopsy investigation, Prof.Dr. Friedrich Feuerhake, Medical Hannover School, personal communication). Stromal cells were positioned at random positions with the uniform density as described in sec. 3.2.5. Collisions between cells were tracked in the region of 600μm radius around the vessel (21141 stromal cells in total in the 1540μm x 1540μm x 490μm box). B cell movement is subjected to periodic boundary condition along the Z-axis: if a B cell reaches the top or bottom boundary of the simulation box, it appears at the opposite side. B cells enter the tissue from the blood vessel with the frequency $f_{\mathrm{B}} = 0.05$ cell/min. I was interested to estimate contact frequency in a steady state, hence after starting the simulation with a prepositioned number of B cells, I tracked the total B cell number to see when the system is stabilized. Indeed, the frequency of contacts was logarithmically dependent on the distance from the vessel, fig. 3.12. Perivascular cells have a higher chance of activation in the frame of our assumptions, since according to the previous section, the first passage time for activation may dramatically vary upon change of the contact frequency, see fig. 3.9. Hence, cell position in the tissue might influence its phenotype because of different contacts frequency, see fig. 3.13.

Conclusion

- I constructed framework for collision detection between cells and tested it in the condition of constant B cell influx to the perivascular area of stromal cells. The frequency of contacts decreases logarithmically with the distance from the blood vessel.
- The stromal cell position may influence the probability of its activation because of the decrease in the cell contact frequency at the periphery and, consequently, the increase of the first passage time for activation.

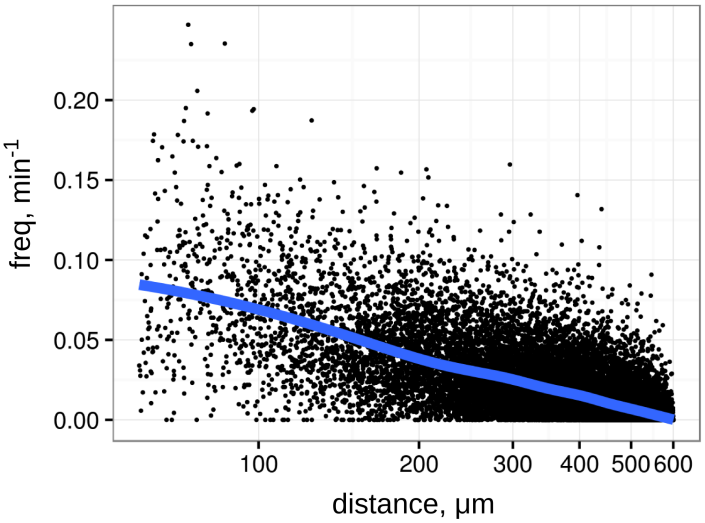

Figure 3.12: Frequency of contacts between stromal cells and B cells depending on the distance from the blood vessel. The smoothing line corresponds to the fit with LOESS regression generated with ggplot2 package for the R statistical environment [222].

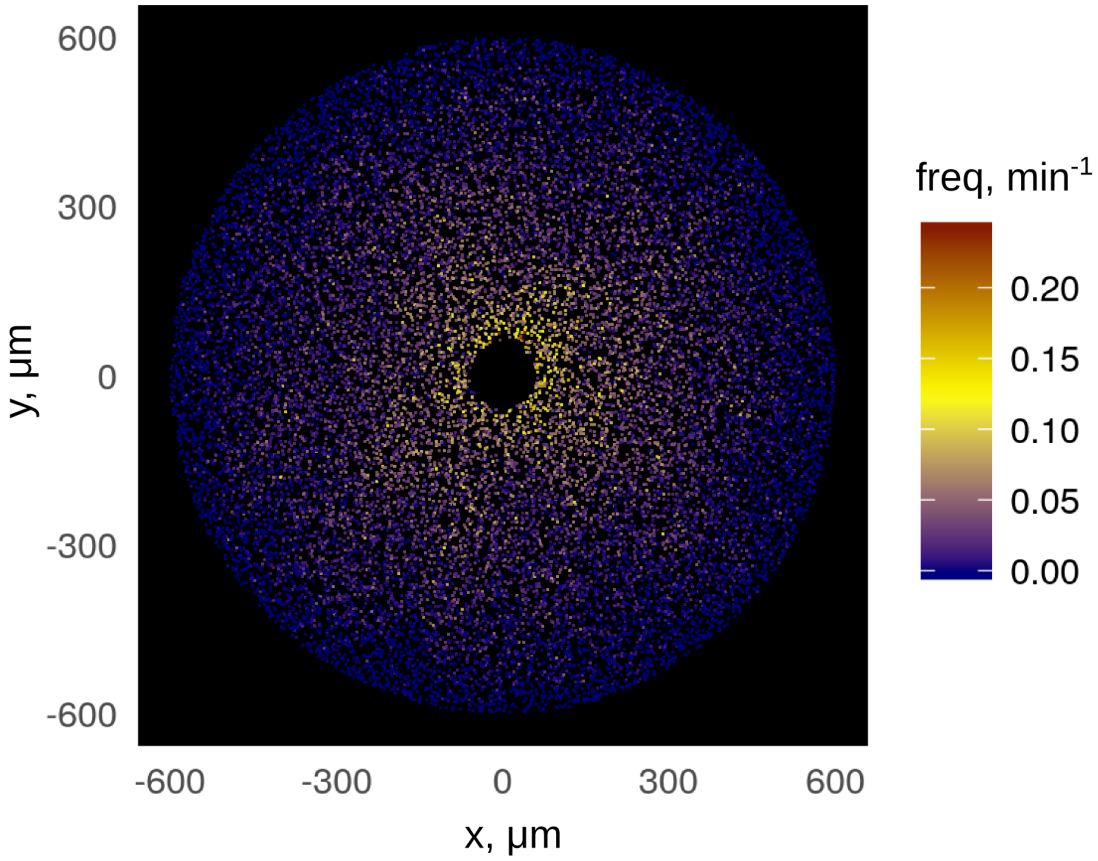

Figure 3.13: Frequency of contacts between stromal cells and B cells in single cell representation.

3.3.3 Chemokine gradient profile

Estimation of concentration with exact and numeric solution

Stromal cells are assumed to secrete the chemokine CXCL13, which spreads in the environment via diffusion and can be degraded by proteolysis. Let us consider a spherical cell secreting the chemokine with the rate q. This system has radial symmetry and the chemokine concentration c can be described with the following diffusion equation

$$\frac{\partial c}{\partial t} = \frac{1}{r^2}\frac{\partial}{\partial r} r^2 \frac{\partial}{\partial r} Dc - \kappa c, \tag{3.51}$$

where D is the diffusion coefficient for CXCL13, κc represents degradation of the chemokine and r is the distance from the cell position. For simplicity, I assume zero boundary condition at infinity and a constant secretion rate at the cell surface:

$$c|_{r\to\infty} = 0 \tag{3.52}$$

$$4\pi\rho^2 D \frac{\partial c}{\partial r}|_{r=\rho} = -q \tag{3.53}$$

where ρ is the cell radius. Here we are interested in a steady-state solution, namely

$$c = \text{const} \rightarrow \frac{\partial c}{\partial t} = 0 \tag{3.54}$$

$$\frac{1}{r^2}\frac{\partial}{\partial r} r^2 \frac{\partial}{\partial r} Dc - \kappa c = 0 \tag{3.55}$$

By substitution $v = rc$ the eq. 3.55 is reduced to

$$\frac{\partial^2 v}{\partial r^2} = \frac{\kappa}{D} v \tag{3.56}$$

with the solution

$$v = C_1 e^{\sqrt{\kappa/D}r} + C_2 e^{-\sqrt{\kappa/D}r}. \tag{3.57}$$

$C_1 = 0$ from the boundary condition of $c = 0$ at infinity, hence, from eq. 3.53 we get

$$c(r) = \frac{q \exp\left(-\sqrt{\frac{\kappa}{D}}r\right)}{4\pi D r \left(\sqrt{\frac{\kappa}{D}}\rho + 1\right) \exp\left(-\sqrt{\frac{\kappa}{D}}\rho\right)}. \tag{3.58}$$

This analytical solution describes the concentration of CXCL13 if the environment size would be infinite. In reality and in our simulations, the system size is limited to the organ size or simulation box, respectively. Since the analytical solution is rather easy to treat, I will use it in order to estimate chemokine profiles for different system parameters. It is interesting to compare the numerical solution with the exact one at the order of distances of the simulation box size. The solutions are very close to each other in the vicinity of the cell and the difference between them does not exceed $2 \cdot 10^{-13}$M, fig. 3.14.

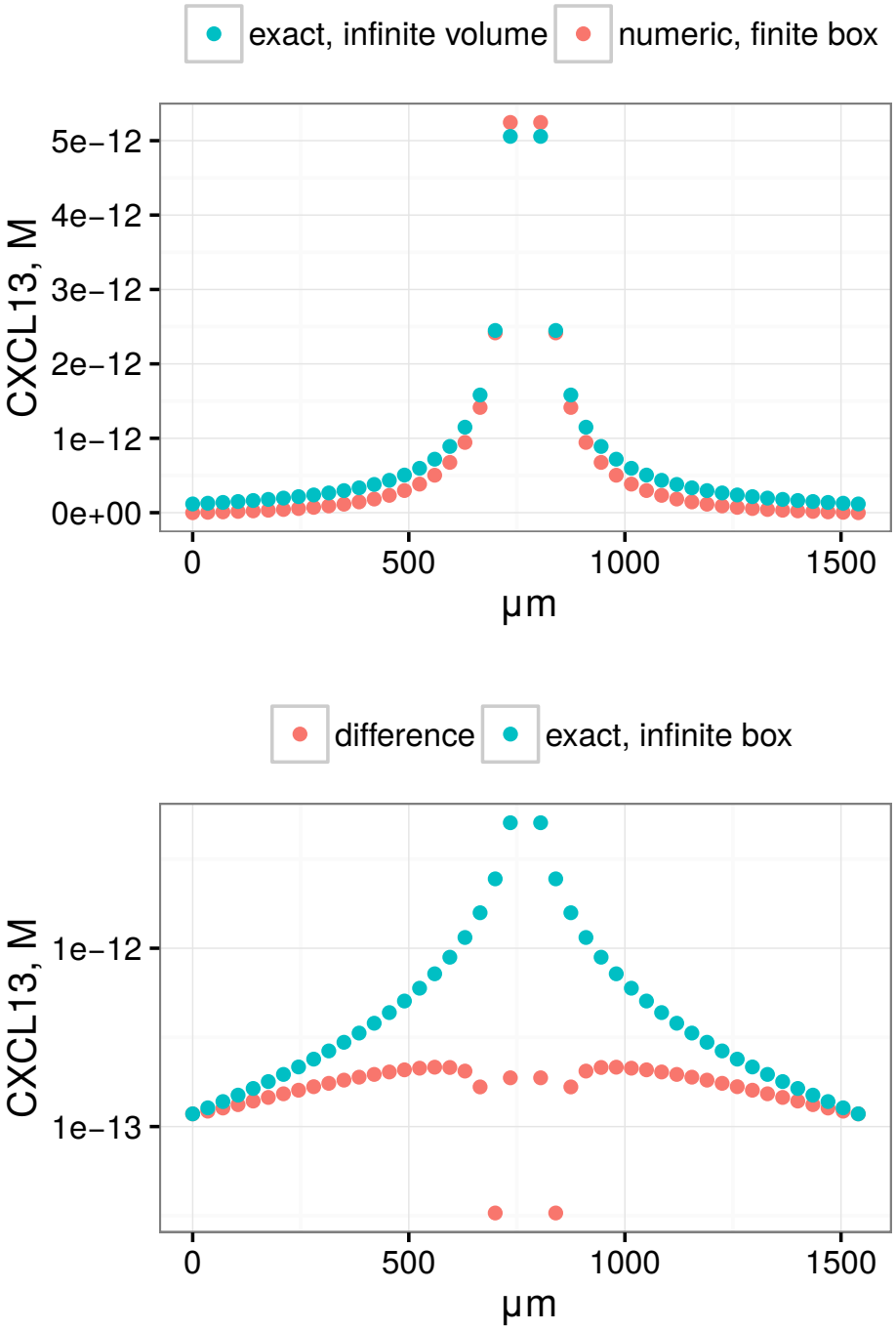

Figure 3.14: Comparison of the exact solution for CXCL13 distribution depending on the distance from the secreting cell in infinite space with the numerical solution for a finite simulation box with zero boundary condition (top); the difference of the exact and the numerical solutions in comparison to the numerical solution (bottom).

The accuracy of the numeric solution can be estimated by direct comparison of solutions made with different step size. For a fixed simulation box size (1540μm), I performed a simulation with 50 secreting cells ($Q = 10^4$ molecules/min) which were positioned as a cluster with such density that the average distance between neighbouring cells was equal to the cell size. I used a lattice with 45 or 89 grid points (equivalent to 44 and 88 grid cells, with 35μm or 17.5μm cell size respectively). For the chemokine concentration, the relative error is of 1% order (fig. 3.15, the left panel). Since cells measure not the absolute concentration when they navigate in the model but the concentration gradient, I was interested to see how the step size influences estimation of the gradient, namely, the difference of the bound receptor $\triangle R_{\mathrm{b}}$ (eq. 3.38), as this is the value used for cell orientation in the simulations. For the estimations of the error in $\triangle R_{\mathrm{b}}$, the same total receptor number $R_{\mathrm{tot}} = 10^5$ as in our agent-based simulations is used.

The step size indeed influences the estimation of $\triangle R_{\mathrm{b}}$, and the error in $\triangle R_{\mathrm{b}}$ reaches the value of 8 in the vicinity of the cluster centre, see fig. 3.15, the right panel. Outside the cluster, the difference is much lower than the threshold of sensitivity $\triangle R_b = 10$, hence the migration of cells which are not trapped into the cluster does not depend on the lattice cell size. This effect is observed because a rectangular grid is used for estimation of the chemokine distribution and its gradient, however, stromal cells are positioned not exactly at the lattice points but at an arbitrary space location. Since secretion is assumed to happen at the closest grid point, a change in grid step size may result into a shift of the approximated location of the chemokine source. Usage of finite element methods with an adaptive grid or a construction of more dense grid in our approach could increase the accuracy, however, at the price of losing of computational speed.

System size effect can be investigated in a similar way as it was done with the lattice cell size. I performed a simulation for the same cluster of 50 secreting stromal cells using simulation boxes with 44 or 88 (a box of double size) lattice cells with 35μm step. The difference in concentration was less than $10^{-13}\mathrm{M}^{-1}$ within a radius of 500μm around the cluster, i.e. the region where its level is detectable for cells, see fig. 3.16, left side. The receptor difference was less than 1 along the whole simulation box space (fig. 3.16, right side) and we may conclude that for clusters near the centre of simulation box the box size does not influence the orientation of the cells.

Conclusion

- The approximation of the chemokine distribution around a secreting cell with the analytical solution for an infinite space and the numerical solution for a finite size simulation box are comparable at the distances of characteristic cluster sizes.
- The step size used in the simulations achieves 1% accuracy for chemokine concentration. The calculation of gradients estimation is influenced by the lattice step size, but outside the cluster it

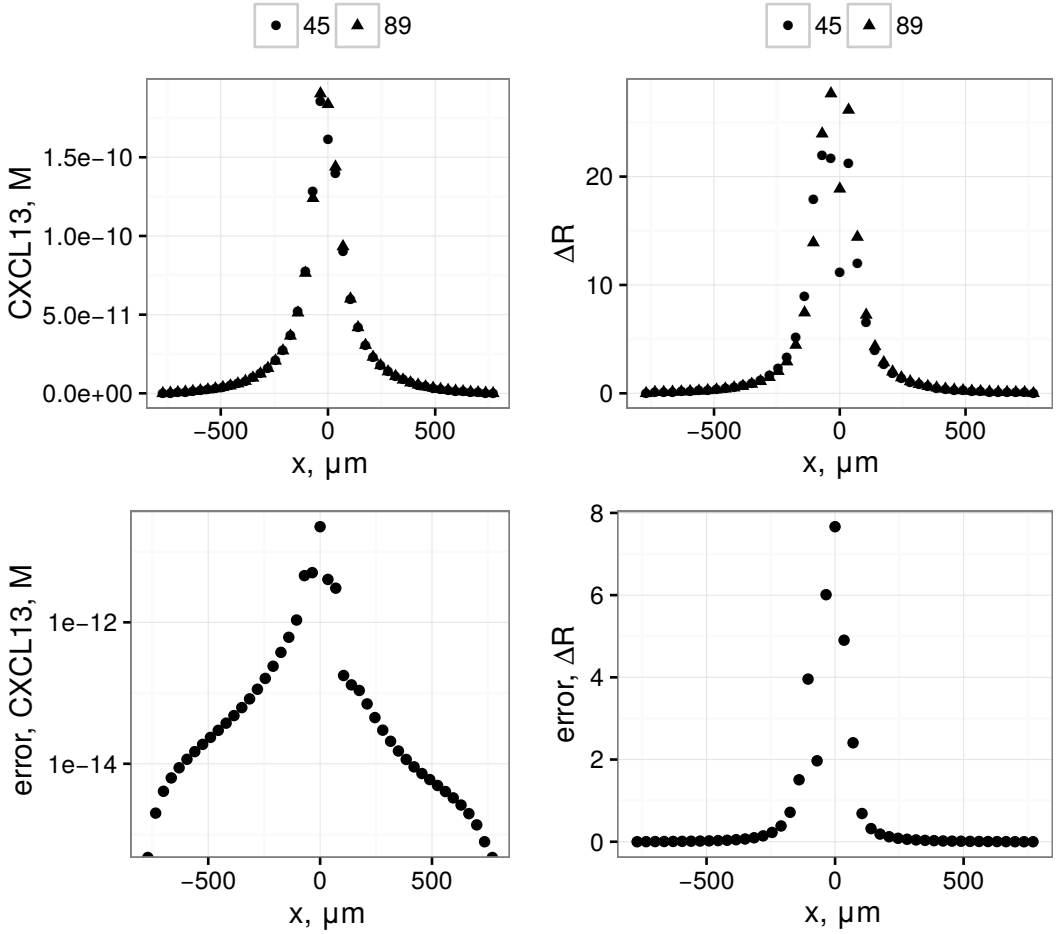

Figure 3.15: Grid cell size effects. CXCL13 concentration and $\triangle R_{\mathrm{b}}$ were compared for $45 \times 45 \times 45$ and $89 \times 89 \times 89$ grids.

is less than the sensitivity threshold of 10 receptors (for cluster of 50 stromal cells). Hence, the description of lymphocyte trapping is not strongly influenced by the step size

- The difference of receptor at opposite cell sides is not influenced (< 0.1) by the simulation box size in the whole simulation box space.

Chemokine field for a single secreting cell

It is interesting to investigate how the chemokine is distributed around a single secreting cell. I varied the secretion rate Q and the degradation rate κ and found out that the degradation of chemokine does not influence the CXCL13 profile much while being in the range of $10^{-5} - 10^{-3}\mathrm{s}^{-1}$, fig. 3.17. The receptor difference at the opposite cell sides $\triangle R_{\mathrm{b}}$ depends on the total surface receptor number R_{total} and on the secretion rate Q of CXCL13, and for $R_{\mathrm{total}} = 10^5$ it achieves the threshold value $\triangle R_{\mathrm{b}} > 10$ only in the vicinity of the cell and if the secretion rate $Q > 10^4$ molecules/min, fig. 3.17, right-up.

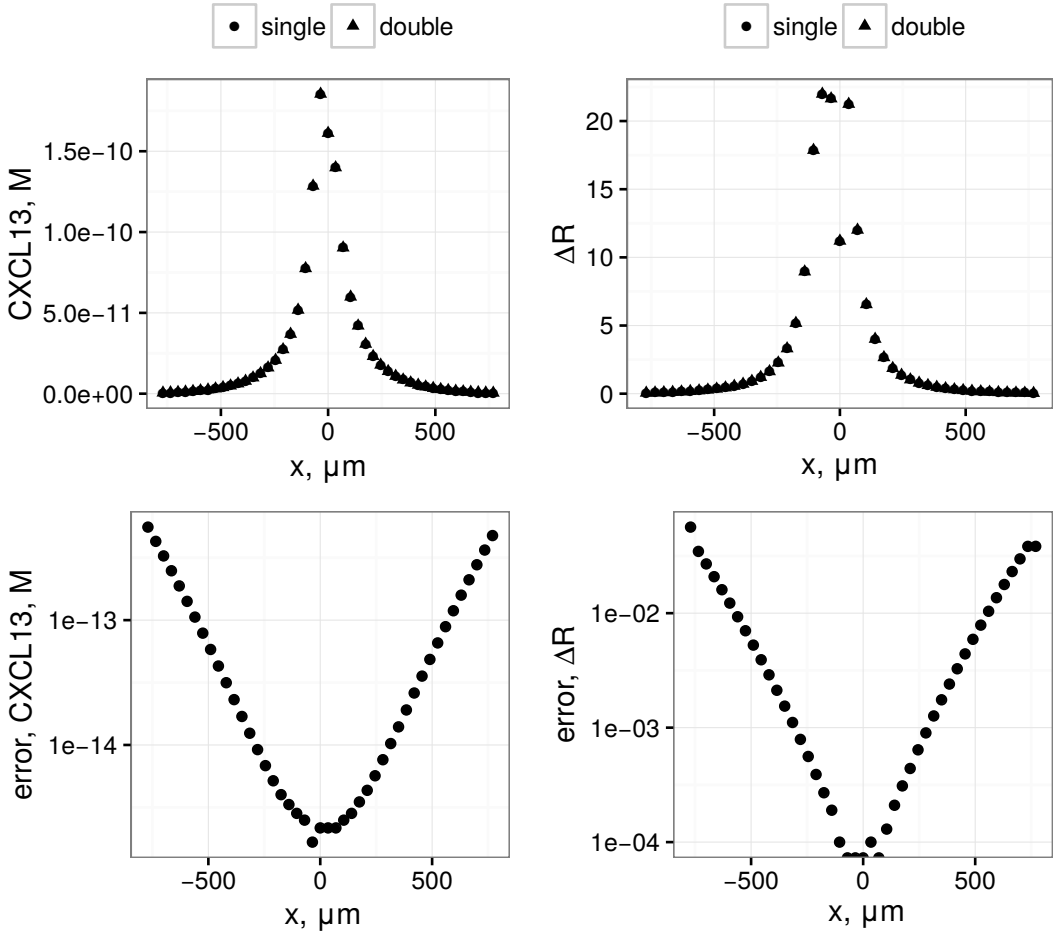

Figure 3.16: System size effects. CXCL13 concentration and $\triangle R_{\mathrm{b}}$ for a single and double size of the simulation box.

I calculated $\triangle R$ for a range of secretion rate Q and total receptor numbers R_{total} and estimated the maximal trapping distances by a single secreting cell, fig. 3.18. This result suggests that the cluster stability can be disturbed via the decrease of available receptors number or of the chemokine concentration. Measurement of q and R_{total} for human cells will help to estimate treatment concentrations for chemokine or receptor blocking molecules.

Next, I tested at which value of the degradation rate the chemokine concentration can be pronouncedly disturbed in the vicinity of the single secreting cell, fig. 3.19. The calculation suggests that the degradation of the chemokine may contribute to change of its concentration at distances longer than 50μm and at the upper limit of the value range of κ, i.e. when the chemokine lifetime is of order of minutes. In this case, one needs to increase the proteolytic degradation rate by 1-3 orders of magnitude in order to noticeably change chemokine concentration in the vicinity of a single secreting cell.

Conclusion

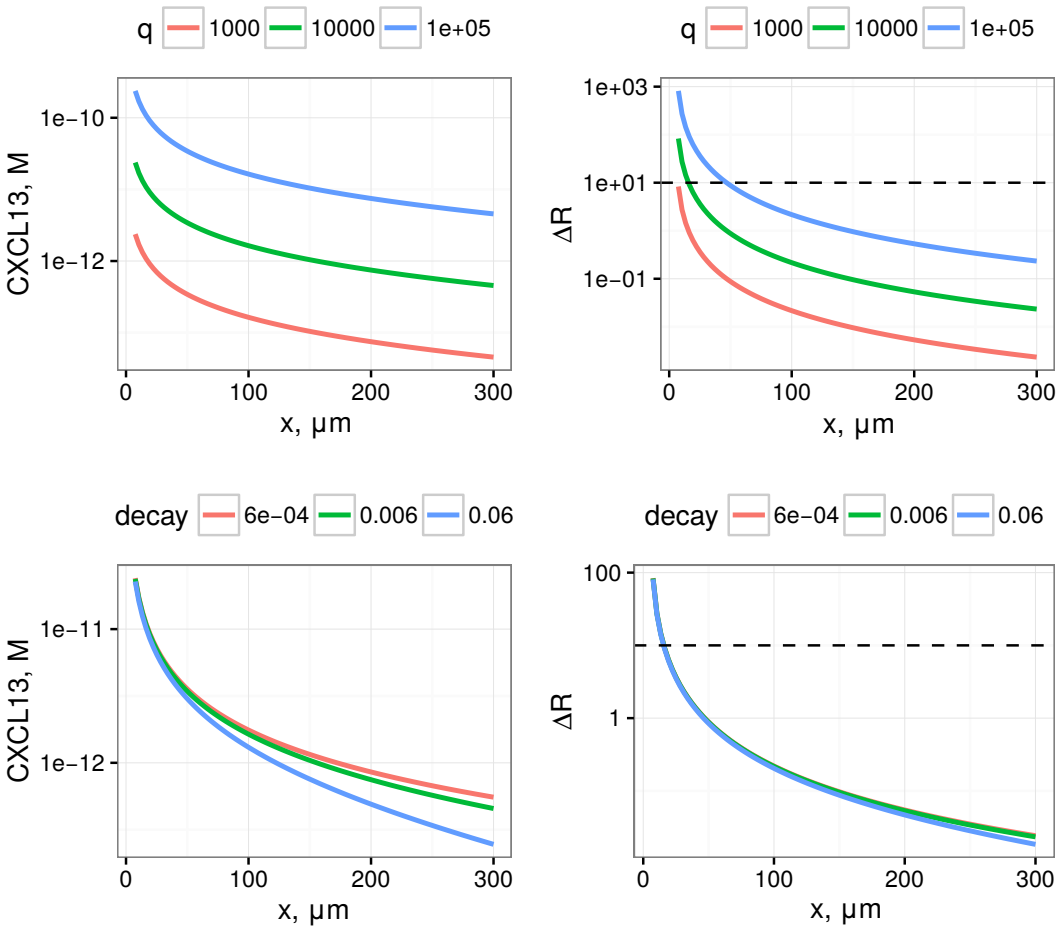

Figure 3.17: The concentration of CXCL13 and the estimated receptor difference at opposite cell sides for $R_{\text{tot}} = 10^5$ for a single stromal cell secreting the chemokine in infinite space.

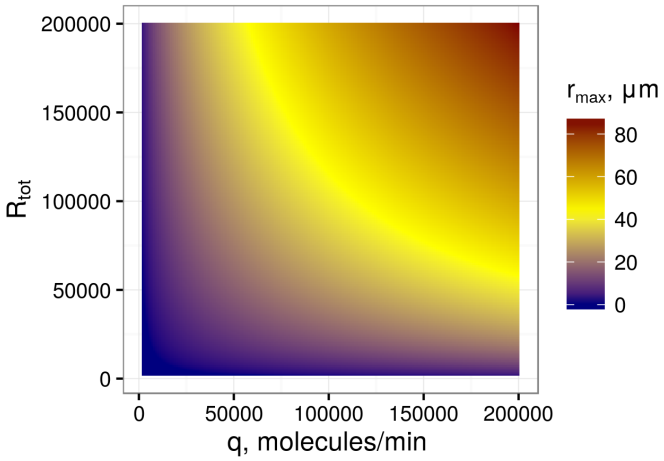

Figure 3.18: Maximal trapping distance by a single secreting cell depending on the secretion rate q and total receptor number R_{total} at the lymphocyte surface.

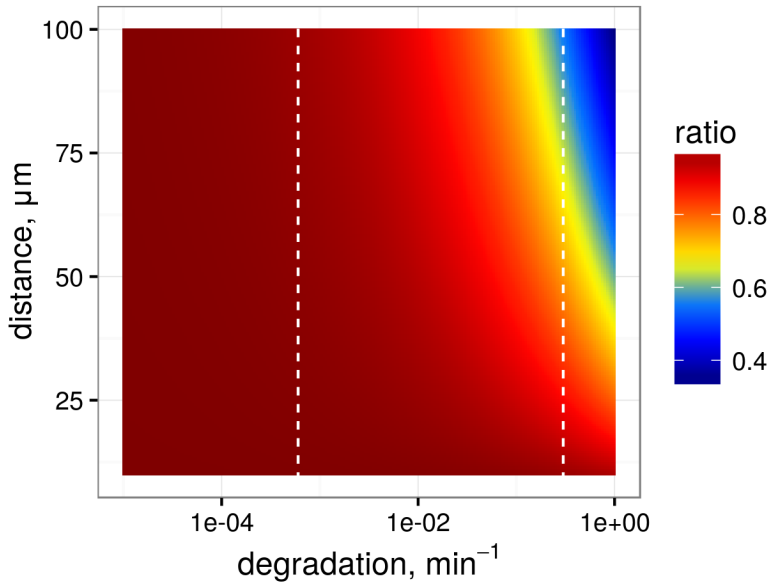

Figure 3.19: Decrease of chemokine concentration depending on the chemokine degradation rate κ. White lines stand for the assumed literature range for κ.

- A single secreting cell is able to generate chemokine gradients which can be sensed by lymphocytes only in a certain range of secretion rates and surface receptor differences.
- Both, chemokine molecules and receptors, are good targets for treatment strategies aiming to destabilize clustering of immune cells.
- The degradation rate does not influence the chemokine profile at the distances of 50μm and one needs to increase amounts of proteolytic enzymes by 1-3 orders of magnitude in order to observe substantial chemokine concentration changes in the vicinity of a single cell.

Contribution of chemokine consumption

Receptor dynamics at the cell surface may influence the chemokine distribution, because bound receptors are subject to internalization with further chemokine degradation inside the cell. It is interesting to estimate how the chemokine field will be disturbed by this phenomenon. First, consider a point source of CXCL13 surrounded by B cells with the density n_{B}. I will use n_{B} which corresponds to rectangular packing of lymphocytes with the distance of 10μm between centres. Using the same boundary conditions as in the previous section, the chemokine distribution $c(\mathbf{x},t)$ can be described

$$\frac{\partial c(\mathbf{x},t)}{\partial t} = D \triangle c(\mathbf{x},t) - \kappa c(\mathbf{x},t) - k_{\mathrm{on}} r(\mathbf{x},t) c(\mathbf{x},t) + k_{\mathrm{off}} r_{\mathrm{b}}(\mathbf{x},t), \tag{3.59}$$

where $r(x,t)$ and $r_{\mathrm{b}}(x,t)$ are distributions of free and bound receptors in the space.

We would like to estimate how much chemokine consumption might influence the chemokine profile. For this, I approximate the chemokine and receptor distributions $c(\mathbf{x}, t)$ and $r(\mathbf{x}, t)$, which depend on discrete lymphocyte positioning, by averaging receptor densities in space according to the lymphocyte density n_{B}. It allows to treat this problem analytically, which helps to simplify the analysis.

In a steady state, for a single cell and chemokine concentration c at its location

$$\dot{R} = -k_{\mathrm{on}} R c + k_{\mathrm{off}} R_{\mathrm{b}} + k_{\mathrm{r}} R_{\mathrm{i}} = 0 \tag{3.60}$$

$$\dot{R_{\mathrm{b}}} = k_{\mathrm{on}} R c - k_{\mathrm{off}} R_{\mathrm{b}} - k_{\mathrm{i}} R_{\mathrm{b}} = 0 \tag{3.61}$$

$$\dot{R_{\mathrm{i}}} = k_{\mathrm{i}} R_{\mathrm{b}} - k_{\mathrm{r}} R_{\mathrm{i}} = 0 \tag{3.62}$$

The total receptor number is $R_{\mathrm{tot}} = R + R_{\mathrm{b}} + R_{\mathrm{i}}$, hence the number of bound receptors for a single cell can be represented as a function of the chemokine concentration:

$$R_{\mathrm{b}} = \frac{R_{\mathrm{tot}} c}{\frac{k_{\mathrm{i}} + k_{\mathrm{off}}}{k_{\mathrm{on}}} + c\left(1 + \frac{k_{\mathrm{i}}}{k_{\mathrm{r}}}\right)} \tag{3.63}$$

Using the values for the kinetic rates one gets

$$R_{\mathrm{b}} = \frac{R_{\mathrm{tot}} c}{10^{-7}\mathrm{M} + 69c} \tag{3.64}$$

This equation can be approximated with the linear relation

$$R_{\mathrm{b}} = \frac{k_{\mathrm{on}} R_{\mathrm{tot}} c}{k_{\mathrm{off}} + k_{\mathrm{i}}} = 10^{7}\mathrm{M}^{-1} \cdot R_{\mathrm{tot}} c \tag{3.65}$$

for chemokine concentrations $c < 10^{-9} M$, which is true for the case of a single secreting cell, for example.

We can substitute terms for binding and unbinding kinetics in the diffusion equation using eq. 3.61 $k_{\mathrm{on}} R c - k_{\mathrm{off}} R_{\mathrm{b}} = k_{\mathrm{i}} R_{\mathrm{b}}$ and by combining receptor numbers for a single cell and cell density n_{B}:

$$D \triangle c - \kappa c - k_{\mathrm{i}} \frac{k_{\mathrm{on}} R_{\mathrm{tot}} n_{\mathrm{B}} c}{k_{\mathrm{off}} + k_{\mathrm{i}}} = 0 \tag{3.66}$$

The last two terms of the eq. 3.66 can be grouped as $(\kappa + k_{\mathrm{i}} \frac{k_{\mathrm{on}} R_{\mathrm{tot}} n_{\mathrm{B}}}{k_{\mathrm{off}} + k_{\mathrm{i}}}) c = \kappa^* c$, which leads to the same form of equation as eq.3.55, only with the modified degradation rate κ^*. The solution reads

$$c(r) = \frac{q \exp\left(-\sqrt{\frac{\kappa^*}{D}} r\right)}{4\pi D r \left(\sqrt{\frac{\kappa^*}{D}} \rho + 1\right) \exp\left(-\sqrt{\frac{\kappa^*}{D}} \rho\right)}. \tag{3.67}$$

In fig. 3.20, one can see that for high receptor numbers ($10^5 - 10^6$), receptor internalisation indeed may decrease the amount of chemokine. However, there are two competing phenomena here: on the one hand, high receptor numbers at the cell surface will result in higher chemokine consumption and

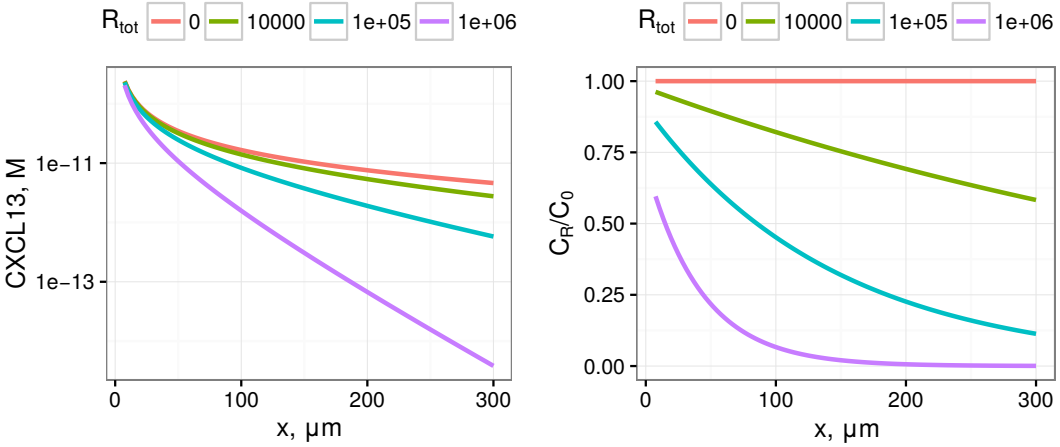

Figure 3.20: CXCL13 distribution in the case of a single secreting cell surrounded by a space filled with densely packed lymphocytes in absolute concentration values (left) and as a fraction with respect to the case of no consumption (right). The estimations are made for the secretion rate $q = 10^5$ min^{-1} and varying total receptor number R_{tot}.

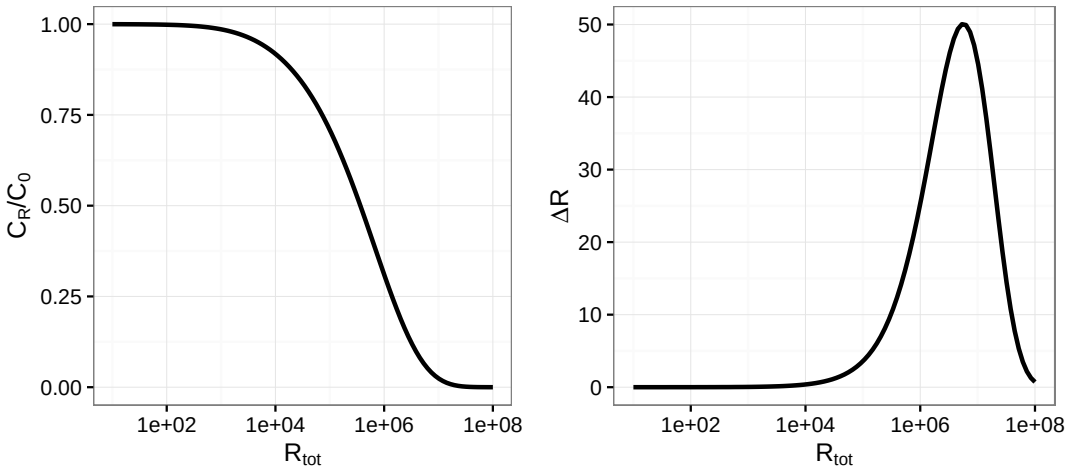

Figure 3.21: Left: Concentration decay due to receptor internalisation depending on the total receptor number R_{tot}. Right: Bound receptor difference at the opposite cell sides as a function of the total receptor number R_{tot}. The estimations are made for the secretion rate $q = 10^5$min^{-1} and for the distance from the secreting cell $r = 50\mu$m.

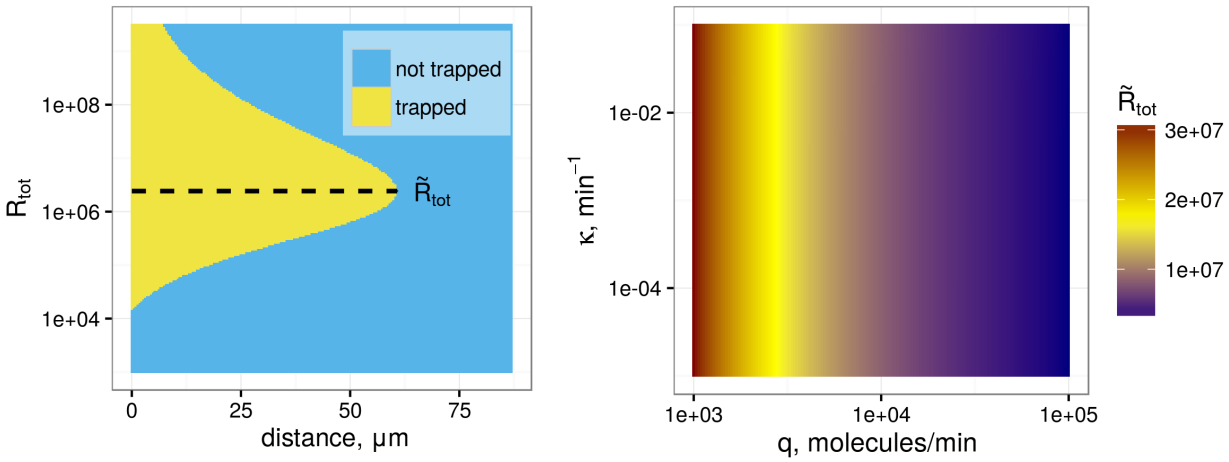

Figure 3.22: Left: Regions in the space where the bound receptor difference is higher than the threshold $\triangle R_b > 10$ (i.e. cell will be trapped by chemokine gradient) depending on the total number of surface receptors. The secretion rate is $q = 10^5 \text{min}^{-1}$. Right: The optimal value of the total receptor number $\tilde{R}_{tot}$ computed for different degradation κ and secretion q rates.

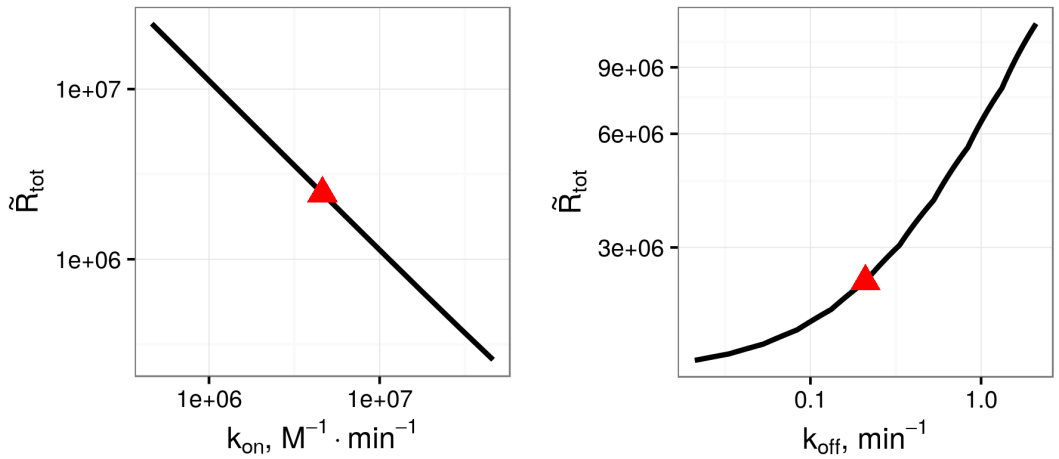

Figure 3.23: Left: $\tilde{R}_{tot}$ as a function of k_{on}. Right: $\tilde{R}_{tot}$ as a function of k_{off}. Red triangles correspond to estimations for k_{on} and k_{off} used in the model.

might destabilize clustering. On the other hand, higher receptor numbers allow better sensitivity, since the critical threshold $\triangle R_{\mathrm{b}} > 10$ can be achieved easier. In steady state $\triangle R_{\mathrm{b}}$ is estimated using eq. 3.65

$$\triangle R_{\mathrm{b}} = \frac{k_{\mathrm{on}} R_{\mathrm{tot}} \triangle c}{2(k_{\mathrm{off}} + k_{\mathrm{i}})}, \tag{3.68}$$

where $\triangle c$ is the difference in CXCL13 concentration at opposite cell sides. It appears that for given kinetic parameters there is a peak for bound receptor differences at around 10^6 receptors/cell (however, it should be less for higher affinity receptors) and at higher receptor numbers, chemokine consumption does not allow chemosensing, fig. 3.21.

For this model, one may define regions in the parameter space where a cell can be or can not be trapped by the gradient. The phase diagram for the receptor number and the distance from the chemokine secreting source shows the maximum trapping distance for different receptor numbers, fig. 3.22, left. There exists an optimal receptor number $\tilde{R}_{\mathrm{tot}}$ in terms of maximal trapping distance, i.e. maximal cluster radius. This value depends on the strength q of the chemokine source, but the degradation rate κ does not influence much $\tilde{R}_{\mathrm{tot}}$, fig. 3.22, right. However, in the case of a single secreting cell, $\tilde{R}_{\mathrm{tot}}$ is of very high values ($10^6 - 10^7$ receptors), which are out of the assumed range for R_{tot} for lymphocytes ($10^4 - 10^5$ receptors). A lower $\tilde{R}_{\mathrm{tot}}$ might be observed for more affine receptor-chemokine pairs, i.e. for higher k_{on} or lower k_{off} values, fig. 3.23. I solved the boundary problem numerically using the R package `bvpSolve` [136], because the linear approximation from eq. 3.65 may deviate from the exact solution for higher affinities.

Conclusion:

- In the model of a point chemokine source in the space of densely packed lymphocytes, receptor internalisation may influence chemokine concentration only at high receptor numbers.
- With increasing receptor numbers, the sensitivity of a cell is higher but this can be abrogated due to increased internalisation.

3.3.4 Gradient inversion due to receptor internalization

Chemokine concentration can be disturbed by receptor dynamics as we discussed in the previous section. This process may lead not only to a decrease in chemokine amount but in change of the gradient as well. To model such a situation I constructed a system consisting of 50 stromal cells and 3000 B cells clusters positioned at a distance of 200 μm between the centres, see fig. 3.24. B cells positions are fixed, i.e. they do not migrate.

A simulation was performed for 100 min and the chemokine concentration and the gradient at different space points were calculated. In the case of a receptor number of $R_{\mathrm{tot}} = 10^5$, there was no gradient inversion observed, see fig. 3.25 (top panel). However, at higher receptor numbers of $R_{\mathrm{tot}} =$

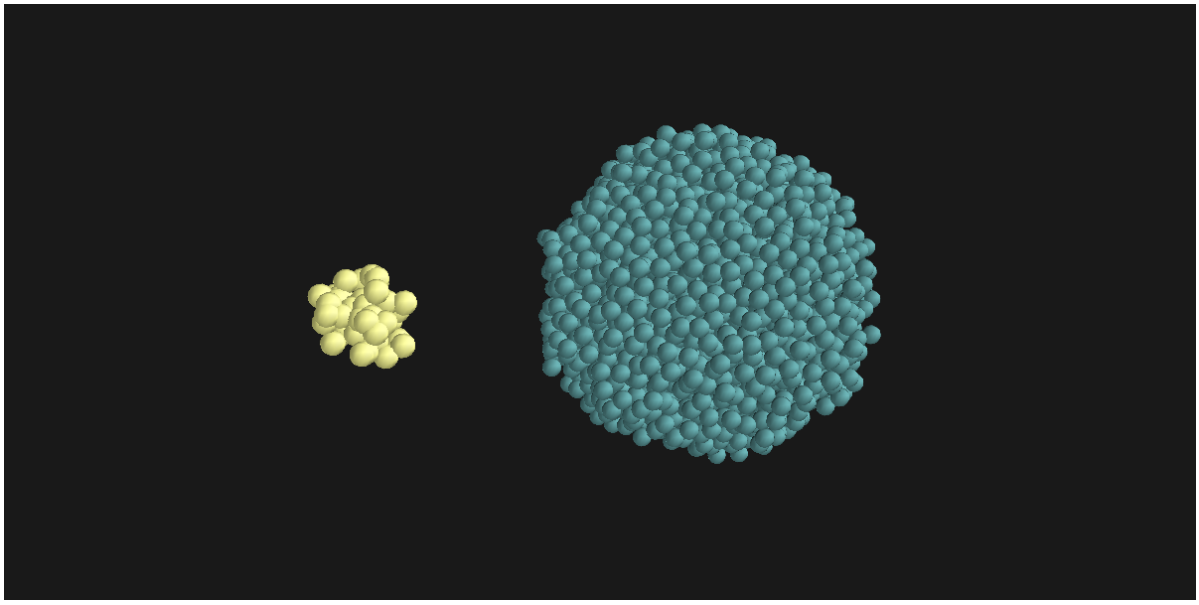

Figure 3.24: A model system of 50 stromal and 3000 B cells positioned in clusters with the distance of 200 μm between their centres.

10^6, the chemokine field was disturbed and the gradient was inverted in the area of the lymphocyte cluster, i.e. a cell being positioned at the farther side of the B cell cluster would migrate to the direction opposite to the stromal cell cluster, fig. 3.25 (bottom panel).

Given that a very high receptor density (10^6 per cell) was needed for gradient inversion in the simulation set-up, even for a rather big B cell clusters (3000 cells), gradient inversion seems to be not achievable *in vivo* for CXCL13. However, the affinity of CXCL13 is one order less than, for example, the affinity of CXCL12. Thus, a disturbance of the gradient profile due to chemokine consumption could be observed for other types of chemokines. Our framework allows to investigate such possibilities if there are available data on receptor dynamics and chemokine diffusion.

Conclusion

- High receptor number might results in chemokine gradient inversion, however it demands high receptor densities in the case of CXCL13.

3.3.5 Simulation of lymphocyte clustering

Having implemented the collision detection algorithm, the description of chemokine diffusion and the receptor dynamics, one can model events of stromal cell activation and lymphocyte clustering. For this, I constructed a model consisting of stromal cells positioned randomly with the same density as in the case of simulation of the contact frequency in section 3.3.2. The stromal cells were located around a

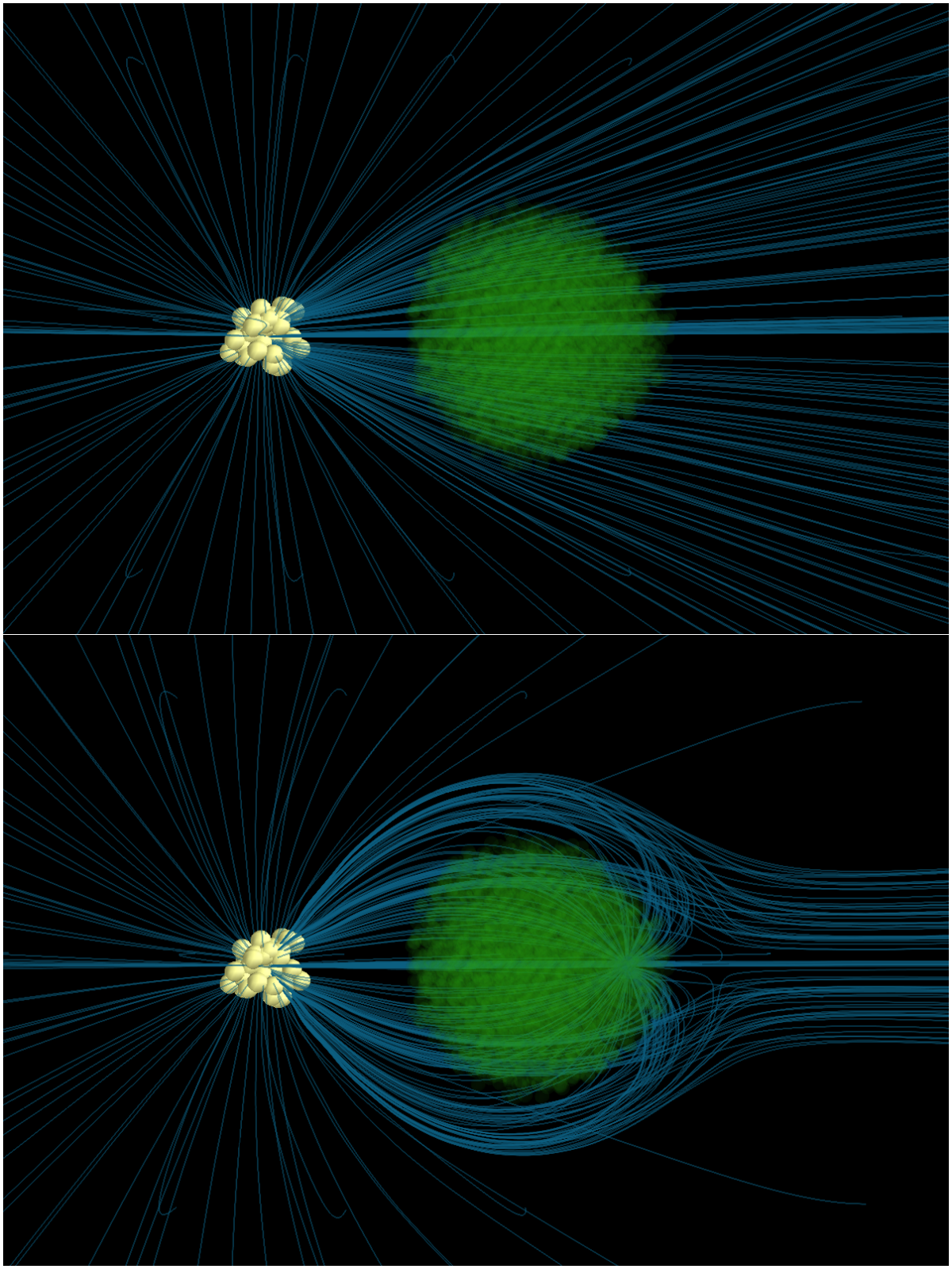

Figure 3.25: Gradient representation for the system from fig. 3.24 for a case of 10^5 (top panel) and 10^6 receptors/lymphocyte (bottom panel). The lines are directed along with the chemokine gradient. The density of lines is not connected with the gradient intensity, but is chosen for a better view of the gradient direction in the inter-cluster area. For rendering of cell distribution and chemokine gradient the Python interface to Mayavi software was used [175].

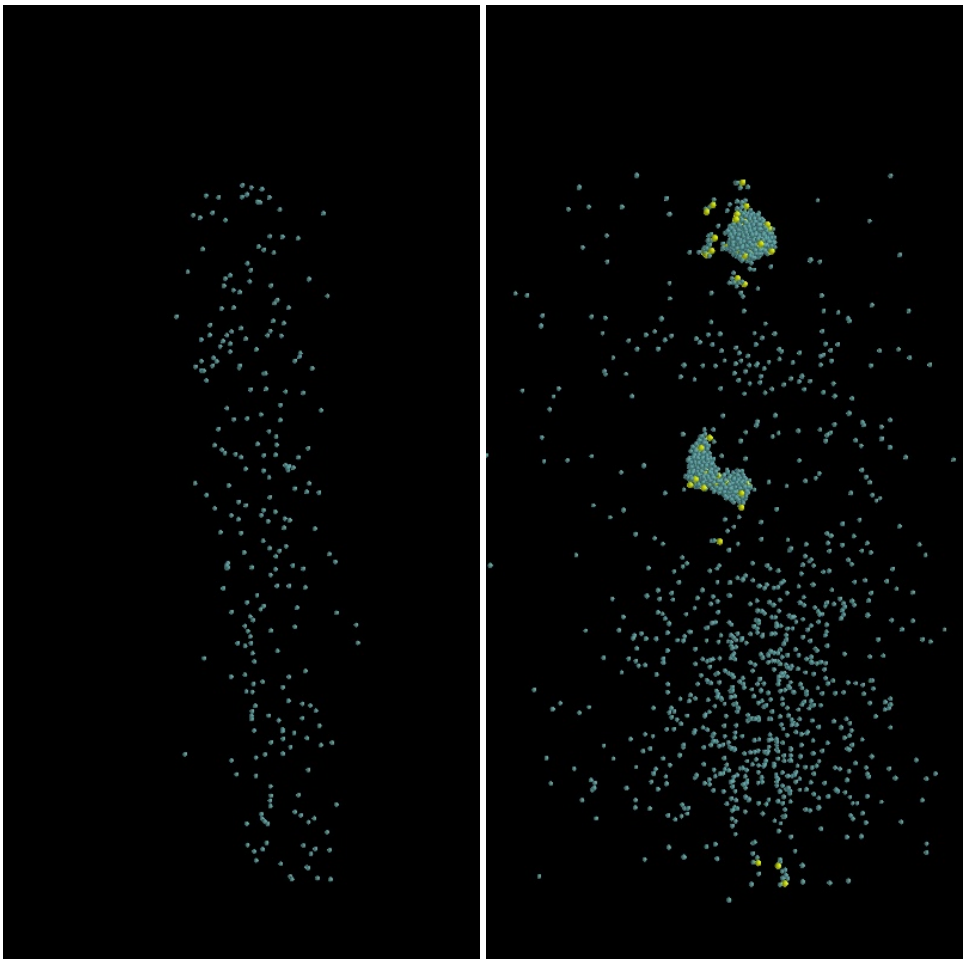

Figure 3.26: Simulation of lymphocytes (blue) influx from the blood vessel into the tissue. Having achieved the threshold signal value ($\theta = 30$), stromal cells get activated (yellow) and start to secrete CXCL13. Non-activated stromal cells are not shown due to their high density. In the beginning of the simulation there are no activated cells (left, 500 min). Gradual increase in lymphocyte density results in development of clusters (right, 5000 min).

"blood vessel" with a diameter of 10 lymphocyte diameters ($d_{\text{vessel}} = 120\mu$m). The perivascular area was limited to the radius of 400μm in the cubic simulation box of 1540μm x 1540μm x 1540μm size. B cells appear in the simulation box via the blood vessel and randomly migrate in the tissue. Upon a contact with a stromal cell, the B cell is stopped for 1 min and continues its migration after then. The stromal cells integrate the abstract signal from contacts with lymphocytes. The signal decays with the rate $d_{\text{S}} = 1/(20\text{min})$. I assumed the frequency of B cell entrance to be 0.5 cells/min which allows to achieve signal values of 10-20 during the simulation. For the activation threshold I used $\theta = 30$.

In these conditions, stromal cells get activated when the concentration of lymphocytes will increase sufficiently or because of random fluctuations in lymphocyte distribution. The result of these simulations is represented in fig. 3.26 after the first 500 minutes after simulation start (left) where no clusters

or activated cells are observed (non-activated cells are not shown for better view). However, due to higher contact frequency in the perivascular area, after 5000 minutes several clusters of activated stromal cells (yellow) and lymphocytes (blue) were observed adjacent to the blood vessel, see fig. 3.26 (right).

Although I can now reproduce cell clustering in the context of stroma activation due to the lymphocyte influx from the blood vessel, these simulations are based on qualitative assumptions about cell signalling. Additional information about how many contacts are needed to upregulate CXCL13 secretion or how much time the memory about interaction lasts would give the opportunity for more realistic simulations.

Agent-based modelling has an advantage in comparison to ordinary differential equations which are also used for description of cell populations, because in such frameworks the spatial aspect is also considered. To illustrate it, I performed a simulation for the same set-up but with a lower threshold value $\theta = 10$ and having 6000 B cells randomly scattered in the simulation box. As it can be expected, in the beginning of the simulation stromal cells will get activated ubiquitously (fig. 3.27, up-left), however because not all the cells get activated simultaneously and there are fluctuations in the density due to random positioning, there are locations with higher concentrations which will attract lymphocytes from the neighbouring activated stroma regions. This will result in development of bigger clusters (fig. 3.27, up-right) which trap lymphocytes from smaller ones. Consequently, the lack of contacts in these neighbouring stroma areas will decrease the number of activated stromal cells or will result in their dissolution, as can be seen from the overshoot at the bottom plot, fig. 3.27. This kind of effect can be observed only due to description of spatial localisation of participating cells and can not be reproduced by an ordinary differential equation model. Although it is modelled in an artificial set-up, these results raise the question whether it is possible to observe fusion of clusters or cell trapping from neighbouring activated regions *in vivo*.

Lymphocyte density directly influences the probability of stromal cells to get activated because higher B cell densities allow more frequent contacts with the stromal cells. I performed simulations for a range of lymphocyte density and activation threshold when stroma activation is observed or not observed throughout the simulated period. In the beginning of the simulation B cells were positioned randomly in the simulation box and their number was constant due to periodic boundary condition at all three axes. If any stromal cell is being activated, the simulation is stopped. Otherwise, the simulation is stopped after 10000 minutes. In agreement with section 3.3.1, the expected activation time was dramatically increasing with the decrease of B cell density and at low B cell numbers the were only few activation events observed, fig. 3.28. More detailed knowledge of activation mechanisms might help to estimate probabilities of stroma activation in order to optimise anti-CD20 immunosuppressing therapy.

Not only lymphocyte density could influence stroma activation, but their motility as well. For the same system, I computed activation times for various B cell speed values. The activation time appeared

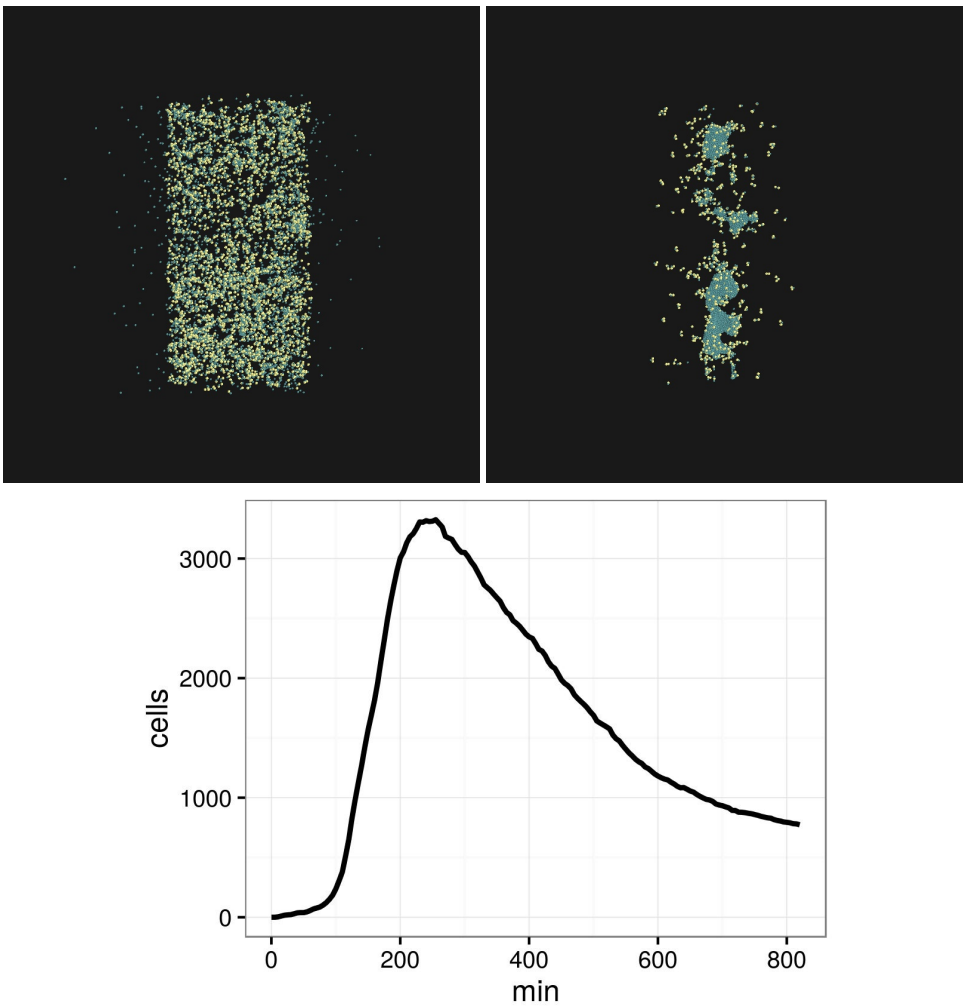

Figure 3.27: An illustration of cluster fusion under the condition of a low activation threshold value ($\theta = 10$). 6000 lymphocytes were randomly positioned in the simulation box before the start of the simulation. In the beginning, stromal cells get activated ubiquitously (top left panel), however, bigger clusters trap lymphocytes from the neighbouring activated stromal cells with the result of small cluster dissolution or their fusion with the bigger ones (top right panel). The number of activated stromal cells during the simulation (bottom panel).

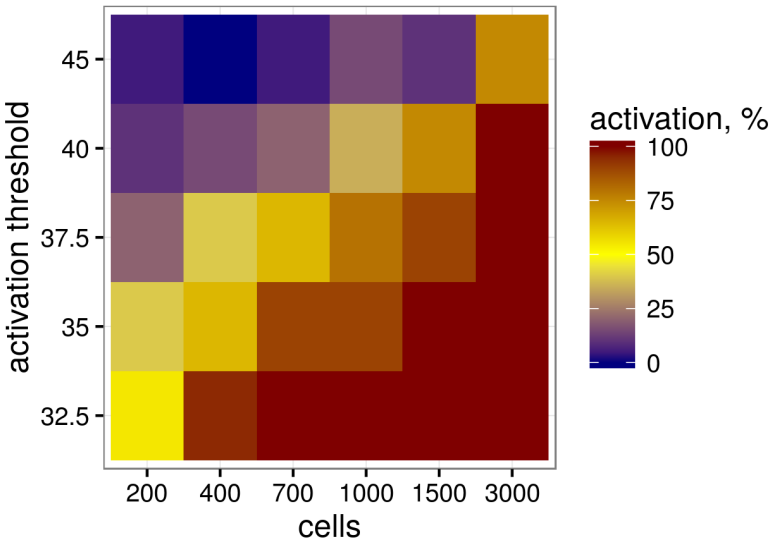

Figure 3.28: Heatmap of frequency of stroma activation for varying activation threshold value and lymphocyte density. For every parameter set, 20 simulations were performed for the time period of 10000 minutes and $d_S = .01\text{min}^{-1}$.

to depend non-monotonically on the speed: the time was shorter for slow and high speeds, fig. 3.29, left. In average, lymphocyte-stroma contacts are more frequent for a higher lymphocyte speed, which results in shorter activation time. If the speed is low, there are less contacts in the system in total. However, if the persistence time remains the same for all simulations, in the case of low speed, it takes more time for lymphocytes to leave a neighbourhood of a contacted stromal cell, which may increase a probability of repetitive contacts, and, hence, stroma activation. It is interesting, that the activation time is different for the case of rectangular packing of stromal cells, fig. 3.29, right. This results need additional investigation in order to understand in details how the activation time depends on the system architecture and whether it is a result of any model artefacts. I do not perform such an analysis here, but plan it for the future work.

Conclusion

- The framework is able to reproduce cluster development in the area of a blood vessel.
- Data about stroma activation are needed in order to fit the model of signal integration.
- The modelling framework allows to grasp spatial effects in a system of chemosensing cells and shows the possibility of cell cluster fusion into bigger clusters.
- B cell density is an important factor for control of stroma activation and investigation of activation mechanisms might have efficient clinical implications.
- Cell motility may contribute to control of the activation time of stromal cells.

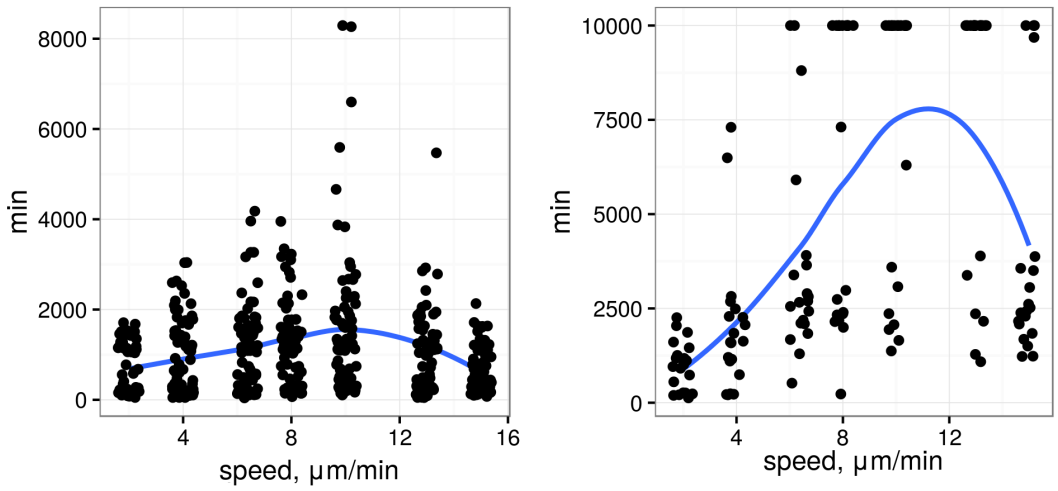

Figure 3.29: Activation time of stroma as a function of B cell speed for random uniform (left) and rectangular stromal cell positioning (right). For every speed value, 70 (random positioning) or 20 (rectangular positioning) simulations were performed up to maximal time of 10000 minutes. Small random disposition is added to the points in order to avoid overplotting for better representation.

3.4 Discussion

In this chapter I present the framework for modelling cell interaction and migration in the context of early TLO development. Unfortunately, the exact mechanism which is responsible for stromal cell differentiation is not known and I substituted it by a phenomenological model of signal integration in the section 3.3.1. Such a straightforward approach illustrates that in a certain range of contact frequency and time of contact memory, the first passage time can dramatically depend on slight changes in the contact frequency. If there will be experimental data on stromal cell activation by contacts with lymphocytes, it will allow to predict probabilities of the development of a pro-TLO environment during a given time period. Up to now, the main treatment during chronic humoral rejection is the therapy directed against B lymphocytes (anti-CD20 antibodies, or Rituximab). Depletion of B cell counts in the organism may prevent B cell-mediated responses as well as delivery of the activation signal to the stroma via contacts with B cells. However it has side-effects. Mathematical modelling may help to optimize the dosage of such treatments and reduce non-favourable side effects or adjust therapy in a way that lymphocyte concentration is below the critical density.

Due to its simplifications, the approach used in section 3.3.1 lacks a spatial component, which can be important in the context of cell migration, as we discuss in the section 3.3.2. In the system of lymphocytes entering the tissue via a blood vessel, one may see that stromal cells located closer to the vessel receive contacts with a higher frequency. In order to perform such kind of simulations, one needs to efficiently handle cell movement and collision. For this purpose, I developed the 3D agent-based

framework which uses a sweep-and-prune algorithm for collision detection and phenomenological implementation of physics only with the purpose of avoiding cell-cell penetration. Such kind of problems are rather frequent in biology currently and the code may be used in other projects where spatial data are available from microscopy or biopsies.

Not only the physical contact plays a role in cell interactions during TLO development but chemokine-mediated interactions as well. I showed that a single cell can generate gradients which can trap lymphocytes at a distance of 50μm only if the receptor density and the secretion rate are rather high (10^5 and 10^5 molecules/min, respectively). This kind of results may be transferred to the level of clusters of activated stromal cells, which allows to estimate a maximally possible trapping distance, and, hence, a B cell cluster size. Such computations can be validated when compared with biopsy data about cell distribution.

There are different factors which influence the chemokine concentration. Some of them do not change it dramatically, for example, the degradation via proteolysis does not substantially decrease the concentration of CXCL13 in the vicinity of a secreting cell. However, the consumption of chemokines due to receptor internalisation may result not only in a decrease of concentration, but also in gradient inversion. This can happen especially for receptor-chemokine pairs with a higher affinity than CXCL13-CXCR5 (e.g. CXCL12-CXCR4).

One can influence cell migration by control of the number of available receptors or chemokine molecules. The estimation of the trapping ability by stromal cell clusters described above can help in the development of anti-chemokine or anti-receptor therapy. Another approach which was also suggested in clinics is based on the opposite idea: instead of decreasing the chemokine concentration, one may use a receptor antagonist, which might decrease the number of receptors available for signalling and, hence, would make cells blind to chemokine gradients. All described approaches can be modelled within our framework, and having measured kinetics data of receptor dynamics and chemokine diffusion in the context of, for example, graft tissue, one may estimate how much of a treatment agent is needed to destabilize cluster formation.

The lack of data about how many contacts are needed in order to activate stromal cells and how frequent they should be does not allow to predict the probability of cluster formation if one has certain assumptions about the B cell influx. Ideally, such an experiment should be performed by direct observation of stroma differentiation when different concentrations of lymphocytes are applied. However, implicit inference about this process can be made via comparing lymphocyte densities for biopsies harbouring TLOs and biopsies that are free of TLOs, although it may vary significantly between patients.

Overall, the presented model is useful in two ways: as a methodological workflow, which can be applied for other systems of migrating cells, and as an instrument for prediction of cluster stability depending on the applied conditions and system parameters.

4

Modelling of germinal center interactions

4.1 Background

Germinal centres (GCs) are structures located predominantly in secondary lymphoid tissue, although matured GCs can be found in TLOs as well, as discussed in chapter 1. GCs were discovered in 1884 by W. Flemming and were thought to be the sites of lymphocyte development. Only later analysis of single GC cells showed that in GCs B lymphocytes are subject to somatic hypermutations (SHM) and selection based on the affinity of the B cell receptor (BCR) to the antigen, i.e. GCs are responsible for the so-called affinity maturation process. The biology of GCs was previously described in the classical work of MacLennan [132] and more recently in a very comprehensive review by Victora and Nussenzweig [213]. In this chapter I construct a model of the interaction of different GCs. Hence, I briefly introduce the main cellular events which happen during the process of affinity maturation, or GC reaction (GCR).

GCs can be functionally and anatomically divided into two regions, the dark (DZ) and the light zone (LZ) [155], fig. 4.1. B cells in the DZ are called centroblasts. They extensively proliferate and are characterised with a very high division rate with a cell cycle in the range of 6-12 hours. Centroblasts share the same morphology and cell size with centrocytes, B cells of the LZ, and these cell types can be distinguished only by difference in expression of surface markers such as CD86, CD83 and CXCR4 receptor [213]. The phenotype of B cells is regulated by the Bcl-6 gene (Bcl for B cell lymphoma) and deficiency in this gene results in the absence of GCs [50]. According to [213], Bcl-6 is responsible for several functions:

- suppression of anti-apoptotic gene Bcl-2 impacts on the B cell survival and selection;
- suppression of p53 and ATR increase cell tolerance to DNA damage due to extensive SHM and division;
- regulation of B cell exit from GCR via inhibition of Blimp-1 expression;
- regulation of selection signals via suppression of CD40 and BCR expression.

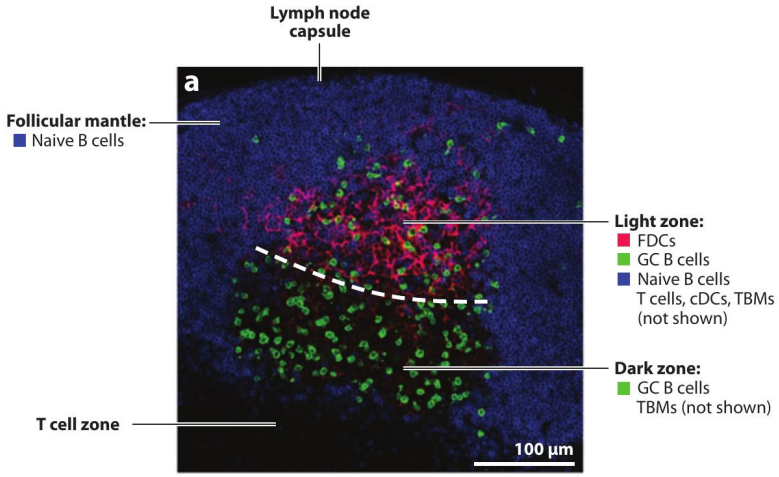

Figure 4.1: The anatomy of GC. The B cell follicle (blue) contains a germinal centre with the dark zone where GC B cells (green) proliferate and mutate and the light zone containing the network of follicular dendritic cells (FDCs, red), T folicular helper cells and other cell types (not stained). Interactions of B cells with FDCs and Tfhs lead to B cell selection in terms of higher affinity to the antigen. Adapted from [213].

Disregulation of B cell fate decisions may result in lymphoma or autoimmunity [157]. In addition, GC B cells express AID which induces VDJ gene rearrangements and SHM in the BCR and together with the high division frequency results in high numbers of new B cell clones [9, 84, 124, 231]. The population of generated clones is constantly tested in interaction with cells from the LZ.

Follicular dendritic cells (FDCs) function was reviewed in chapter 1, retain antigen at their surface in the form of immune complexes, i.e. antibodies bound to antigen. FDCs are able to retain antigen for a very long time and, although affinity maturation was observed even in their absence, they are important for immune responses in suboptimal conditions when the amount of antigen is limited [184]. They are characterised by expression of complement receptors the CR1 and CR2 participating in the presentation of antigen to GC B cells as well as of adhesion molecules like VCAM-1 and ICAM-1 which are important for the formation of immunological synapses with B cells, fig. 2.5. FDCs sustain surveillance of GC B cells by secretion of BAFF. They are also responsible for B and T cell positioning due to secretion of CXCL13, a ligand for CXCR5 receptor located at the surface of GC B cells and T follicular cells (Tfhs). LZ B cells collect antigen located on the surface of FDCs and present it to Tfhs (T follicular helper cells) as MHC-II-peptide complexes [47, 133].

Analysis of the migration patterns and of individual mutations in B cell clones resulted in the proposal of a cyclic-reentry model by [100], in which B cells are involved in several rounds of proliferation and selection. Having passed selection in the LZ, B cells either recycle back to the DZ and continue division and SHM or differentiate to plasmablasts (PBs) or memory cells. According to an alternative model, all B cells return to the DZ where the fate decision takes place [55, 141].

The mechanisms of this fate decision are not clearly known yet. By default, GC B cells are programmed to die by apoptosis [123] and upon successful interactions with FDC and Tfh, they may be rescued from cell death. The contribution of interactions with FDCs via BCR to the selection process is still unclear and in [213], T cell help is hypothesized to be the limiting factor in the GCR based on theoretical and experimental investigations. Tfhs were shown to interact with several GC B cells at the same time and they are able to polarize towards the cell bearing higher density of antigen-MHC complexes at the surface. In experimental setup where B cells were artificially loaded with antigen using antigen-antibodies fusion proteins, Tfhs were selecting these cells irrespective of their affinity, and, as a result, affinity maturation was disrupted [214]. Since cells with higher affinity BCR have an advantage in collecting antigen and hence in presenting it to Tfh [22, 51], this two-step selection system allows to increase the average affinity of B cell clones during the GCR [58, 59]. Although the critical role of Tfh in B cell selection was shown, what signals influence the further B cell differentiation to antibody secreting PBs or to memory B cells is not discovered yet.

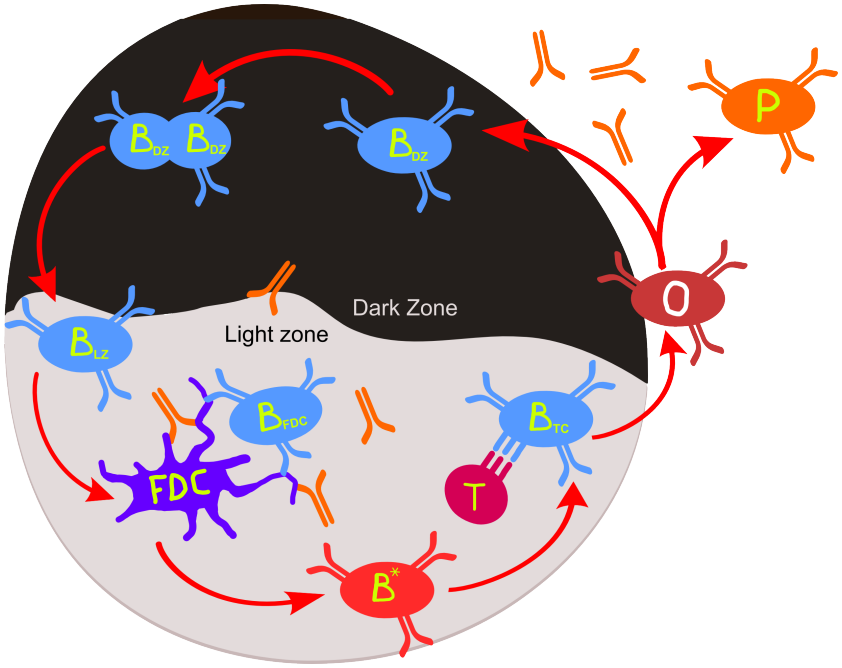

Figure 4.2: Schematic representation of the GC reaction. B_{DZ}, B_{LZ} correspond to B cells in the dark and the light zones; T to Tfh; B_{FDC}, B_{TC} are B cells in interaction with FDC and Tfh, respectively; O is an " output" B cell after interaction with Tfh; P are PBs. Memory B cells are not considered in this study. Antibodies (orange molecules) are produced by PBs and can penetrate the GC and bind the antigen presented on the surface of FDCs.

GCs are predominantly discussed as isolated structures. However it is interesting to investigate how they might interact with each other. Recently, Tfhs were shown to migrate between different GCs [190], but besides cellular interaction, there might be communication mediated by molecules. Antibodies produced by PBs from one GC may penetrate the same and other GCs and bind to the antigen presented

Figure 4.3: Secreted antibodies penetrate the GCs itself as well as other ones what results in antigen masking at the FDCs surface influencing antigen access for B cells.

on the FDC surface [232], fig. 4.3. This disturbs recognition of the antigen by low affinity B cell clones, increasing the selection pressure during the GCR and changing the reaction kinetics [232]. In the light of these results, it is interesting to investigate how GCs may influence each other in terms of the GCR kinetics and how the affinity maturation changes depending on the system size or the starting time of the GCR. I constructed a model describing GCR kinetics using ordinary differential equations and compared the development of the immune response in different simulation setups.

4.2 Mathematical model

Representation of clones and mutations

There are several published models of the GC reaction based on systems of ordinary differential equations (ODE) [101, 138] or agent-based approaches [62], but none of them considers GCs as a system of interacting instances. In our model, cell dynamics and chemical kinetics of antibody-antigen binding were described with a system of coupled ODE. I used the phenomenological concept of 4 dimensional shape space to describe clones of different affinity, see for example [138]. In this representation, a clone is coded with 4 integers which might correspond to some physical properties of the B cell receptor, and a mutation corresponds to one step in any direction in the shape space. This approach allows to describe the dynamics of clones with different affinities, although this simplified representation is not based on any measurable mapping of sequences to affinities. Our model has to be considered as a qualitative approach rather than a precise predictive model in this respect. The simulation starts with clones located at a distance of 5 mutations from the optimal clone [140]. The number of clones located at the distance of not more than 10 mutations from the optimal clone is 10^4 for a 4D shape space. To simplify our calculations, I substituted numbers of clones located at equal distance by their total number, i.e. transformed the system from 4D representation to 1D (similar to models using affinity classes representation [101]):

$$B(i) = \sum_{\vec{j}:|\vec{j}-\vec{o}|=i} b_j, \tag{4.1}$$

where $B(i)$ is the total cell number of clones located at distance i from the optimal clone $\vec{o}$, $|\cdot|$ denotes the Hamming distance, and b_j is the number of cells of clone $\vec{j}$.

In the discrete 4D space, not all clones at the same Hamming distance are located in the same configuration. For example, assuming $\{0,0,0,0\}$ as the optimal clone, 7 possible mutations of the clone $\{2,0,0,0\}$ lead to a lower affinity configuration and 1 mutation leads to a higher affinity clone $\{1,0,0,0\}$ (i.e. smaller distance to the optimal clone). In contrast, for the clone $\{1,1,0,0\}$, which has the same Hammings distance as $\{2,0,0,0\}$, only 6 mutations lead to lower affinity and 2 to higher. In Fig. 4.4 the corresponding situation is illustrated for a 2D case. For every configuration, the exact number of such transitions to higher and lower affinity can be calculated. Since all numbers of the clones located at the same distance were substituted by their total number $B(i)$, I calculate the total number of possible transitions from all configurations located at the distance i to higher (t_+) or to lower (t_-) affine states to estimate which proportion of cells of $B(i)$ mutate to a higher or lower affinity state. With p being the proliferation rate, m the mutation probability, and assuming equal probability for all mutations, the rate of transitions $i+1 \to i$ reads

$$\frac{t_-(i+1)}{t_-(i+1)+t_+(i+1)} pmB(i+1), \tag{4.2}$$

where $t_\pm(i+1)$ is the number of possible transitions from $i+1$ to higher (+) or lower distance (–). t_+ can be computed iteratively as $t_+(0)=8, t_+(1)=8c_1-t_+(0),\ldots,t_+(k+1)=8c_k-t_+(k)$, and $t_+(k)\equiv t_-(k+1)$, where c_k is the number of clones in the shape space which are located at a distance k from the optimal clone

$$c_k = \sum_{l=1}^{\min(4,k)} C_{k-1}^{l-1}\cdot 2^l \cdot C_4^l, \tag{4.3}$$

where $C_n^k = \frac{n!}{k!(n-k)!}$. Having the numbers of cells for clones $i\pm 1$ the number of cells to mutate into the clone i becomes

$$N(B(i-1),B(i+1)) = \underbrace{\frac{t_-(i+1)}{t_-(i+1)+t_+(i+1)}B(i+1)}_{i+1\to i} + \underbrace{\frac{t_+(i-1)}{t_-(i-1)+t_+(i-1)}B(i-1)}_{i-1\to i} \tag{4.4}$$

Cell interactions

The rate g_{FDC} of contact formation of B cells with FDCs is proportional to the number of available sites with antigen. I assume that every FDC has 6 sites (like cube sides). With 200 cells the total number of FDC sites is estimated as $\#(\text{FDC sites}) = 200\times 6 = 1200$. Not all sites are used simultaneously and the system is not sensitive to this parameter. Hence, a precise estimation of the FDC network interaction capacity is not necessary. I assume that a B cell is not able to interact with a certain site on an FDC if another B cell has already occupied it or the antigen is masked with antibody of higher affinity than that of the BCR. A cell which has a high affinity is assumed to have a higher probability of interacting with an FDC. This is implemented by weighting the rate of contact formation g_{FDC} with the function $\rho(i)$,

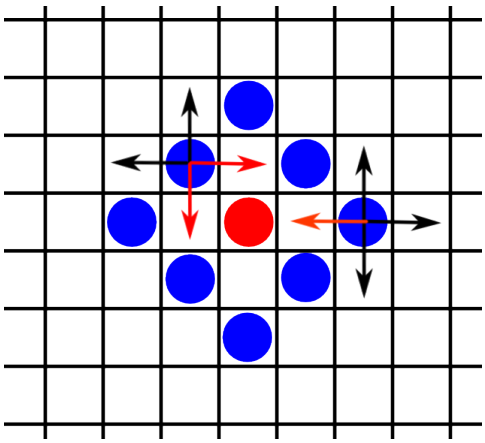

Figure 4.4: Example of clone configurations. Different configurations of clones on a 2D grid lead to different numbers of transitions to higher and lower affinity. The red circle is the optimal clone, the blue circles are the clones located at a distance of 2 mutations from the optimum. The red arrows show beneficial mutations, while black arrows show mutations leading to lower affinity to the optimal clone.

which monotonically increases with affinity. Within these assumptions, the rate of interaction becomes

$$g_{\text{FDC}}(i) = g^0_{\text{FDC}}\rho(i)\alpha(i)\frac{\#(\text{ FDC sites}) - \sum_i B_{\text{FDC}}(i)}{\#(\text{ FDC sites})}\frac{G}{G_0}, \tag{4.5}$$

where g^0_{FDC} is the rate of contact formation in the absence of antigen masking and when all sites are free, $\alpha(i)$ is the proportion of antigen available for clone i, i.e. free antigen and immune complexes with antibodies of lower than i's affinity, $\rho(i) = \exp(-i^2/2.8^2)$ is the affinity function defined in [140], and G, G_0 are current and initial antigen amounts respectively. The rate of interaction with Tfhs is described in an analogous way:

$$g_{\text{TC}}(i) = g^0_{\text{TC}}\beta(i), \tag{4.6}$$

where g^0_{TC} is the rate of contact formation if all Tfhs are free.

It was shown in [51], that T cells do not distinguish between B cells of different affinities, but preferentially interact with B lymphocytes presenting more antigen on their surface. I assume that B cells with higher affinity collect more antigen [142, 214] and that the probability of interaction with Tfhs $\beta(i)$ is proportional to the number of free Tfhs plus the number of Tfhs in interaction with lower affinity than corresponding to clones i

$$\beta(i) = \frac{\#(\text{ Tfh}) - \sum_{j\leq i} B_{\text{TC}}(j)}{\#(\text{ Tfh})} \quad . \tag{4.7}$$

This probability enters Eq. 4.6.

Since the threshold of entrance into the GC in the beginning of the reaction is low [188], I assume that any interaction with FDC leads a B cell to the next selection step independently of its affinity. The only difference between clones at this stage is the probability $\rho(i)$ to be involved in an interaction in Eq. 4.6.

The kinetics are modelled based on rate equations. The model distinguishes two morphological zones which are associated with the presence of B cells of different phenotypical characteristics [107]. The cells which are located in the DZ ($B_{\mathrm{DZ}}(i)$) proliferate with rate p and differentiate to the light zone (LZ) phenotype with rate g_{LZ}. At every division, a cell mutates with probability m as its neighbours do. The number of neighbours is defined by Eq. 4.4. Output cells $O(i)$ are selected for recycling with probability $(1-r)$. After one division (factor 2 before $(1-r)$) they return to the B_{DZ} state:

$$\dot{B}_{\mathrm{DZ}}(i) = (p - 2mp - g_{\mathrm{LZ}})B_{\mathrm{DZ}}(i) + pmN(B(i-1), B(i+1)) + 2(1-r)p\,O(i) \quad . \tag{4.8}$$

B cells in the LZ die via apoptosis with rate d and interact with FDCs with rate g_{FDC}:

$$\dot{B}_{\mathrm{LZ}}(i) = g_{\mathrm{LZ}}B_{\mathrm{DZ}}(i) - (g_{\mathrm{FDC}} + d)B_{\mathrm{LZ}}(i) \quad . \tag{4.9}$$

The cells that interact with FDCs $B_{\mathrm{FDC}}(i)$ turn to the "FDC selected" state $B^*(i)$ with rate h_{FDC}, which was derived from the average duration of interaction:

$$\dot{B}_{\mathrm{FDC}}(i) = g_{\mathrm{FDC}}B_{\mathrm{LZ}}(i) - h_{\mathrm{FDC}}B_{\mathrm{FDC}}(i) \quad . \tag{4.10}$$

The cells in the state $B^*(i)$ search for Tfhs and die with a decreased apoptosis rate d_{selected}:

$$\dot{B}^*(i) = h_{\mathrm{FDC}}B_{\mathrm{FDC}}(i) - (g_{\mathrm{TC}} + d_{\mathrm{selected}})B^*(i) \quad . \tag{4.11}$$

In analogy to the interaction with FDCs, interaction with Tfh (B_{TC}) induces differentiation to the output state $O(i)$ with rate h_{TC}:

$$\dot{B}_{\mathrm{TC}}(i) = g_{\mathrm{TC}}B^*(i) - h_{\mathrm{TC}}B_{\mathrm{TC}}(i) \quad . \tag{4.12}$$

Output cells $O(i)$ divide with the same rate p as the DZ cells and differentiate to PBs with the probability r or go back to the DZ otherwise (see Eq. 4.8):

$$\dot{O}(i) = h_{\mathrm{TC}}B_{\mathrm{TC}}(i) - pO(i) \quad . \tag{4.13}$$

PBs die with apoptosis rate d_P:

$$\dot{P}(i) = 2rpO(i) - d_{\mathrm{P}}P(i) \quad . \tag{4.14}$$

At each interaction with an FDC, an amount q of antigen is consumed:

$$\dot{G} = -\sum_i qh_{\mathrm{FDC}}B_{\mathrm{FDC}}(i), \tag{4.15}$$

where G is the antigen concentration, h_{FDC} is the rate of interaction of a B cell with an FDC, and $B_{\mathrm{FDC}}(i)$ is the number of B cells at Hamming distance i in interaction with an FDC (see Eq. 4.10).

Antigen masking is calculated in equilibrium of immune complexes and antibodies produced by PBs:

$$\dot{A}(i) = \frac{ns}{V_{\text{blood}}} P(i) - d_A A(i) \tag{4.16}$$

$$C(i) = \frac{A(i) G_{\text{free}}}{K_i + G_{\text{free}}} \tag{4.17}$$

$$G = G_{\text{free}} + \sum_i C(i) \tag{4.18}$$

$$K_i := 10^{-5.5-0.4(10-i))}, \tag{4.19}$$

where $A(i)$ is the concentration of antibodies, $C(i)$ is the concentration of immune complexes, K_i is the dissociation constant, d_A is the antibody decay rate, s is the secretion rate of antibodies for a single cell, G_{free} is the concentration of free antigen, and n is the number of GCs in the range of 300-500 [95]. I use $n = 300$ to investigate whether inter-GC interaction via antibodies is still observable at lower numbers of GCs. For higher numbers n, the effect of inter-GC interaction is more pronounced. I assume that antibodies are present in excess to antigen in GCs. Otherwise the immune response would be inefficient because a significant part of antibodies would be bound to antigen in GCs but not to a pathogen. If the concentration of antigen is very low, the ratio [free antigen]:[immune complex] becomes

$$\frac{G_{\text{free}}}{C(i)} = \frac{K_i}{A_i} \quad . \tag{4.20}$$

Since only the percentage of antigen bound in complexes is relevant, I can use an arbitrarily small value for the initial $G_0 = 10^{-16}$M. The size of antigen quanta enters the fitting routine.

The immune power (IP) metric is defined as the percentage of the antigen which would be covered with antibodies of given concentrations. For the calculation of IP values I use the concentration of antibodies produced by one GC multiplied by $n = 300$. The choice of the antigen concentration is arbitrary and is chosen as $G = 10^{-6}$M for presentation reasons. Then, the concentration of unbound antigen G_{free} can be calculated and determines the fraction of bound antigen to

$$\text{IP} = \frac{G - G_{\text{free}}}{G} \quad . \tag{4.21}$$

Parameter fitting

For most of the parameters, values from experiments or theoretical estimations were used (Table 4.1)). The model was fitted to experimental measurements of GC size [204] by minimizing the residual sum of squares (RSS) [219] using the C++ library for nonlinear optimization NLOPT (Steven G. Johnson, http://ab-initio.mit.edu/nlopt), Fig.4.5. To incorporate data about antigen consumption to the fitting I modified the RSS function by adding a weighted term

$$\text{RSS}^* = \text{RSS} + w \cdot \left(\frac{A_{\text{end}}}{A_0} - 0.25 \right)^2 \quad , \tag{4.22}$$

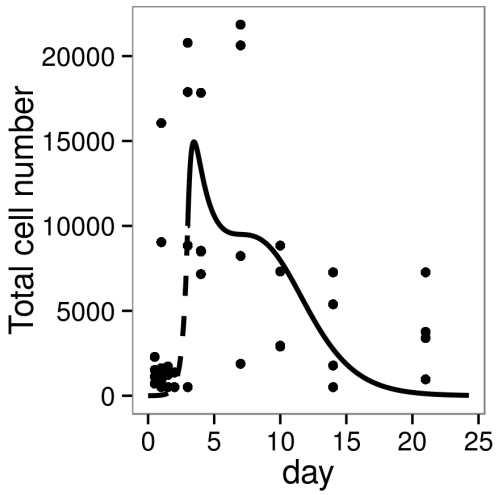

Figure 4.5: Model fitting. Result of model fitting to GC size kinetics from [204]. Monoclonal expansion period (dashed line) is followed by the established GC (solid line).

where I assume that A_{end}, the amount of antigen in the end of the GC reaction, should be approximately one quarter of the initial antigen amount A_0 according the antigen kinetic data [200]. The value $w = 100$ was found to be appropriate in the sense that the system follows the dynamics of GC size but does not run out of antigen. The first 3 days are described by exponential monoclonal expansion with proliferation rate p. The simulation of the GC reaction after expansion starts with 10000 cells which is based on the assumption that the radius of a GC is 160μm, the average B lymphocyte cell size is 15μm [209], and that the GC cells are densely packed.

Antigen quanta q, the rate of BCs to get LZ phenotype g_{LZ} and the rate to find an FDC g_{FDC} are the fit parameters. The 95% confidence intervals (CI) were calculated using nonparametric bootstrapping [40]. For the parameter g^0_{FDC} the CI is (0.43,2.3) and for g_{LZ} the CI is (0.13,0.22). Antigen quanta and g_{FDC} are mutually dependent parameters, since the larger antigen quanta is, the less frequently B cell should interact with FDCs in order to keep antigen amount in an appropriate range. That is why I fixed the value of antigen quanta and estimated the CI only for g_{FDC}.

Estimation of B cell-Tfh interaction rate

The rate of contact formation between B cells and Tfh g^0_{TC} in Eq. 4.6 was approximated based on constraints on the mean free path length. The speed of lymphocytes is $v_{\text{BC}} = 8\mu$m/min [143, 220] and the concentration of Tfh is $n_{\text{T}} = 10^4$cells/mm^3 [190]. For a B lymphocyte with a diameter of 15μm [209] and a T cell with a diameter of 8.5μm [93], the mean free path of a B cell between interactions with Tfh gets

Table 4.1: Model parameters.

Notation	Meaning	Value	Unit	Reference
V_{blood}	blood volume	4	ml	[232]
s	antibody production rate	2×10^{-18}	1/hr/cell	[177]
p	proliferation rate	$\log 2/6$	hr^{-1}	[58]
g_{LZ}	rate to get LZ phenotype	0.15	hr^{-1}	fitted
g^0_{FDC}	rate to find FDC	0.61	hr^{-1}	fitted
g^0_{TC}	rate to find TC	3	hr^{-1}	estimated
d	apoptosis rate	0.1	hr^{-1}	[122]
h_{FDC}	rate of interaction with FDC	2	hr^{-1}	[211]
h_{TC}	rate of interaction with Tfh	2	hr^{-1}	[142]
r	probability to differentiate	0.2		[141]
d_{Selected}	apoptosis rate of activated cells	0.02	hr^{-1}	[138]
d_{P}	PBs apoptosis	$1/4$	day^{-1}	[99]
d_{A}	antibody decay	$\log 2/10$	day^{-1}	[232]
q	antigen quanta	4.6×10^{-21}	M^{-1}	fitted
	FDC number	200	cells	[62]
	FDC dendrites pro cell	6		[142]
n	number of GCs	300		[95], see text

$$\lambda = \frac{1}{\sqrt{2}\sigma n_{\text{T}}} = \frac{1}{\sqrt{2}\pi \cdot (7.5 + 4.25\mu\text{ m})^2 \cdot 10^4 \text{cells/mm}^3} = 0.163\text{mm [38]} \tag{4.23}$$

$$\tau_{\text{Tfh}} = \frac{\lambda}{v_{\text{BC}}} = \frac{0.163\text{mm}}{8\mu\text{m/min}} = 20\text{min} \Rightarrow \frac{1}{\tau_{\text{Tfh}}} = 3\text{hr}^{-1} \approx g^0_{\text{TC}}, \tag{4.24}$$

where $\sigma = \pi r^2_{\text{BC}}$ is the cross section of a lymphocyte, τ_{Tfh} is the free path duration.

It is difficult to estimate the rate of interaction with FDC directly because FDCs form a network of dendrites and B cells need to collect multiple portions of antigen what leads to a sequence of multiple interactions with different FDCs. Therefore the rate g_{FDC} was treated as a fit parameter.

4.3 Results

How to compare the efficiency of humoral immune response in silico?

GCs generate antibody forming plasma cells. The produced antibodies are supposed to bind fragments of the pathogen and either neutralize or opsonise it. The efficiency of this process depends on antibody concentration and affinity of the antibody for the antigen. With the aim of comparison of GCs I define a new measure of GC efficiencies in binding pathogenic antigen. I consider the limit of antibodies in excess of antigen and use classical chemical kinetics to determine the fraction of bound antigen. For a concentration of antibodies equal to its dissociation constant K, half of the antigen is bound in immune complexes. To cover the same percentage of antigen with antibodies of K/10 affinity, the required

antibody concentration is 10 times higher. Both these results of a GC reaction are considered of equal efficiency because the same fraction of antigen is bound.

In the spirit of this simple thought, I propose to use the percentage of antigen bound by GC derived antibodies as a measure IP for the efficiency of the GC reaction

$$\text{IP} = \frac{[\text{antigen in complex}]}{[\text{total antigen}]}, \tag{4.25}$$

where the brackets denote concentrations and IP stands for "immune power". The total antigen concentration for computing the IP can be chosen freely and may be adjusted to optimise the illustration of results.

During GC simulations, the IP is continuously computed in order to generate a time course of GC efficiencies in binding antigen and to compare the strength of immune responses in different GC models. Since the model does not distinguish neutralizing and non-neutralizing antibodies, the IP is a simplification which restricts the analysis to functional antibodies.

Strong selection pressure does not guarantee efficient immune responses.

Antibodies derived from GC reactions diffuse over the whole organ. Antibody feedback was shown to influence selection during GC reactions [139, 232]. Masking of antigen by antibodies increases selection pressure and might prevent access of low affinity B cell clones to antigen. At the same time higher selection pressure induced by high-affinity antibodies might reduce the number of PBs that leave the GC.

These adverse effects of antibody feedback on the GC motivate the question how the strength of antibody feedback would impact on GC efficiency in terms of IP. The strength of antibody feedback can be modulated by tuning the number of GCs. This is equivalent to scaling the antibody productivity of PBs. In the reference system, 300 GCs were assumed. For a system with reduced antibody feedback the number of GCs was reduced to 30, which reduced the amount of antibodies competing with GC B cells for antigen correspondingly.

The difference in selection pressure was reflected in the GC population kinetics (Fig. 4.6A). With reduced selection pressure, a regrowth of the GC B cell population was observed due to lack of adaptation of the antigen coverage to the progress of affinity maturation of B cells.

With reduced selection pressure, the average affinity of PBs gets lower as well (Fig. 4.6B), but the number of PBs (not shown) and the IP per GC is higher (Fig. 4.6C).

The plasma cell number, and therefore the antibody concentration depend on the number of GCs in our system. To test how the IP changes with the amount of antibody produced, I performed simulations from 1 - 1000 GCs. In addition, for every number of GCs N I compute the IP for a system of a single GC which is scaled to the system of N GCs, i.e. I multiply concentration of antibodies by N during

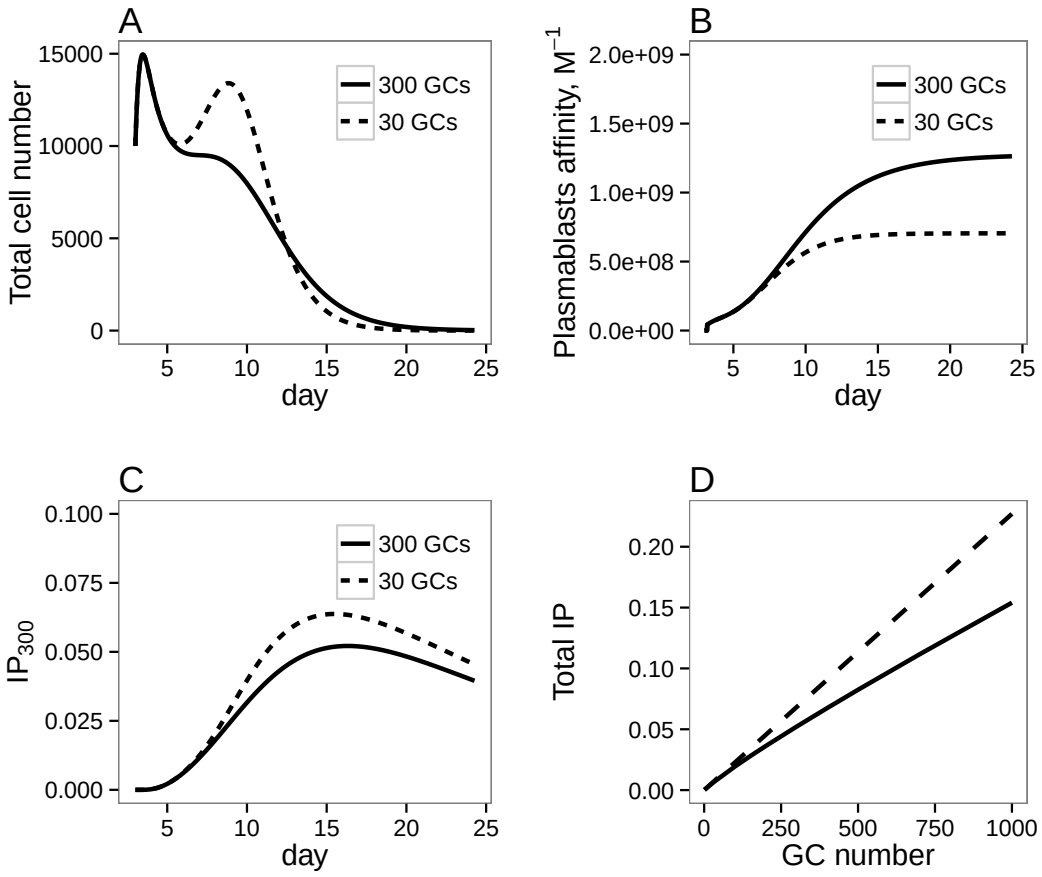

Figure 4.6: Influence of antibody feedback onto GC dynamics. A-C: Total cell number, average PB affinity and the IP for GCs developed in condition of normal (full lines) and reduced (dashed lines) antibody feedback. The strength of antibody feedback was modulated by the number of simultaneous GCs. The IP corresponds to a system of 300 GCs and is scaled appropriately in case of 30 GCs. D: The total IP depending on the number of GCs (solid line), where more GCs mimic increasing antibody feedback, is compared to the IP of a single GC scaled to the corresponding number of GCs (dashed line).

IP calculation. If there is only one GC in the system the feedback of antibodies is minimal, hence comparison of the IPs between the system of N GCs and the IP of the single GC system scaled to the same size allows us to see how GC-GC interaction influence the efficiency of the immune response. Although the IP monotonically increases with the GC number, the feedback effect increases as well (the difference between the solid and the dashed lines in Fig. 4.6D), further limiting the contribution of each GC.

Late developing GCs are suppressed by early ones.

Antibodies derived from one GC can penetrate all GCs in the organism. Next, I asked whether this interaction supports or suppresses the emergence of late GCs. I considered a model with 300 GCs which started simultaneously under normal conditions and one GC which was initiated 3 days later than the others. The later appearing GC develops under the influence of antibodies being generated by the other 300 GCs, and I monitored its affinity maturation, PBs and IP.

The simulations suggest that early GCs boost late GCs in terms of affinity maturation. Since antigen masking by antibodies from the early GCs increases the selection pressure in the late GC, a higher average affinity of PBs is found (Fig. 4.7B). However, in terms of cell numbers the late GC was strongly suppressed (Fig. 4.7A). As a consequence, the IP of the late GC is decreased as well (Fig. 4.7C).

I varied the time of the delay and found that late GCs do not contribute to the immune response significantly: the IP of a GC started 5 days later is only around 10% of the early GC(Fig. 4.7D).

Simultaneous development of GCs is more beneficial

The GC response may be delayed, for example, in the neonatal organism where the FDC network is still developing [166] or in the aged organism where antigen transport is impaired [105]. It is interesting how such delays in the GC development may influence the efficiency of the immune response. In this section, I focus only on the influence of the starting time of a GC reaction on its dynamics without consideration of case specific factors like changes in antigen transport with age or the process of FDC maturation in neonatal mice.

I compared two different cases: a) a “simultaneous” model with start of 300 GCs at day 0; b) a “sequential” model, in which 30 new GCs start every day during 10 days. The initial amount of antigen in newly developed GCs was set to the current amount of the antigen in the GCs developed at day 0. The first 30 GCs in the “sequential“ case are developing under reduced antibody feedback, which is identical to the simulation in Fig. 4.6. They generate more antibodies and cells in comparison to the “simultaneous“ system. However, this is not enough to compensate for the suppression of the later GCs, because the overall IP for the ”sequential“ system appeared to be lower, Fig. 4.8. This result shows that delays in GC reaction result in poorer output even without consideration of additional pathological conditions which caused this delay.

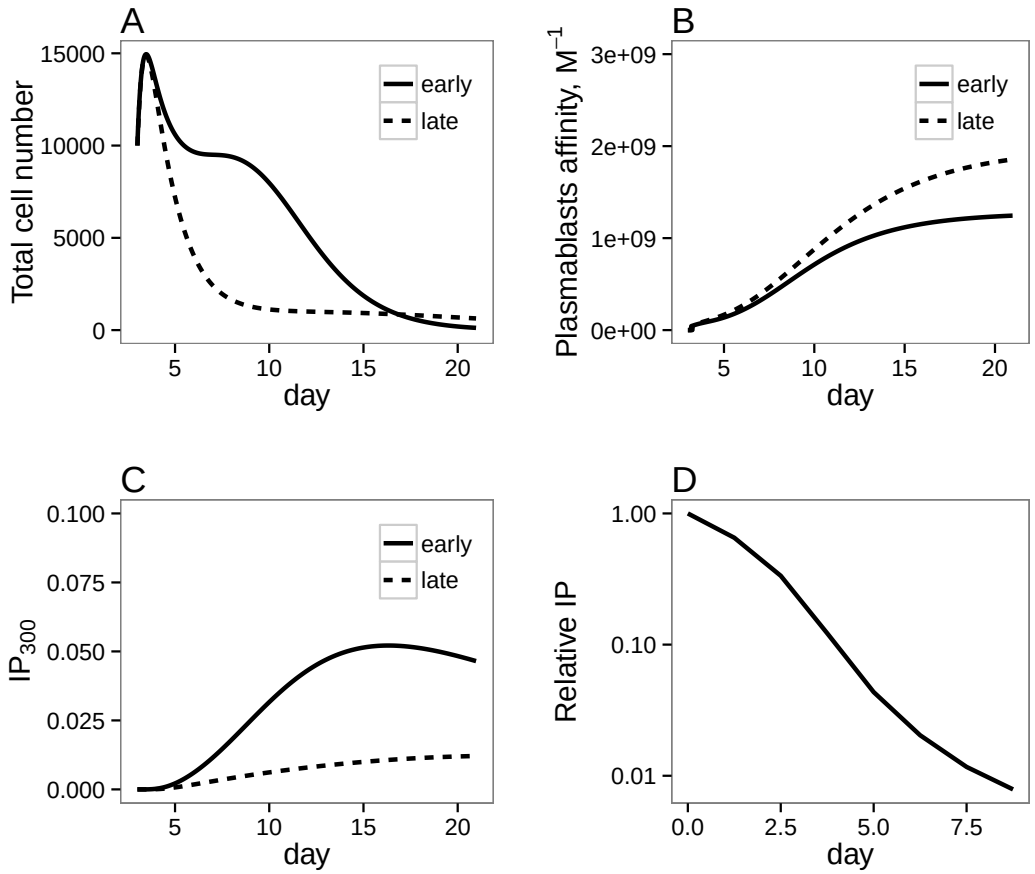

Figure 4.7: The impact of retarded GC reactions. A-C: Total cell number, average PB affinity, and the IP (scaled as in Fig. 4.6) of an early GC (full lines) is compared to a GC which initiated 3 days later (dashed lines). The graph for the late GC is shifted 3 days backward for the sake of better comparison. D: The ratio of the IP of the late to the early GC is shown for increasing delay of the late GC.

4.4 Discussion

GCs are mostly considered as isolated structures. In this study I introduce the first model considering interactions between different GCs. I show that GCs appearing later contribute little to an immune response and that the influence becomes negligible with increasing delay. According to this result, synchronous GC initiation leads to more efficient antibody response than sequential one.

The model provides evidence for an impact of antibody feedback onto affinity maturation and the size of GC responses. Stronger antibody feedback increases GC B cell affinity but at the expense of the number of PB generated. Thus, there is a trade-off between quantity and quality of generated output [139]. In addition, the overall GC population kinetics are strongly influenced by this feedback mechanism as also observed in experiment [232]. The reduced size of late GC reactions over-compensates the

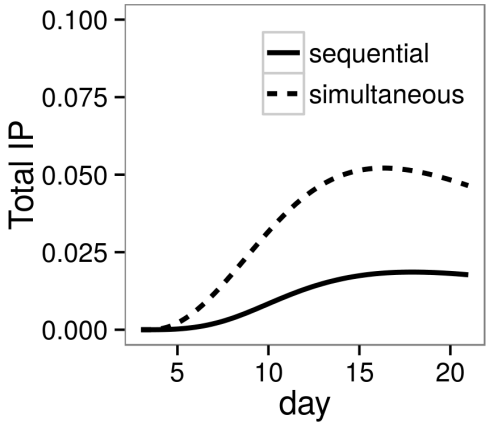

Figure 4.8: Immune efficiency of simultaneous versus sequential GCs. The development of the IP over three weeks for 300 simultaneously started GCs (dashed line) is compared to 30 GCs started every day for 10 days (full line).

positive effect of antibody feedback onto affinity maturation in late appearing GCs, leading to lower IP. However, the increased selection pressure is able to synchronize B cell affinity between early and late GCs. Thus, late GCs which would be increased in size by external manipulation are likely to foster the efficiency of immune responses.

The model predicts that reduced antibody feedback leads to GCs of larger size. Transgenic mice which are deficient for the secreted form of IgM [57] can be considered as such a system with reduced antibody feedback. Indeed, these mice exhibit larger GC size in comparison to controls [232]. Part of the observed effect might be due to prolonged GC reactions as the data were taken 21 day after immunization. This latter interpretation is consistent with the previous finding that antibody feedback has a major role in GC shut-down [139].

The desired GC output may well depend on the immune stimulus in question. In the case of a primary response to infection, it is important to cover as much antigen as possible with antibodies. In this case, the average affinity of antibodies is not the best measure of response efficiency, since GCs may generate only small numbers of high affinity PBs to each individual epitope. Thus, the response to individual epitopes would remain weak. The newly introduced ”immune power” metric, which literally represents the coverage of epitope by antibodies, is proposed as a better measure of GC efficiency in antibody responses. In contrast, in the context of vaccination, the aim may be mainly the generation of B cell memory. It is not clear yet, how specific or diverse an optimal pool of B cell memory cells should be in order to account for mutated pathogens [78]. The most important value might be the average affinity of the generated diverse pool rather than the degree of antigen coverage. In this case, optimisation of the GC conditions based on the average affinity as a metric of efficiency would be beneficial. The model provides a tool to design conditions of optimisation for both scenarios.

While the optimal GC efficiency is the result of a subtle balance between affinity and number of generated PBs, the number of GCs is an important parameter as well. Increasing the number of GCs has a double beneficial effect: Affinity maturation is accelerated and the total number of generated PBs is increased. However, the efficiency of individual GC is reduced. Also, the organisms cannot initiate unlimited numbers of GCs for the limitation of other resources, which are not included in the modelling approach. According to the simulation results, the organism has to maximize the number of GCs while preserving a reasonable resource investment.

Our model supports the view that the phase of GC initiation is an essential parameter for the success of an immune response. The efficiency of simultaneously started GCs is higher compared to a sequential start of the same total number of GCs. If antigen is not properly provided to lymphocytes, a delay of GC reactions may be induced, which would lead to a weakened humoral immune response. Fast and coordinated antigen delivery and GC onset should be considered as a potential mechanism in situations of suboptimal vaccine response, e.g. the slowly emerging vaccination response in the elderly immune system [5, 13]. While aged mice quickly produce high titres of low affinity antibody, high affinity antibody is severely reduced and this is associated with smaller GCs [81, 108]. This may be related to aged FDC having changes in the efficiency to interact with antibody and immune complex [15], which could lead to reduced antibody feedback. Furthermore, aged mice respond to vaccination with reduced numbers of GC, which is thought to be dependent on delayed antigen transport [197].

With the presented model I provide evidence for the need to investigate the interaction of GCs in order to gain a better understanding of the efficiency of antibody optimisation on the systems level. Besides antibody feedback, other means of GC-GC interactions like exchange of cells [190] or other molecules should be considered.

5

Quantification of virus-specific CD8 T cell killing efficiency in vivo

5.1 Background

Cytotoxic T cells (CTLs) are $CD8^+$ T lymphocytes which participate in the immune response against infected host cells or cancer cells. CTLs express a T cell receptor (TCR) which recognizes antigens presented in complex with MHC-I (Major histocompatibility complex of class I) molecules at the cell surface. If the affinity of such an interaction is high, CTLs stay in contact with the target cell and secrete granzymes, perforin and granulysin. Perforin molecules form cylindrical pores in the host cell membrane and also assist in delivery of granzymes into the cytoplasm, which leads to activation of pro-apoptotic reaction cascades, DNA fragmentation and, finally, target cell death. Additionally, CTLs express Fas ligand (FasL). Binding of FasL to Fas which is located at the target surface can induce apoptosis as well [161]. Such so-called effector functions of CTLs allow efficient elimination of infected, damaged or cancer cells.

The ability of CTLs to specifically recognize and to kill certain cells might be useful in the treatment of diseases. For example, CTLs which have specificity to tumour antigens may contribute to antitumour immune response [54]. The efficiency of such adoptive immunotherapy directly depends on the kinetic characteristics of CTL killing, that is why experimental measurements of CTL killing rate is of high interest. Following virus infection, transfer of virus-specific CTLs might also be a possible therapeutic intervention, for example, in cytomegalovirus (CMV)-infected immunodeficient human patients.

There are a number of studies where CTL killing was described *in vitro* using a chromium assay [28] or by direct single cell observation [223]. In [223] it was shown that CTLs are very rapid in killing and may deliver lethal hit to several targets simultaneously. However, until now there were no studies of *in vivo* CTL killing models where CTL activity was measured at single cell level and with high spatial resolution. CTL responses *in vivo* may differ from *in vitro* because in the latter, CTLs and targets are mixed passively, but, in contrast, T cells need to migrate inside tissue in order to reach a target. The other difference between these experimental conditions is that *in vivo* there are other cell types present which may contribute to the regulation of the CTL response.

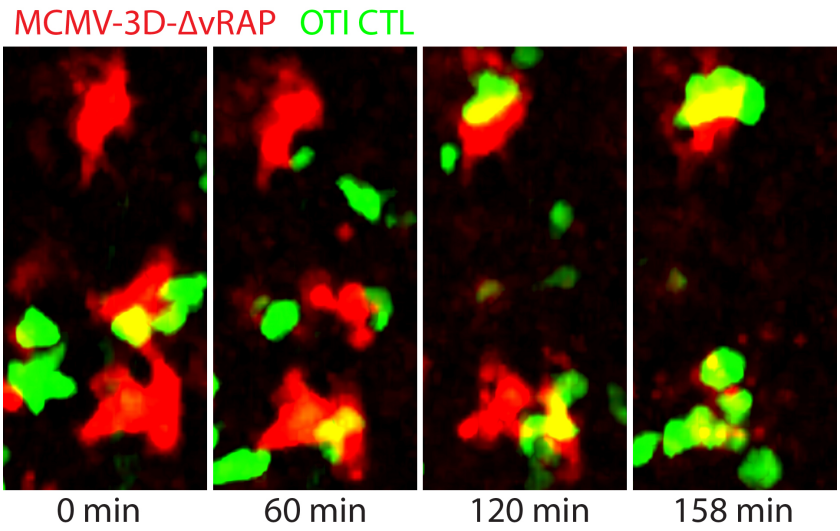

Figure 5.1: Microscopy observation of CTLs (green) at the sites of infected with MCMV cells. A courtesy of Stephan Halle, the group of Prof. Dr. Reinhold Förster, Institute of Immunology, Hanover Medical School.

In order to estimate killing kinetics of CTLs *in vivo*, two-photon microscopy was utilized to observe the behaviour of the target and the T cells in mice infected with murine cytomegalovirus (MCMV). MCMV-specific T cells were isolated and delivered via intra-lymphatic injection. After one day, infected cells and CTLs were counted using two-photon microscopy, fig. 5.1. Varying the concentration of injected CTLs and using different cell sorting techniques data about the efficiency of *in vivo* CTL killing were collected, fig. 5.2. To estimate the rate of killing I utilized a simple mass-action kinetic model.

5.2 Mathematical Model and Results

Kinetic model

The kinetics of CTL killing were previously modelled using different approaches. I used the simplest approximation of mass-action kinetics, since the aim of the study was only to estimate the range of the killing rate but not to investigate spatial effects or to include any additional cell interactions or proliferation. A similar model can be found also in [144] based on data from *Cr* release assay, however, an approximation of enzyme-like reaction kinetics or more complex agent-based approaches were also applied to the same system [79, 169].

According to the mass-action approximation, the number of infected cell I is described as

$$\frac{dI}{dt} = -kTI, \tag{5.1}$$

where T is the number of T cells and k is the killing rate. This model uses the assumption of a well-mixed system, where the probability of contacts between T and infected cells are the same and independent

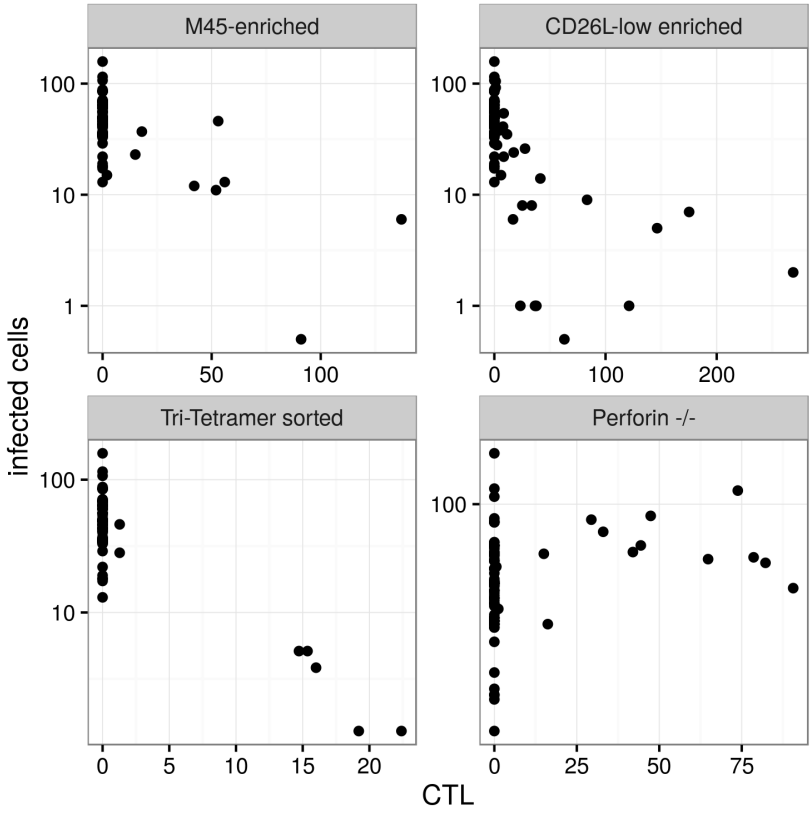

Figure 5.2: The number of infected cells depending on the CTL number at the day 1 after CTL injection. CTLs were obtained from wild type mice. Killing efficiency was measured for CTLs, sorted with different approaches, which allow various purity: Tri-Tetramer- (purity $\approx 90\%$), M45-Tetramer (purity $\approx 60\%$) and CD26$^{\text{low}}$- enriched (negatively sorted by depletion of CD26$^{\text{high}}$ and CD8^{-} cells). The CTLs from the Perforin$^{-/-}$ knock out mice were used for comparison as they lack cytotoxic activity. The data were generated at the group of Prof. Dr. Reinhold Förster, Institute of Immunology, Hanover Medical School

of the previous interactions for a given T and I. The number of infected cells at the time point t is

$$I(t) = I_0 \exp(-kTt), \tag{5.2}$$

where I_0 is the initial number of infected cells. I assume apoptosis of target cells to happen only due to interaction with CTLs, because in control experiments in the absence of CTLs no cytotoxic activity from MCMV was observed during the time of measurement. The number of T cells is assumed to be constant as well and I assume that virus spreading between cells is slower in comparison to CTL killing.

The experiments were performed at two different scales with a size of the image frame equal to 400μm x 400μm or 500μm x 500μm, hence I rescaled the numbers of cells to the 400μm x 400μm experiment. As no killing activity was observed during first 10 hours of the experiment, I assumed the duration of the experiment to be $t = 14$hr.

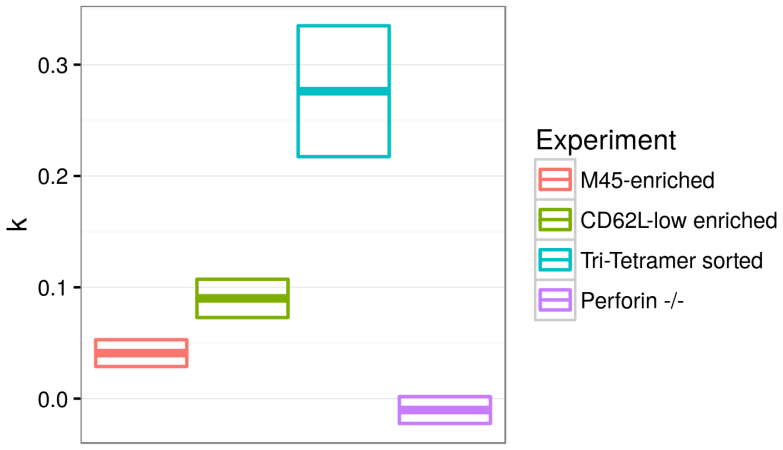

Figure 5.3: Estimations of the parameter k ($[\text{day}]^{-1}[\text{cell}]^{-1}$) and its 95% confidence interval for different experimental conditions.

I assume that the initial number of infected cells I_0 is log-normally distributed. In this case the number of survived cells can be described with the following linear model

$$\log I_{\text{exp}} = \log I_0 - kTt + \varepsilon, \tag{5.3}$$

where $\varepsilon \sim \mathcal{N}(0, \sigma)$ is normally distributed.

The killing rates k for every experiment and the initial infected cell number I_0 were estimated using multiple linear regression with R statistical environment [172]. Zero values are considered as censored measurements and the substitute method was used to treat them [152]. Outliers were detected using robust regression as described in [146]. I did not impose condition for k to be strictly positive, hence for the perforin$^{-/-}$ mice estimation of k may reach negative values, fig. 5.3.

In contrast to such a description of the killing kinetics using the k rate, it is more common among experimentalists to calculate so-called per capita killing rate (PCKR)

$$\text{PCKR} = \frac{I(t_{\text{end}}) - I(t_{\text{start}})}{T(t_{\text{end}} - t_{\text{start}})}, \tag{5.4}$$

where I_* are the numbers of infected cells in the start and the end of the experiment, T is the CTL number and t_* are the experiment time points. For our system, the PCKR lies in the range of 2-10 cells/CTL/day. However, the PCKR depends on the CTL number and the duration of the experiment and I would not recommend to use it for comparison.

Probabilistic model

CTL killing kinetics was also investigated from a probabilistic point of view. For example, in the analysis of Cr assay data [163] it was concluded that T cells deliver lethal hits at random times (and sequentially,

CTL number	p-value
2	5.7e-01
3	1.7e-04
4	1.3e-02
5	2.3e-02
6	1.2e-01
7	3.0e-01
9	5.8e-01
14	8.9e-01

Table 5.1: The p-value from the binomial test for observed frequencies of CTL killing.

if there are several targets). Here I assume that for a given CTL-target contact there is a certain probability that the CTL delivers a lethal hit. I used *in vivo* two-photon microscopy records to estimate if the number of contacts has any impact on the probability of cell death. If there is no memory, i.e. previous contacts do not change the probability to die after the next one, then the probability to be killed can be derived from the probability of death in a single interaction p_1. Let a cell gets 3 hits, any 1 or 2 or 3 of them may be lethal ones with the same probability p_1. The probability p_{die} to be involved in at least one lethal interaction will be $p_{\text{die}} = 1 - (1 - p_1)^3$ or in general case of n interactions

$$p_{\text{die}}(n) = 1 - (1 - p_1)^n \tag{5.5}$$

I tested this hypothesis on the collected data on cell death frequency for observed numbers of contacts using the binomial test, table 5.1. Since the observation of high contact numbers for the same target is a very rare event, we did not have many experimental data and for 6 and more contacts the hypothesis of the suggested model is not rejected at the significance level of 0.05. However, for 3 and 4 contacts the targets were killed with statistically significantly higher probability than expected, hence the previous contacts with CTLs seem to contribute to the cell death.

5.3 Discussion

Here I implemented simple kinetic and probabilistic models of CTL killing and fitted them to the experimental observations generated from *in vivo* two-photon imaging. I estimated the killing efficiency of CTLs for a given experimental setup, which appeared to be in the range of 2-10 cells/CTL/day. There is no consensus about this value in the community, most probably due to varying experimental conditions. The frequency of contacts between CTL and target cells depends not on the absolute number of cells but on their concentrations. For different sites of the body the motility of CTLs may vary as well as the density of infected cells. These factors will contribute to differences in PCKR and k estimations.

The most interesting result is the analysis of single cell interactions which shows that the process of killing has memory, i.e. the probability of target cell death depends on its contact history. The probability increases already after 3 contacts with CTLs. Experimental data about contact times and *Ca* signalling

in target cells might give more information about CTL killing activity. Such modelling may describe the phenomena and invoke new questions and experiments in the CTL biology.

6

Summary and Outlook

In the previous chapters, I applied mathematical modelling approaches to describe processes in the immune system. These methods allow to quantitatively estimate parameters of the systems and to test hypothesis about a possible mechanism. In the case of CTL killing model, I used a simple kinetic model to estimate the range for CTL killing rate, and showed that previous contacts with T cells change the probability of a target cell to die. This result shows that the killing process has memory, i.e. previous contacts influence fate of target cells.

In the field of mathematical modelling one often faces a lack of experimental data, but in certain cases one may perform simulations in order to see the qualitative behaviour of the system and to suggest new experiments in this direction. In our model of interacting GCs, I compare the development of GCs in the early and the late environments and hypothesize that early GCs may suppress the later ones. A more precise model can be based on experiments in which individual GC kinetics is measured depending on the concentration of antigen specific antibodies if artificially injected.

Biological systems consist of objects which perform their function at different scales. This demands to construct multi-scale models and to implement a variety of approaches. In the GC model, I use ODE to describe cell populations and antibody concentrations, where spatial aspects were not considered. However, modelling of cell clustering demands description of molecular diffusion and cell behaviour defined by its location. Multiscale modelling is a developing branch of computational biology, however, there are no established standard frameworks for simulations. In contrast, ODE models may utilise any of available ODE solvers implemented in a variety of programming languages. Construction of 3D agent-based models involves a high number of assumptions about details which are neglected in population-based ODE models. It results in a challenge of model parametrisation and extensive literature analysis for available data. In addition, a modeller has to make a decision on the question about which processes are to be included into the model and which of them can be neglected. Although it does not represent any technical knowledge about mathematical modelling, this is a very important aspect which may influence the direction of model development and demands effective communication with clinical experts. In this project, I developed a framework which includes efficient collision detection between migrating cells, description of chemokine diffusion and its internalisation due to binding

to the receptors. Although it may reproduce cell clustering around cells which secrete the chemokine, there is a number of possible improvements in terms of implementation. Firstly, the collision algorithm and diffusion solver can be parallelised in order to handle bigger systems with more participating cells and to describe chemokine profiles with higher precision. Secondly, the chemokine concentration could be described using finite element method. This approach is more flexible in terms of form of simulated domain, i.e. it allows to more easily adapt PDE to domains of arbitrary shape, and, hence, to incorporate more details about organ structure. Another benefit of using finite element method is more precise modelling of chemokine secretion, because a node of the finite element mesh can be positioned exactly to the location of the secreting cell.

Additionally, the simulation outcome is not represented by a single measurable value, but by the list of cell positions and chemokine concentrations instead. Here we face the problem of comparison of the model simulation with patient biopsies which is to be resolved in the future. The kinetic rates of receptor dynamics and chemokine binding measured for CXCR5-CXCL13 receptor-ligand pair or similar molecules allowed us to estimate characteristics of clustering, such as trapping distances or receptor densities at which gradient inversion is possible. The missing part from experimental support is in the information about stroma activation. The knowledge of critical contacts frequency needed for stroma differentiation would allow to model cluster formation more precisely in the condition of lymphocyte influx into the tissue.

Apart of fundamental interest, mathematical modelling of immune responses might have implications in clinics. Simulation of GC reactions might help in optimization of immunization conditions in order to boost the immune response and to select more affine B cell clones, since there is a way to influence the selection process via injections of specific antibodies. Although the GC model has not been applied to any patient data yet, the other two projects, namely, the model of TLO development and the model of CTL killing, were developed in close communication with our clinical partners.

Immunosuppressive therapy is an approach to control conditions of kidney transplants. The usage of anti-CD20 antibodies (e.g. Rituximab) results in depletion of the B cell population. Although this help to decrease graft damage, which is caused by antibody-mediated response, the suppressed immune system can not efficiently eliminate infected or cancer cells. In order to diminish side effects of the immunosupperssion, the dosage of the treatment can be controlled according to graft biopsy results. For example, if there will be a direct evidence of the contribution of TLOs in graft rejection in human, mathematical modelling might provide suggestions for the treatment in order to avoid formation of this structures. In this case, the agent-based model might predict the probability for stromal cell activation on the basis of the lymphocyte densities in biopsies of transplanted grafts, which would result in a suggestion about increase or decrease of treatment dose. Unfortunately, we lack the information about stroma activation mechanisms. Additional experiments, which are directed on the quantification of

stroma activation for different lymphocytes densities, could help to fit the agent-based model in order to generate biopsy-based predictions.

TLOs are observed not only in transplantation, but in autoimmune diseases, e.g. rheumatoid arthritis. These immune cell clusters were shown to be a source of auto-antigenic cells. If the treatment directed against TLO formation can be used for such conditions, the information about cluster stability may be taken into consideration during adjustment of anti-chemokine or receptor antagonist therapies. Injection of receptor antagonists can block lymphocyte navigation, which would result in cluster dissolution. Ideally, the outcome of the model would be suggestion of a dose of therapeutic agent, which can block long-range cell interactions governed by chemokine gradients. If this kind of therapy could be used together with or substitute anti-CD20 treatment, which is currently used in many cases, patients might benefit because there will be reduced depletion of the whole B cell population. Moreover, local administration of the therapeutic agent would prevent only cell clustering in the graft.

Although the current model does not provide predictions about TLO formation in the context of patient tissue and can not be used in clinics right now, with this work I hope to provoke new experiments in order to identify the role of immune cell clusters in graft rejection and other pathological conditions.

Another example for application of mathematical modelling is CTL-based therapy. Adoptive transfer of T cells is a very promising approach which can be used to treat cancer or infection diseases. Quantitative characterisation of CTL killing efficiency might help to optimise therapy effect and its costs. In order to know, how many cells are needed to be delivered to a patient, one needs to estimate the killing rate by CTLs *in vivo*. Mathematical models of killing kinetics can provide these estimations and predict population dynamics in time. Besides killing rate estimations, I show that multiple contacts can dramatically increase probability of infected cells to die. This result raises a question of mechanisms of CTL killing which is very interesting in the context of fundamental T cell biology.

A

Analysis of GC size in spleen samples

The power of immune response varies among different immunisation conditions, and antibody feedback might be changed too, what may influence GC size.

To compare germinal centre size in different immunisation conditions we analysed microscopy images of spleen samples from mice which were immunised only intravenously or intravenously and into food pad. We used the Python interface to OpenCV computer vision library[25].

The samples were stained for PNA-binding GC B cells (green) and for surface immunoglobulin IgD, which is expressed at the surface of naive B cells in B cell follicles (red), see fig. A.1. The median filter was applied to the images in order to decrease noise and to delete small nonspecific staining areas. After then images were subjected to thresholding with the threshold value chosen according to visual evaluation of the result and applied to all images. The GCs area was measured using ImageJ[2] by manually picking specifically stained green areas in the red follicles.

Comparison of GC sizes from samples coded as 1-4 for intravenous immunisation and 5-7 for intravenous and foot pad immunisation did not show any significant difference (Wilcoxon test with p-value 0.54). Experiments with other form of immunisation like intraperitoneal or comparison between organs, for example, GC sizes in spleen versus LNs, may help to estimate the impact of antibodies onto GC reaction.

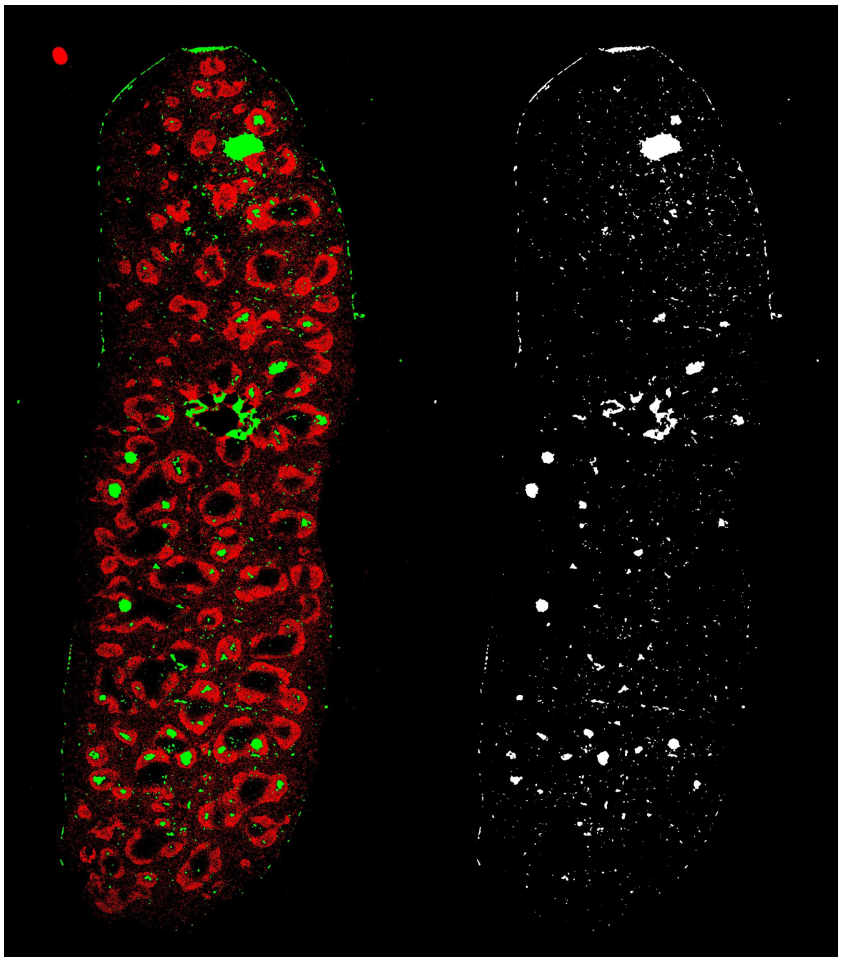

Figure A.1: Processed image of the spleen splice. Green arease correspond to GC B cells (PNA) and is shown separately at the right image. Red regions are B cell follicles stained with anti-IgD antibodies. The samples contains nonspecific staining, hence GC areas were selected manually.

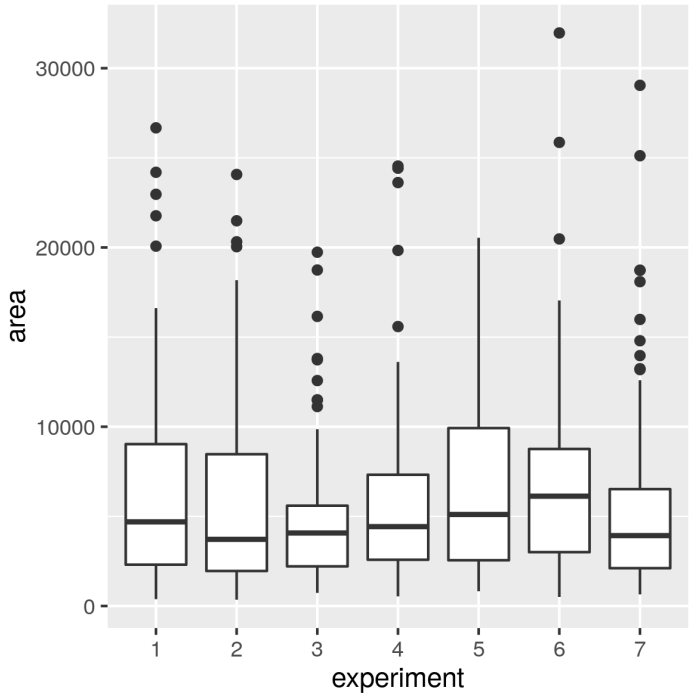

Figure A.2: GC size in i.v. immunisation (1-4 experiments) and i.v. + footpad (5-7)

Bibliography

[1] Abbas, A., Lichtman, A., and Pillai, S. (2010). *Cellular and molecular immunology*. Philadelphia, PA: Saunders.

[2] Abràmoff, M. D., Magalhães, P. J., and Ram, S. J. (2004). Image processing with imagej. *Biophotonics international*, 11(7):36–42.

[3] Acton, S. E., Astarita, J. L., Malhotra, D., Lukacs-Kornek, V., Franz, B., Hess, P. R., Jakus, Z., Kuligowski, M., Fletcher, A. L., Elpek, K. G., et al. (2012). Podoplanin-rich stromal networks induce dendritic cell motility via activation of the c-type lectin receptor clec-2. *Immunity*, 37(2):276–289.

[4] Acton, S. E., Farrugia, A. J., Astarita, J. L., Mourão-Sá, D., Jenkins, R. P., Nye, E., Hooper, S., van Blijswijk, J., Rogers, N. C., Snelgrove, K. J., et al. (2014). Dendritic cells control fibroblastic reticular network tension and lymph node expansion. *Nature*, 514(7523):498–502.

[5] Ademokun, A., Wu, Y.-C., Martin, V., Mitra, R., Sack, U., Baxendale, H., Kipling, D., and Dunn-Walters, D. K. (2011). Vaccination-induced changes in human B-cell repertoire and pneumococcal igm and iga antibody at different ages. *Aging cell*, 10(6):922–930.

[6] Aguzzi, A., Kranich, J., and Krautler, N. J. (2014). Follicular dendritic cells: origin, phenotype, and function in health and disease. *Trends in immunology*, 35(3):105–113.

[7] Aliahmad, P., de la Torre, B., and Kaye, J. (2010). Shared dependence on the dna-binding factor tox for the development of lymphoid tissue-inducer cell and nk cell lineages. *Nature immunology*, 11(10):945–952.

[8] Allen, C. D. and Cyster, J. G. (2008). Follicular dendritic cell networks of primary follicles and germinal centers: phenotype and function. In *Seminars in immunology*, volume 20, pages 14–25. Elsevier.

[9] Allen, C. D., Okada, T., Tang, H. L., and Cyster, J. G. (2007). Imaging of germinal center selection events during affinity maturation. *Science*, 315(5811):528–531.

[10] Aloisi, F. and Pujol-Borrell, R. (2006). Lymphoid neogenesis in chronic inflammatory diseases. *Nature Reviews Immunology*, 6(3):205–217.

[11] Amé-Thomas, P., Maby-El Hajjami, H., Monvoisin, C., Jean, R., Monnier, D., Caulet-Maugendre, S., Guillaudeux, T., Lamy, T., Fest, T., and Tarte, K. (2007). Human mesenchymal stem cells isolated from bone marrow and lymphoid organs support tumor b-cell growth: role of stromal cells in follicular lymphoma pathogenesis. *Blood*, 109(2):693–702.

[12] Ansel, K. M., Ngo, V. N., Hyman, P. L., Luther, S. A., Förster, R., Sedgwick, J. D., Browning, J. L., Lipp, M., and Cyster, J. G. (2000). A chemokine-driven positive feedback loop organizes lymphoid follicles. *Nature*, 406(6793):309–314.

[13] Aspinall, R., Del Giudice, G., Effros, R. B., Grubeck-Loebenstein, B., and Sambhara, S. (2007). Challenges for vaccination in the elderly. *Immun Ageing*, 4(9):1807–1814.

[14] Astarita, J. L., Cremasco, V., Fu, J., Darnell, M. C., Peck, J. R., Nieves-Bonilla, J. M., Song, K., Kondo, Y., Woodruff, M. C., Gogineni, A., et al. (2015). The clec-2-podoplanin axis controls the contractility of fibroblastic reticular cells and lymph node microarchitecture. *Nature immunology*, 16(1):75–84.

[15] Aydar, Y., Wu, J., Song, J., Szakal, A. K., and Tew, J. G. (2004). FcγRII expression on follicular dendritic cells and immunoreceptor tyrosine-based inhibition motif signaling in B cells. *European journal of immunology*, 34(1):98–107.

[16] Bajénoff, M. and Germain, R. N. (2009). B-cell follicle development remodels the conduit system and allows soluble antigen delivery to follicular dendritic cells. *Blood*, 114(24):4989–4997.

[17] Bandi, S. and Thalmann, D. (1995). An adaptive spatial subdivision of the object space for fast collision detection of animated rigid bodies. In *Computer Graphics Forum*, volume 14, pages 259–270. Wiley Online Library.

[18] Bar-Even, A., Paulsson, J., Maheshri, N., Carmi, M., O'Shea, E., Pilpel, Y., and Barkai, N. (2006). Noise in protein expression scales with natural protein abundance. *Nature genetics*, 38(6):636–643.

[19] Baraff, D. (1992). *Dynamic simulation of non-penetrating rigid body simulation*. PhD thesis, PhD thesis, Cornell University.

[20] Barone, F., Bombardieri, M., Rosado, M. M., Morgan, P. R., Challacombe, S. J., De Vita, S., Carsetti, R., Spencer, J., Valesini, G., and Pitzalis, C. (2008). Cxcl13, ccl21, and cxcl12 expression in salivary glands of patients with sjögren's syndrome and malt lymphoma: association with reactive and malignant areas of lymphoid organization. *The Journal of Immunology*, 180(7):5130–5140.

[21] Barroso, R., Muñoz, L. M., Barrondo, S., Vega, B., Holgado, B. L., Lucas, P., Baíllo, A., Sallés, J., Rodríguez-Frade, J. M., and Mellado, M. (2012). Ebi2 regulates cxcl13-mediated responses by heterodimerization with cxcr5. *The FASEB Journal*, 26(12):4841–4854.

[22] Batista, F. D., Arana, E., Barral, P., Carrasco, Y. R., Depoil, D., Eckl-Dorna, J., Fleire, S., Howe, K., Vehlow, A., Weber, M., et al. (2007). The role of integrins and coreceptors in refining thresholds for B-cell responses. *Immunological reviews*, 218(1):197–213.

[23] Bellmann-Sickert, K. and Beck-Sickinger, A. G. (2011). Palmitoylated sdf1 α shows increased resistance against proteolytic degradation in liver homogenates. *ChemMedChem*, 6(1):193–200.

[24] Bentley, J. L. and Friedman, J. H. (1979). Data structures for range searching. *ACM Computing Surveys (CSUR)*, 11(4):397–409.

[25] Bradski, G. et al. (2000). The opencv library. *Doctor Dobbs Journal*, 25(11):120–126.

[26] Brendolan, A. and Caamaño, J. H. (2012). Mesenchymal cell differentiation during lymph node organogenesis. *Frontiers in immunology*, 3.

[27] Browning, J. L., Allaire, N., Ngam-ek, A., Notidis, E., Hunt, J., Perrin, S., and Fava, R. A. (2005). Lymphotoxin-β receptor signaling is required for the homeostatic control of hev differentiation and function. *Immunity*, 23(5):539–550.

[28] Brunner, K., Mauel, J., Cerottini, J.-C., and Chapuis, B. (1968). Quantitative assay of the lytic action of immune lymphoid cells of 51cr-labelled allogeneic target cells in vitro; inhibition by isoantibody and by drugs. *Immunology*, 14(2):181.

[29] Buckley, C. D., Barone, F., Nayar, S., Bénézech, C., and Caamaño, J. (2015). Stromal cells in chronic inflammation and tertiary lymphoid organ formation. *Annual review of immunology*, 33:715–745.

[30] Butcher, J. (2003). *Numerical Methods for Ordinary Differential Equations*. Wiley.

[31] Caamaño, J. H., Rizzo, C. A., Durham, S. K., Barton, D. S., Raventós-Suárez, C., Snapper, C. M., and Bravo, R. (1998). Nuclear factor (nf)-κb2 (p100/p52) is required for normal splenic microarchitecture and b cell–mediated immune responses. *The Journal of experimental medicine*, 187(2):185–196.

[32] Carlsen, H. S., Baekkevold, E. S., Morton, H. C., Haraldsen, G., and Brandtzaeg, P. (2004). Monocyte-like and mature macrophages produce cxcl13 (b cell–attracting chemokine 1) in inflammatory lesions with lymphoid neogenesis. *Blood*, 104(10):3021–3027.

[33] Carrasco, Y. R. and Batista, F. D. (2006). B cell recognition of membrane-bound antigen: an exquisite way of sensing ligands. *Current opinion in immunology*, 18(3):286–291.

[34] Carslaw, H. S. (1921). Introduction to the mathematical theory of the conduction of heat in solids. *Lon don*.

[35] Castagnaro, L., Lenti, E., Maruzzelli, S., Spinardi, L., Migliori, E., Farinello, D., Sitia, G., Harrelson, Z., Evans, S. M., Guidotti, L. G., et al. (2013). Nkx2-5+ islet1+ mesenchymal precursors generate distinct spleen stromal cell subsets and participate in restoring stromal network integrity. *Immunity*, 38(4):782–791.

[36] Cavnar, S., Ray, P., Moudgil, P., Chang, S., Luker, K., Linderman, J., Takayama, S., and Luker, G. (2014). Microfluidic source-sink model reveals effects of biophysically distinct cxcl12 isoforms in breast cancer chemotaxis. *Integrative Biology*, 6(5):564–576.

[37] Chang, S. L., Cavnar, S. P., Takayama, S., Luker, G. D., and Linderman, J. J. (2015). Cell, isoform, and environment factors shape gradients and modulate chemotaxis.

[38] Chapman, S. and Cowling, T. (1991). The mathematical theory of non-uniform gases. *The Mathematical Theory of Non-uniform Gases, by Sydney Chapman and TG Cowling and Foreword by C. Cercignani, pp. 447. ISBN 052140844X. Cambridge, UK: Cambridge University Press, January 1991.*, 1.

[39] Chen, S.-C., Vassileva, G., Kinsley, D., Holzmann, S., Manfra, D., Wiekowski, M. T., Romani, N., and Lira, S. A. (2002). Ectopic expression of the murine chemokines ccl21a and ccl21b induces the formation of lymph node-like structures in pancreas, but not skin, of transgenic mice. *The Journal of Immunology*, 168(3):1001–1008.

[40] Chernick, M. R. (2011). *Bootstrap methods: A guide for practitioners and researchers*, volume 619. John Wiley & Sons.

[41] Chieppa, M., Bianchi, G., Doni, A., Del Prete, A., Sironi, M., Laskarin, G., Monti, P., Piemonti, L., Biondi, A., Mantovani, A., et al. (2003). Cross-linking of the mannose receptor on monocyte-derived dendritic cells activates an anti-inflammatory immunosuppressive program. *The Journal of Immunology*, 171(9):4552–4560.

[42] Clatworthy, M. R., Watson, C. J., Plotnek, G., Bardsley, V., Chaudhry, A. N., Bradley, J. A., and Smith, K. G. (2009). B-cell–depleting induction therapy and acute cellular rejection. *New England Journal of Medicine*, 360(25):2683–2685.

[43] Coelho, F. M., Natale, D., Soriano, S. F., Hons, M., Swoger, J., Mayer, J., Danuser, R., Scandella, E., Pieczyk, M., Zerwes, H.-G., et al. (2013). Naive b-cell trafficking is shaped by local chemokine availability and lfa-1–independent stromal interactions. *Blood*, 121(20):4101–4109.

[44] Coggins, N. L., Trakimas, D., Chang, S. L., Ehrlich, A., Ray, P., Luker, K. E., Linderman, J. J., and Luker, G. D. (2014). Cxcr7 controls competition for recruitment of β-arrestin 2 in cells expressing both cxcr4 and cxcr7.

[45] Cohen, J. D., Lin, M. C., Manocha, D., and Ponamgi, M. (1995). I-collide: An interactive and exact collision detection system for large-scale environments. In *Proceedings of the 1995 symposium on Interactive 3D graphics*, pages 189–ff. ACM.

[46] Cording, S., Wahl, B., Kulkarni, D., Chopra, H., Pezoldt, J., Buettner, M., Dummer, A., Hadis, U., Heimesaat, M., Bereswill, S., et al. (2014). The intestinal micro-environment imprints stromal cells to promote efficient treg induction in gut-draining lymph nodes. *Mucosal immunology*, 7(2):359–368.

[47] Crotty, S. (2011). Follicular Helper CD4 T Cells (Tfh). *Annual review of immunology*, 29:621–663.

[48] Cupedo, T., Jansen, W., Kraal, G., and Mebius, R. E. (2004). Induction of secondary and tertiary lymphoid structures in the skin. *Immunity*, 21(5):655–667.

[49] Demetris, A., Murase, N., Lee, R., Randhawa, P., Zeevi, A., Pham, S., Duquesnoy, R., Fung, J., and Starzl, T. (1997). Chronic rejection. a general overview of histopathology and pathophysiology with emphasis on liver, heart and intestinal allografts. *Annals of transplantation: quarterly of the Polish Transplantation Society*, 2(2):27.

[50] Dent, A. L., Shaffer, A. L., Yu, X., Allman, D., and Staudt, L. M. (1997). Control of inflammation, cytokine expression, and germinal center formation by bcl-6. *Science*, 276(5312):589–592.

[51] Depoil, D., Zaru, R., Guiraud, M., Chauveau, A., Harriague, J., Bismuth, G., Utzny, C., Müller, S., and Valitutti, S. (2005). Immunological synapses are versatile structures enabling selective T cell polarization. *Immunity*, 22(2):185–194.

[52] Dong, H. P., Elstrand, M. B., Holth, A., Silins, I., Berner, A., Trope, C. G., Davidson, B., and Risberg, B. (2006). Nk-and b-cell infiltration correlates with worse outcome in metastatic ovarian carcinoma. *American journal of clinical pathology*, 125(3):451–458.

[53] Dougall, W. C., Glaccum, M., Charrier, K., Rohrbach, K., Brasel, K., De Smedt, T., Daro, E., Smith, J., Tometsko, M. E., Maliszewski, C. R., et al. (1999). Rank is essential for osteoclast and lymph node development. *Genes & development*, 13(18):2412–2424.

[54] Dudley, M. E. and Rosenberg, S. A. (2003). Adoptive-cell-transfer therapy for the treatment of patients with cancer. *Nature Reviews Cancer*, 3(9):666–675.

[55] Dustin, M. L. and Meyer-Hermann, M. (2012). Antigen feast or famine. *Science*, 335(6067):408–409.

[56] Eberl, G., Marmon, S., Sunshine, M.-J., Rennert, P. D., Choi, Y., and Littman, D. R. (2004). An essential function for the nuclear receptor rorγt in the generation of fetal lymphoid tissue inducer cells. *Nature immunology*, 5(1):64–73.

[57] Ehrenstein, M. R., O'Keefe, T. L., Davies, S. L., and Neuberger, M. S. (1998). Targeted gene disruption reveals a role for natural secretory igm in the maturation of the primary immune response. *Proceedings of the National Academy of Sciences*, 95(17):10089–10093.

[58] Eisen, H. N. (2014). Affinity enhancement of antibodies: How low-affinity antibodies produced early in immune responses are followed by high-affinity antibodies later and in memory B-cell responses. *Cancer immunology research*, 2(5):381–392.

[59] Eisen, H. N. and Siskind, G. W. (1964). Variations in affinities of antibodies during the immune response. *Biochemistry*, 3(7):996–1008.

[60] Ekland, E. H., Forster, R., Lipp, M., and Cyster, J. G. (2004). Requirements for follicular exclusion and competitive elimination of autoantigen-binding b cells. *The Journal of Immunology*, 172(8):4700–4708.

[61] Emilie, D., Devergne, O., Raphael, M., Coumbaras, L., and Galanaud, P. (1992). Production of interleukin-6 in high grade b lymphomas. In *Mechanisms in B-Cell Neoplasia 1992*, pages 349–355. Springer.

[62] Figge, M. T., Garin, A., Gunzer, M., Kosco-Vilbois, M., Toellner, K.-M., and Meyer-Hermann, M. (2008). Deriving a germinal center lymphocyte migration model from two-photon data. *The Journal of experimental medicine*, 205(13):3019–3029.

[63] Fleige, H., Haas, J. D., Stahl, F. R., Willenzon, S., Prinz, I., and Förster, R. (2012). Induction of balt in the absence of il-17. *Nature immunology*, 13(1):1–1.

[64] Fleige, H., Ravens, S., Moschovakis, G. L., Bölter, J., Willenzon, S., Sutter, G., Häussler, S., Kalinke, U., Prinz, I., and Förster, R. (2014). Il-17–induced cxcl12 recruits b cells and induces follicle formation in balt in the absence of differentiated fdcs. *The Journal of experimental medicine*, 211(4):643–651.

[65] Fletcher, A. L., Acton, S. E., and Knoblich, K. (2015). Lymph node fibroblastic reticular cells in health and disease. *Nature Reviews Immunology*, 15(6):350–361.

[66] Fletcher, A. L., Lukacs-Kornek, V., Reynoso, E. D., Pinner, S. E., Bellemare-Pelletier, A., Curry, M. S., Collier, A.-R., Boyd, R. L., and Turley, S. J. (2010). Lymph node fibroblastic reticular cells directly present peripheral tissue antigen under steady-state and inflammatory conditions. *The Journal of experimental medicine*, 207(4):689–697.

[67] Fletcher, A. L., Malhotra, D., and Turley, S. J. (2011). Lymph node stroma broaden the peripheral tolerance paradigm. *Trends in immunology*, 32(1):12–18.

[68] Franzoso, G., Carlson, L., Poljak, L., Shores, E. W., Epstein, S., Leonardi, A., Grinberg, A., Tran, T., Scharton-Kersten, T., Anver, M., et al. (1998). Mice deficient in nuclear factor (nf)-κb/p52 present with defects in humoral responses, germinal center reactions, and splenic microarchitecture. *The Journal of experimental medicine*, 187(2):147–159.

[69] Fu, Y.-X. and Chaplin, D. D. (1999). Development and maturation of secondary lymphoid tissues. *Annual review of immunology*, 17(1):399–433.

[70] Garin, A., Meyer-Hermann, M., Contie, M., Figge, M. T., Buatois, V., Gunzer, M., Toellner, K.-M., Elson, G., and Kosco-Vilbois, M. H. (2010). Toll-like receptor 4 signaling by follicular dendritic cells is pivotal for germinal center onset and affinity maturation. *Immunity*, 33(1):84–95.

[71] Geherin, S. A., Fintushel, S. R., Lee, M. H., Wilson, R. P., Patel, R. T., Alt, C., Young, A. J., Hay, J. B., and Debes, G. F. (2012). The skin, a novel niche for recirculating b cells. *The Journal of Immunology*, 188(12):6027–6035.

[72] Georgopoulos, K., Bigby, M., Wang, J.-H., Molnar, A., Wu, P., Winandy, S., and Sharpe, A. (1994). The ikaros gene is required for the development of all lymphoid lineages. *Cell*, 79(1):143–156.

[73] Germain, C., Gnjatic, S., and Dieu-Nosjean, M.-C. (2015). Tertiary lymphoid structure-associated b cells are key players in anti-tumor immunity. *Frontiers in immunology*, 6.

[74] Germain, C., Gnjatic, S., Tamzalit, F., Knockaert, S., Remark, R., Goc, J., Lepelley, A., Becht, E., Katsahian, S., Bizouard, G., et al. (2014). Presence of b cells in tertiary lymphoid structures is associated with a protective immunity in patients with lung cancer. *American journal of respiratory and critical care medicine*, 189(7):832–844.

[75] GeurtsvanKessel, C. H., Willart, M. A., Bergen, I. M., van Rijt, L. S., Muskens, F., Elewaut, D., Osterhaus, A. D., Hendriks, R., Rimmelzwaan, G. F., and Lambrecht, B. N. (2009). Dendritic cells are crucial for maintenance of tertiary lymphoid structures in the lung of influenza virus–infected mice. *The Journal of experimental medicine*, 206(11):2339–2349.

[76] Gnjatic, S., Ritter, E., Büchler, M. W., Giese, N. A., Brors, B., Frei, C., Murray, A., Halama, N., Zörnig, I., Chen, Y.-T., et al. (2010). Seromic profiling of ovarian and pancreatic cancer. *Proceedings of the National Academy of Sciences*, 107(11):5088–5093.

[77] Gonzalez, S. F., Lukacs-Kornek, V., Kuligowski, M. P., Pitcher, L. A., Degn, S. E., Kim, Y.-A., Cloninger, M. J., Martinez-Pomares, L., Gordon, S., Turley, S. J., et al. (2010). Capture of influenza by medullary dendritic cells via sign-r1 is essential for humoral immunity in draining lymph nodes. *Nature immunology*, 11(5):427–434.

[78] Good-Jacobson, K. L. and Shlomchik, M. J. (2010). Plasticity and heterogeneity in the generation of memory B cells and long-lived plasma cells: the influence of germinal center interactions and dynamics. *The Journal of Immunology*, 185(6):3117–3125.

[79] Graw, F. and Regoes, R. R. (2009). Investigating ctl mediated killing with a 3d cellular automaton. *PLoS Comput Biol*, 5(8):e1000466.

[80] Halle, S., Dujardin, H. C., Bakocevic, N., Fleige, H., Danzer, H., Willenzon, S., Suezer, Y., Hämmerling, G., Garbi, N., Sutter, G., et al. (2009). Induced bronchus-associated lymphoid tissue serves as a general priming site for t cells and is maintained by dendritic cells. *The Journal of experimental medicine*, 206(12):2593–2601.

[81] Han, S., Yang, K., Ozen, Z., Peng, W., Marinova, E., Kelsoe, G., and Zheng, B. (2003). Enhanced differentiation of splenic plasma cells but diminished long-lived high-affinity bone marrow plasma cells in aged mice. *The Journal of Immunology*, 170(3):1267–1273.

[82] Hanayama, R., Tanaka, M., Miwa, K., Shinohara, A., Iwamatsu, A., and Nagata, S. (2002). Identification of a factor that links apoptotic cells to phagocytes. *Nature*, 417(6885):182–187.

[83] Hanayama, R., Tanaka, M., Miyasaka, K., Aozasa, K., Koike, M., Uchiyama, Y., and Nagata, S. (2004). Autoimmune disease and impaired uptake of apoptotic cells in mfg-e8-deficient mice. *Science*, 304(5674):1147–1150.

[84] Hauser, A. E., Junt, T., Mempel, T. R., Sneddon, M. W., Kleinstein, S. H., Henrickson, S. E., von Andrian, U. H., Shlomchik, M. J., and Haberman, A. M. (2007). Definition of germinal-center B cell migration in vivo reveals predominant intrazonal circulation patterns. *Immunity*, 26(5):655–667.

[85] Heesters, B. A., Chatterjee, P., Kim, Y.-A., Gonzalez, S. F., Kuligowski, M. P., Kirchhausen, T., and Carroll, M. C. (2013). Endocytosis and recycling of immune complexes by follicular dendritic cells enhances b cell antigen binding and activation. *Immunity*, 38(6):1164–1175.

[86] Heesters, B. A., Myers, R. C., and Carroll, M. C. (2014). Follicular dendritic cells: dynamic antigen libraries. *Nature Reviews Immunology*, 14(7):495–504.

[87] Henry, R. A. and Kendall, P. L. (2010). Cxcl13 blockade disrupts b lymphocyte organization in tertiary lymphoid structures without altering b cell receptor bias or preventing diabetes in nonobese diabetic mice. *The Journal of Immunology*, 185(3):1460–1465.

[88] Herzog, B. H., Fu, J., Wilson, S. J., Hess, P. R., Sen, A., McDaniel, J. M., Pan, Y., Sheng, M., Yago, T., Silasi-Mansat, R., et al. (2013). Podoplanin maintains high endothelial venule integrity by interacting with platelet clec-2. *Nature*, 502(7469):105–109.

[89] Hesselgesser, J., Liang, M., Hoxie, J., Greenberg, M., Brass, L. F., Orsini, M. J., Taub, D., and Horuk, R. (1998). Identification and characterization of the cxcr4 chemokine receptor in human t cell lines: ligand binding, biological activity, and hiv-1 infectivity. *The Journal of Immunology*, 160(2):877–883.

[90] Hruban, R., Beschorner, W., Baumgartner, W., Achuff, S., Traill, T., Digennaro, K., Reitz, B., and Hutchins, G. (1988). Depletion of bronchus-associated lymphoid tissue associated with lung allograft rejection. *The American journal of pathology*, 132(1):6.

[91] Hsao, H.-M., Li, W., Gelman, A. E., Krupnick, A. S., and Kreisel, D. (2015). The role of lymphoid neogenesis in allografts. *American Journal of Transplantation*.

[92] Huggenberger, R., Siddiqui, S. S., Brander, D., Ullmann, S., Zimmermann, K., Antsiferova, M., Werner, S., Alitalo, K., and Detmar, M. (2011). An important role of lymphatic vessel activation in limiting acute inflammation. *Blood*, 117(17):4667–4678.

[93] Inglis, D. W., Davis, J. A., Zieziulewicz, T. J., Lawrence, D. A., Austin, R. H., and Sturm, J. C. (2008). Determining blood cell size using microfluidic hydrodynamics. *Journal of immunological methods*, 329(1):151–156.

[94] Issa, A., Le, T. X., Shoushtari, A. N., Shields, J. D., and Swartz, M. A. (2009). Vascular endothelial growth factor-c and cc chemokine receptor 7 in tumor cell–lymphatic cross-talk promote invasive phenotype. *Cancer research*, 69(1):349–357.

[95] Jacob, J., Kassir, R., and Kelsoe, G. (1991). In situ studies of the primary immune response to (4-hydroxy-3-nitrophenyl) acetyl. I. the architecture and dynamics of responding cell populations. *The Journal of experimental medicine*, 173(5):1165–1175.

[96] Jonker, M., Wubben, J. A., A't Hart, B., and Haanstra, K. G. (2015). Lymphoid-like structures with distinct b cell areas in kidney allografts are not predictive for graft rejection. a non-human primate study. *Inflammation*, 38(6):2191–2202.

[97] Katakai, T., Hara, T., Sugai, M., Gonda, H., and Shimizu, A. (2004). Lymph node fibroblastic reticular cells construct the stromal reticulum via contact with lymphocytes. *The Journal of experimental medicine*, 200(6):783–795.

[98] Katakai, T., Suto, H., Sugai, M., Gonda, H., Togawa, A., Suematsu, S., Ebisuno, Y., Katagiri, K., Kinashi, T., and Shimizu, A. (2008). Organizer-like reticular stromal cell layer common to adult secondary lymphoid organs. *The Journal of Immunology*, 181(9):6189–6200.

[99] Kauffman, S. A. and Perelson, A. S. (1991). *Molecular evolution on rugged landscapes: proteins, RNA, and the immune system : the proceedings of the Workshop on Applied Molecular Evolution and the Maturation of the Immune Response*. Addison Wesley, first edition.

[100] Kepler, T. B. and Perelson, A. S. (1993). Cyclic re-entry of germinal center b cells and the efficiency of affinity maturation. *Immunology today*, 14(8):412–415.

[101] Keşmir, C. and De Boer, R. J. (1999). A mathematical model on germinal center kinetics and termination. *The Journal of Immunology*, 163(5):2463–2469.

[102] Khader, S. A., Rangel-Moreno, J., Fountain, J. J., Martino, C. A., Reiley, W. W., Pearl, J. E., Winslow, G. M., Woodland, D. L., Randall, T. D., and Cooper, A. M. (2009). In a murine tuberculosis model, the absence of homeostatic chemokines delays granuloma formation and protective immunity. *The Journal of Immunology*, 183(12):8004–8014.

[103] Koopman, G., Keehnen, R. M., Lindhout, E., Newman, W., Shimizu, Y., Van Seventer, G., De Groot, C., and Pals, S. T. (1994). Adhesion through the lfa-1 (cd11a/cd18)-icam-1 (cd54) and the vla-4 (cd49d)-vcam-1 (cd106) pathways prevents apoptosis of germinal center b cells. *The Journal of Immunology*, 152(8):3760–3767.

[104] Kopf, M., Herren, S., Wiles, M. V., Pepys, M. B., and Kosco-Vilbois, M. H. (1998). Interleukin 6 influences germinal center development and antibody production via a contribution of c3 complement component. *The Journal of experimental medicine*, 188(10):1895–1906.

[105] Kosco, M., Burton, G., Kapasi, Z., Szakal, A., and Tew, J. (1989). Antibody-forming cell induction during an early phase of germinal centre development and its delay with ageing. *Immunology*, 68(3):312.

[106] Kosco-Vilbois, M. H. (2003). Are follicular dendritic cells really good for nothing? *Nature Reviews Immunology*, 3(9):764–769.

[107] Krafft, C., Salzer, R., Soff, G., and Meyer-Hermann, M. (2005). Identification of B and T cells in human spleen sections by infrared microspectroscopic imaging. *Cytometry Part A*, 64(2):53–61.

[108] Kraft, R., Bachmann, M., Bachmann, K., Buerki, H., Hess, M., Cottier, H., and Stoner, R. (1987). Satisfactory primary tetanus antitoxin responses but markedly reduced germinal centre formation in first draining lymph nodes of ageing mice. *Clinical and experimental immunology*, 67(2):447.

[109] Kranich, J., Krautler, N. J., Heinen, E., Polymenidou, M., Bridel, C., Schildknecht, A., Huber, C., Kosco-Vilbois, M. H., Zinkernagel, R., Miele, G., et al. (2008). Follicular dendritic cells control engulfment of apoptotic bodies by secreting mfge8. *The Journal of experimental medicine*, 205(6):1293–1302.

[110] Kratz, A., Campos-Neto, A., Hanson, M. S., and Ruddle, N. H. (1996). Chronic inflammation caused by lymphotoxin is lymphoid neogenesis. *The Journal of experimental medicine*, 183(4):1461–1472.

[111] Krautler, N. J., Kana, V., Kranich, J., Tian, Y., Perera, D., Lemm, D., Schwarz, P., Armulik, A., Browning, J. L., Tallquist, M., et al. (2012). Follicular dendritic cells emerge from ubiquitous perivascular precursors. *Cell*, 150(1):194–206.

[112] Ladics, T. (2012). Application of operator splitting to solve reaction-diffusion equations. *Proc. 9th Coll. QTDE*, 9:1–20.

[113] Lambeir, A.-M., Proost, P., Durinx, C., Bal, G., Senten, K., Augustyns, K., Scharpé, S., Van Damme, J., and De Meester, I. (2001). Kinetic investigation of chemokine truncation by cd26/dipeptidyl peptidase iv reveals a striking selectivity within the chemokine family. *Journal of Biological Chemistry*, 276(32):29839–29845.

[114] Lane, P., McConnell, F., Withers, D., Gaspal, F., Saini, M., and Anderson, G. (2009). Lymphoid tissue inducer cells: bridges between the ancient innate and the modern adaptive immune systems. *Mucosal immunology*, 2(6):472–477.

[115] Lane, P. J., Gaspal, F. M., McConnell, F. M., Kim, M. Y., Anderson, G., and Withers, D. R. (2012). Lymphoid tissue inducer cells: innate cells critical for cd4+ t cell memory responses? *Annals of the New York Academy of Sciences*, 1247(1):1–15.

[116] Lauffenburger, D. A., Tranquillo, R. T., and Zigmond, S. H. (1988). Concentration gradients of chemotactic factors in chemotaxis assays. *Methods in enzymology*, 162:85.

[117] Lebre, M. C., Burwell, T., Vieira, P. L., Lora, J., Coyle, A. J., Kapsenberg, M. L., Clausen, B. E., and De Jong, E. C. (2005). Differential expression of inflammatory chemokines by th1-and th2-cell promoting dendritic cells: a role for different mature dendritic cell populations in attracting appropriate effector cells to peripheral sites of inflammation. *Immunology and cell biology*, 83(5):525–535.

[118] Liang, H., Chen, Q., Coles, A. H., Anderson, S. J., Pihan, G., Bradley, A., Gerstein, R., Jurecic, R., and Jones, S. N. (2003). Wnt5a inhibits b cell proliferation and functions as a tumor suppressor in hematopoietic tissue. *Cancer cell*, 4(5):349–360.

[119] Lin, F. and Butcher, E. C. (2008). Modeling the role of homologous receptor desensitization in cell gradient sensing. *The Journal of Immunology*, 181(12):8335–8343.

[120] Link, A., Hardie, D. L., Favre, S., Britschgi, M. R., Adams, D. H., Sixt, M., Cyster, J. G., Buckley, C. D., and Luther, S. A. (2011). Association of t-zone reticular networks and conduits with ectopic lymphoid tissues in mice and humans. *The American journal of pathology*, 178(4):1662–1675.

[121] Link, A., Vogt, T. K., Favre, S., Britschgi, M. R., Acha-Orbea, H., Hinz, B., Cyster, J. G., and Luther, S. A. (2007). Fibroblastic reticular cells in lymph nodes regulate the homeostasis of naive t cells. *Nature immunology*, 8(11):1255–1265.

[122] Liu, Y.-J., Barthelemy, C., de Bouteiller, O., and Banchereau, J. (1994). The differences in survival and phenotype between centroblasts and centrocytes. In *In Vivo Immunology*, pages 213–218. Springer.

[123] Liu, Y.-J., Joshua, D. E., Williams, G. T., Smith, C. A., Gordon, J., and MacLennan, I. C. M. (1989). Mechanism of antigen-driven selection in germinal centres. *Nature*, 342(6252):929–931.

[124] Liu, Y.-J., Zhang, J., Lane, P. J., Chan, E. Y.-T., and Maclennan, I. (1991). Sites of specific B cell activation in primary and secondary responses to T cell-dependent and T cell-independent antigens. *European journal of immunology*, 21(12):2951–2962.

[125] Llopis, N. (2009). Data-oriented design (or why you might be shooting yourself in the foot with oop). http://gamesfromwithin.com/data-oriented-design.

[126] Lötzer, K., Döpping, S., Connert, S., Gräbner, R., Spanbroek, R., Lemser, B., Beer, M., Hildner, M., Hehlgans, T., van der Wall, M., et al. (2010). Mouse aorta smooth muscle cells differentiate into lymphoid tissue organizer-like cells on combined tumor necrosis factor receptor-1/lymphotoxin β-receptor nf-κb signaling. *Arteriosclerosis, thrombosis, and vascular biology*, 30(3):395–402.

[127] Lucas, T. A. (2008). Operator splitting for an immunology model using reaction-diffusion equations with stochastic source terms. *SIAM Journal on Numerical Analysis*, 46(6):3113–3135.

[128] Luther, S. A., Ansel, K. M., and Cyster, J. G. (2003). Overlapping roles of cxcl13, interleukin 7 receptor α, and ccr7 ligands in lymph node development. *The Journal of experimental medicine*, 197(9):1191–1198.

[129] Luther, S. A., Bidgol, A., Hargreaves, D. C., Schmidt, A., Xu, Y., Paniyadi, J., Matloubian, M., and Cyster, J. G. (2002). Differing activities of homeostatic chemokines ccl19, ccl21, and cxcl12 in lymphocyte and dendritic cell recruitment and lymphoid neogenesis. *The Journal of Immunology*, 169(1):424–433.

[130] Luther, S. A., Lopez, T., Bai, W., Hanahan, D., and Cyster, J. G. (2000a). Blc expression in pancreatic islets causes b cell recruitment and lymphotoxin-dependent lymphoid neogenesis. *Immunity*, 12(5):471–481.

[131] Luther, S. A., Tang, H. L., Hyman, P. L., Farr, A. G., and Cyster, J. G. (2000b). Coexpression of the chemokines elc and slc by t zone stromal cells and deletion of the elc gene in the plt/plt mouse. *Proceedings of the National Academy of Sciences*, 97(23):12694–12699.

[132] MacLennan, I. C. (1994). Germinal centers. *Annual review of immunology*, 12(1):117–139.

[133] Mandels, T., Phippsi, R., Abbot, A., and Tew, J. (1980). The follicular dendritic cell: long term antigen retention during immunity. *Immunological reviews*, 53(1):29–59.

[134] Manzo, A., Paoletti, S., Carulli, M., Blades, M. C., Barone, F., Yanni, G., FitzGerald, O., Bresnihan, B., Caporali, R., Montecucco, C., et al. (2005). Systematic microanatomical analysis of cxcl13 and ccl21 in situ production and progressive lymphoid organization in rheumatoid synovitis. *European journal of immunology*, 35(5):1347–1359.

[135] Matsumoto, M., Lo, S. F., Carruthers, C. J., Min, J., Mariathasan, S., Huang, G., Plas, D. R., Martin, S. M., Geha, R. S., Nahm, M. H., et al. (1996). Affinity maturation without germinal centres in lymphotoxin-α-deficient mice. *Nature*, 382(6590):462–466.

[136] Mazzia, F., Cash, J. R., and Soetaert, K. (2014). Solving boundary value problems in the open source software r: Package bvpsolve. *Opuscula mathematica*, 34(2):387–403.

[137] Meier, D., Bornmann, C., Chappaz, S., Schmutz, S., Otten, L. A., Ceredig, R., Acha-Orbea, H., and Finke, D. (2007). Ectopic lymphoid-organ development occurs through interleukin 7-mediated enhanced survival of lymphoid-tissue-inducer cells. *Immunity*, 26(5):643–654.

[138] Meyer-Hermann, M. (2007). A concerted action of B cell selection mechanisms. *Advances in Complex Systems*, 10(04):557–580.

[139] Meyer-Hermann, M. (2014). Overcoming the dichotomy of quantity and quality in antibody responses. *The Journal of Immunology*, 193(11):5414–5419.

[140] Meyer-Hermann, M., Deutsch, A., and Or-Guil, M. (2001). Recycling probability and dynamical properties of germinal center reactions. *Journal of Theoretical Biology*, 210(3):265–285.

[141] Meyer-Hermann, M., Mohr, E., Pelletier, N., Zhang, Y., Victora, G., and Toellner, K.-M. (2012). A Theory of Germinal Center B Cell Selection, Division, and Exit. *Cell Reports*, 2(1):162–174.

[142] Meyer-Hermann, M. E., Maini, P. K., and Iber, D. (2006). An analysis of B cell selection mechanisms in germinal centers. *Mathematical Medicine and Biology*, 23(3):255–277.

[143] Miller, M. J., Wei, S. H., Parker, I., and Cahalan, M. D. (2002). Two-photon imaging of lymphocyte motility and antigen response in intact lymph node. *Science*, 296(5574):1869–1873.

[144] Miller, R. and Dunkley, M. (1974). Quantitative analysis of the 51cr release cytotoxicity assay for cytotoxic lymphocytes. *Cellular immunology*, 14(2):284–302.

[145] Mirtich, B. (1997). Efficient algorithms for two-phase collision detection. *Practical motion planning in robotics: current approaches and future directions*, pages 203–223.

[146] Motulsky, H. J. and Brown, R. E. (2006). Detecting outliers when fitting data with nonlinear regression–a new method based on robust nonlinear regression and the false discovery rate. *BMC bioinformatics*, 7(1):123.

[147] Moyron-Quiroz, J. E., Rangel-Moreno, J., Hartson, L., Kusser, K., Tighe, M. P., Klonowski, K. D., Lefrançois, L., Cauley, L. S., Harmsen, A. G., Lund, F. E., et al. (2006). Persistence and responsiveness of immunologic memory in the absence of secondary lymphoid organs. *Immunity*, 25(4):643–654.

[148] Moyron-Quiroz, J. E., Rangel-Moreno, J., Kusser, K., Hartson, L., Sprague, F., Goodrich, S., Woodland, D. L., Lund, F. E., and Randall, T. D. (2004). Role of inducible bronchus associated lymphoid tissue (ibalt) in respiratory immunity. *Nature medicine*, 10(9):927–934.

[149] Muth, B., Müller, M.-K., Eberhard, P., and Luding, S. (2007). Collision detection and administration methods for many particles with different sizes.

[150] Myers, R. C., King, R. G., Carter, R. H., and Justement, L. B. (2013). Lymphotoxin $\alpha 1\beta 2$ expression on b cells is required for follicular dendritic cell activation during the germinal center response. *European journal of immunology*, 43(2):348–359.

[151] Nasr, I., Reel, M., Oberbarnscheidt, M., Mounzer, R., Baddoura, F., Ruddle, N., and Lakkis, F. (2007). Tertiary lymphoid tissues generate effector and memory t cells that lead to allograft rejection. *American journal of transplantation*, 7(5):1071–1079.

[152] Nehls, G. J. and Akland, G. G. (1973). Procedures for handling aerometric data. *Journal of the Air Pollution Control Association*, 23(3):180–184.

[153] Neyt, K., Perros, F., GeurtsvanKessel, C. H., Hammad, H., and Lambrecht, B. N. (2012). Tertiary lymphoid organs in infection and autoimmunity. *Trends in immunology*, 33(6):297–305.

[154] Ngo, V. N., Cornall, R. J., and Cyster, J. G. (2001). Splenic t zone development is b cell dependent. *The Journal of experimental medicine*, 194(11):1649–1660.

[155] Nieuwenhuis, P. and Opstelten, D. (1984). Functional anatomy of germinal centers. *American journal of anatomy*, 170(3):421–435.

[156] Nimmagadda, S., Pullambhatla, M., Stone, K., Green, G., Bhujwalla, Z. M., and Pomper, M. G. (2010). Molecular imaging of cxcr4 receptor expression in human cancer xenografts with [64cu] amd3100 positron emission tomography. *Cancer research*, 70(10):3935–3944.

[157] Nussenzweig, A. and Nussenzweig, M. C. (2010). Origin of chromosomal translocations in lymphoid cancer. *Cell*, 141(1):27–38.

[158] Onder, L., Danuser, R., Scandella, E., Firner, S., Chai, Q., Hehlgans, T., Stein, J. V., and Ludewig, B. (2013). Endothelial cell–specific lymphotoxin-β receptor signaling is critical for lymph node and high endothelial venule formation. *The Journal of experimental medicine*, 210(3):465–473.

[159] Onder, L., Narang, P., Scandella, E., Chai, Q., Iolyeva, M., Hoorweg, K., Halin, C., Richie, E., Kaye, P., Westermann, J., et al. (2012). Il-7–producing stromal cells are critical for lymph node remodeling. *Blood*, 120(24):4675–4683.

[160] Osada, M., Inoue, O., Ding, G., Shirai, T., Ichise, H., Hirayama, K., Takano, K., Yatomi, Y., Hirashima, M., Fujii, H., et al. (2012). Platelet activation receptor clec-2 regulates blood/lymphatic vessel separation by inhibiting proliferation, migration, and tube formation of lymphatic endothelial cells. *Journal of Biological Chemistry*, 287(26):22241–22252.

[161] Owen, J. A., Punt, J., Stranford, S. A., and Jones, P. P. (2013). *Kuby immunology*. WH Freeman New York.

[162] Pallier, A., Hillion, S., Danger, R., Giral, M., Racapé, M., Degauque, N., Dugast, E., Ashton-Chess, J., Pettré, S., Lozano, J. J., et al. (2010). Patients with drug-free long-term graft function display increased numbers of peripheral b cells with a memory and inhibitory phenotype. *Kidney international*, 78(5):503–513.

[163] Perelson, A. and Bell, G. (1982). Delivery of lethal hits by cytotoxic t lymphocytes in multicellular conjugates occurs sequentially but at random times. *The Journal of Immunology*, 129(6):2796–2801.

[164] Pham, T. H., Baluk, P., Xu, Y., Grigorova, I., Bankovich, A. J., Pappu, R., Coughlin, S. R., McDonald, D. M., Schwab, S. R., and Cyster, J. G. (2010). Lymphatic endothelial cell sphingosine kinase activity is required for lymphocyte egress and lymphatic patterning. *The Journal of experimental medicine*, 207(1):17–27.

[165] Phan, T. G., Grigorova, I., Okada, T., and Cyster, J. G. (2007). Subcapsular encounter and complement-dependent transport of immune complexes by lymph node b cells. *Nature immunology*, 8(9):992–1000.

[166] Pihlgren, M., Tougne, C., Bozzotti, P., Fulurija, A., Duchosal, M. A., Lambert, P.-H., and Siegrist, C.-A. (2003). Unresponsiveness to lymphoid-mediated signals at the neonatal follicular dendritic cell precursor level contributes to delayed germinal center induction and limitations of neonatal antibody responses to t-dependent antigens. *The Journal of Immunology*, 170(6):2824–2832.

[167] Pitzalis, C., Jones, G. W., Bombardieri, M., and Jones, S. A. (2014). Ectopic lymphoid-like structures in infection, cancer and autoimmunity. *Nature Reviews Immunology*, 14(7):447–462.

[168] Poljak, L., Carlson, L., Cunningham, K., Kosco-Vilbois, M. H., and Siebenlist, U. (1999). Distinct activities of p52/nf-κb required for proper secondary lymphoid organ microarchitecture: functions enhanced by bcl-3. *The Journal of Immunology*, 163(12):6581–6588.

[169] Pollack, S. B. and Emmons, S. L. (1979). Kinetic analysis of human spontaneous cell-mediated cytotoxicity. *The Journal of Immunology*, 123(1):160–165.

[170] Proost, P., Menten, P., Struyf, S., Schutyser, E., De Meester, I., and Van Damme, J. (2000). Cleavage by cd26/dipeptidyl peptidase iv converts the chemokine ld78β into a most efficient monocyte attractant and ccr1 agonist. *Blood*, 96(5):1674–1680.

[171] Quartuccio, L., Fabris, M., Moretti, M., Barone, F., Bombardieri, M., Rupolo, M., Lombardi, S., Pitzalis, C., Beltrami, C. A., Curcio, F., et al. (2008). Resistance to rituximab therapy and local baff overexpression in sjögren's syndrome-related myoepithelial sialadenitis and low-grade parotid b-cell lymphoma. *The open rheumatology journal*, 2(1).

[172] R Core Team (2013). *R: A Language and Environment for Statistical Computing*. R Foundation for Statistical Computing, Vienna, Austria.

[173] Rachmilewitz, J. and Lanzavecchia, A. (2002). A temporal and spatial summation model for t-cell activation: signal integration and antigen decoding. *Trends in immunology*, 23(12):592–595.

[174] Rahman, Z. S., Rao, S. P., Kalled, S. L., and Manser, T. (2003). Normal induction but attenuated progression of germinal center responses in baff and baff-r signaling–deficient mice. *The Journal of experimental medicine*, 198(8):1157–1169.

[175] Ramachandran, P. and Varoquaux, G. (2011). Mayavi: 3d visualization of scientific data. *Computing in Science & Engineering*, 13(2):40–51.

[176] Randall, K. L., Lambe, T., Johnson, A., Treanor, B., Kucharska, E., Domaschenz, H., Whittle, B., Tze, L. E., Enders, A., Crockford, T. L., et al. (2009). Dock8 mutations cripple b cell immunological synapses, germinal centers and long-lived antibody production. *Nature immunology*, 10(12):1283–1291.

[177] Randall, T. D., Parkhouse, R., and Corley, R. B. (1992). J chain synthesis and secretion of hexameric IgM is differentially regulated by lipopolysaccharide and interleukin 5. *Proceedings of the National Academy of Sciences*, 89(3):962–966.

[178] Randolph, G. J., Angeli, V., and Swartz, M. A. (2005). Dendritic-cell trafficking to lymph nodes through lymphatic vessels. *Nature Reviews Immunology*, 5(8):617–628.

[179] Rangel-Moreno, J., Moyron-Quiroz, J. E., Hartson, L., Kusser, K., and Randall, T. D. (2007). Pulmonary expression of cxc chemokine ligand 13, cc chemokine ligand 19, and cc chemokine ligand 21 is essential for local immunity to influenza. *Proceedings of the National Academy of Sciences*, 104(25):10577–10582.

[180] Reppas, A., Alfonso, J., and Hatzikirou, H. (2015). In silico tumor control induced via alternating immunostimulating and immunosuppressive phases. *Virulence*, pages 1–13.

[181] Reuschenbach, M., von Knebel Doeberitz, M., and Wentzensen, N. (2009). A systematic review of humoral immune responses against tumor antigens. *Cancer immunology, immunotherapy*, 58(10):1535–1544.

[182] Roozendaal, R. and Mebius, R. E. (2011). Stromal cell-immune cell interactions. *Annual review of immunology*, 29:23–43.

[183] Roozendaal, R., Mempel, T. R., Pitcher, L. A., Gonzalez, S. F., Verschoor, A., Mebius, R. E., von Andrian, U. H., and Carroll, M. C. (2009). Conduits mediate transport of low-molecular-weight antigen to lymph node follicles. *Immunity*, 30(2):264–276.

[184] Rutemark, C., Bergman, A., Getahun, A., Hallgren, J., Henningsson, F., and Heyman, B. (2012). Complement receptors 1 and 2 in murine antibody responses to igm-complexed and uncomplexed sheep erythrocytes. *PloS one*, 7(7):e41968.

[185] Sallusto, F., Palermo, B., Lenig, D., Miettinen, M., Matikainen, S., Julkunen, I., Forster, R., Burgstahler, R., Lipp, M., Lanzavecchia, A., et al. (1999). Distinct patterns and kinetics of chemokine production regulate dendritic cell function. *European journal of immunology*, 29(5):1617–1625.

[186] Schaller, G. and Meyer-Hermann, M. (2004). Kinetic and dynamic delaunay tetrahedralizations in three dimensions. *Computer Physics Communications*, 162(1):9–23.

[187] Schaller, G. and Meyer-Hermann, M. (2005). Multicellular tumor spheroid in an off-lattice voronoi-delaunay cell model. *Physical Review E*, 71(5):051910.

[188] Schwickert, T. A., Victora, G. D., Fooksman, D. R., Kamphorst, A. O., Mugnier, M. R., Gitlin, A. D., Dustin, M. L., and Nussenzweig, M. C. (2011). A dynamic T cell–limited checkpoint regulates affinity-dependent B cell entry into the germinal center. *The Journal of experimental medicine*, 208(6):1243–1252.

[189] Serafini, B., Rosicarelli, B., Magliozzi, R., Stigliano, E., and Aloisi, F. (2004). Detection of ectopic b-cell follicles with germinal centers in the meninges of patients with secondary progressive multiple sclerosis. *Brain pathology*, 14(2):164–174.

[190] Shulman, Z., Gitlin, A. D., Targ, S., Jankovic, M., Pasqual, G., Nussenzweig, M. C., and Victora, G. D. (2013). T Follicular Helper Cell Dynamics in Germinal Centers. *Science*, 673.

[191] Siegert, S., Huang, H.-Y., Yang, C.-Y., Scarpellino, L., Carrie, L., Essex, S., Nelson, P. J., Heikenwalder, M., Acha-Orbea, H., Buckley, C. D., et al. (2011). Fibroblastic reticular cells from lymph nodes attenuate t cell expansion by producing nitric oxide. *PLoS One*, 6(11):e27618.

[192] Siliņa, K., Rulle, U., Kalniņa, Z., and Linē, A. (2014). Manipulation of tumour-infiltrating b cells and tertiary lymphoid structures: a novel anti-cancer treatment avenue? *Cancer Immunology, Immunotherapy*, 63(7):643–662.

[193] Sofroniou, M. and Spaletta, G. (2006). Hybrid solvers for composition and splitting methods. *Journal of computational and applied mathematics*, 185(2):278–291.

[194] Stranford, S., Ruddle, N. H., et al. (2012). Follicular dendritic cells, conduits, lymphatic vessels, and high endothelial venules in tertiary lymphoid organs: parallels with lymph node stroma. *Front Immunol*, 3(350.10):3389.

[195] Swirski, F. K., Nahrendorf, M., Etzrodt, M., Wildgruber, M., Cortez-Retamozo, V., Panizzi, P., Figueiredo, J.-L., Kohler, R. H., Chudnovskiy, A., Waterman, P., et al. (2009). Identification of splenic reservoir monocytes and their deployment to inflammatory sites. *Science*, 325(5940):612–616.

[196] Szakal, A. K., Gieringer, R. L., Kosco, M. H., and Tew, J. G. (1985). Isolated follicular dendritic cells: cytochemical antigen localization, nomarski, sem, and tem morphology. *The Journal of Immunology*, 134(3):1349–1359.

[197] Szakal, A. K., Taylor, J. K., Smith, J. P., Kosco, M. H., Burton, G. F., and Tew, J. J. (1990). Kinetics of germinal center development in lymph nodes of young and aging immune mice. *The Anatomical Record*, 227(4):475–485.

[198] Takatori, H., Kanno, Y., Watford, W. T., Tato, C. M., Weiss, G., Ivanov, I. I., Littman, D. R., and O'Shea, J. J. (2009). Lymphoid tissue inducer–like cells are an innate source of il-17 and il-22. *The Journal of experimental medicine*, 206(1):35–41.

[199] Tanford, C. et al. (1961). *Physical chemistry of macromolecules*. Wiley.

[200] Tew, J. and Mandel, T. (1979). Prolonged antigen half-life in the lymphoid follicles of specifically immunized mice. *Immunology*, 37(1):69.

[201] Thaunat, O. (2011). Pathophysiologic significance of b-cell clusters in chronically rejected grafts. *Transplantation*, 92(2):121–126.

[202] Thaunat, O., Patey, N., Caligiuri, G., Gautreau, C., Mamani-Matsuda, M., Mekki, Y., Dieu-Nosjean, M.-C., Eberl, G., Ecochard, R., Michel, J.-B., et al. (2010). Chronic rejection triggers the development of an aggressive intragraft immune response through recapitulation of lymphoid organogenesis. *The Journal of Immunology*, 185(1):717–728.

[203] Timmer, T. C., Baltus, B., Vondenhoff, M., Huizinga, T. W., Tak, P. P., Verweij, C. L., Mebius, R. E., and van der Pouw Kraan, T. C. (2007). Inflammation and ectopic lymphoid structures in rheumatoid arthritis synovial tissues dissected by genomics technology: identification of the interleukin-7 signaling pathway in tissues with lymphoid neogenesis. *Arthritis & Rheumatism*, 56(8):2492–2502.

[204] Toellner, K.-M., Gulbranson-Judge, A., Taylor, D. R., Sze, D. M.-Y., and MacLennan, I. (1996). Immunoglobulin switch transcript production in vivo related to the site and time of antigen-specific B cell activation. *The Journal of experimental medicine*, 183(5):2303–2312.

[205] Tong, S. and Yuan, F. (2001). Numerical simulations of angiogenesis in the cornea. *Microvascular research*, 61(1):14–27.

[206] Tracy, D. J., Buss, S. R., and Woods, B. M. (2009). Efficient large-scale sweep and prune methods with aabb insertion and removal. In *Virtual Reality Conference, 2009. VR 2009. IEEE*, pages 191–198. IEEE.

[207] Tranquillo, R. T., Lauffenburger, D. A., and Zigmond, S. (1988). A stochastic model for leukocyte random motility and chemotaxis based on receptor binding fluctuations. *The Journal of cell biology*, 106(2):303–309.

[208] Tsuji, M., Suzuki, K., Kitamura, H., Maruya, M., Kinoshita, K., Ivanov, I. I., Itoh, K., Littman, D. R., and Fagarasan, S. (2008). Requirement for lymphoid tissue-inducer cells in isolated follicle formation and t cell-independent immunoglobulin a generation in the gut. *Immunity*, 29(2):261–271.

[209] Turgeon, M. L. (2005). *Clinical hematology: theory and procedures*, volume 936. Lippincott Williams & Wilkins.

[210] van de Pavert, S. A., Olivier, B. J., Goverse, G., Vondenhoff, M. F., Greuter, M., Beke, P., Kusser, K., Höpken, U. E., Lipp, M., Niederreither, K., et al. (2009). Chemokine cxcl13 is essential for lymph node initiation and is induced by retinoic acid and neuronal stimulation. *Nature immunology*, 10(11):1193–1199.

[211] van Eijk, M., Medema, J. P., and de Groot, C. (2001). Cutting edge: cellular fas-associated death domain-like il-1-converting enzyme-inhibitory protein protects germinal center B cells from apoptosis during germinal center reactions. *The journal of immunology*, 166(11):6473–6476.

[212] Verlet, L. (1967). Computer" experiments" on classical fluids. i. thermodynamical properties of lennard-jones molecules. *Physical review*, 159(1):98.

[213] Victora, G. D. and Nussenzweig, M. C. (2012). Germinal centers. *Annual review of immunology*, 30:429–457.

[214] Victora, G. D., Schwickert, T. A., Fooksman, D. R., Kamphorst, A. O., Meyer-Hermann, M., Dustin, M. L., and Nussenzweig, M. C. (2010). Germinal center dynamics revealed by multiphoton microscopy with a photoactivatable fluorescent reporter. *Cell*, 143(4):592–605.

[215] Victoratos, P., Lagnel, J., Tzima, S., Alimzhanov, M. B., Rajewsky, K., Pasparakis, M., and Kollias, G. (2006). Fdc-specific functions of p55tnfr and ikk2 in the development of fdc networks and of antibody responses. *Immunity*, 24(1):65–77.

[216] Vinuesa, C. G., Linterman, M. A., Goodnow, C. C., and Randall, K. L. (2010). T cells and follicular dendritic cells in germinal center b-cell formation and selection. *Immunological reviews*, 237(1):72–89.

[217] Wang, X., Cho, B., Suzuki, K., Xu, Y., Green, J. A., An, J., and Cyster, J. G. (2011). Follicular dendritic cells help establish follicle identity and promote b cell retention in germinal centers. *The Journal of experimental medicine*, 208(12):2497–2510.

[218] Wang, Y. and Irvine, D. J. (2013). Convolution of chemoattractant secretion rate, source density, and receptor desensitization direct diverse migration patterns in leukocytes. *Integrative Biology*, 5(3):481–494.

[219] Weber, P., Hasenauer, J., Allgöwer, F., and Radde, N. (2011). Parameter estimation and identifiability of biological networks using relative data. In *Proceedings of the 18th IFAC World Congress (Milano 2011)*, pages 11648–11653.

[220] Wei, S. H., Parker, I., Miller, M. J., and Cahalan, M. D. (2003). A stochastic view of lymphocyte motility and trafficking within the lymph node. *Immunological reviews*, 195(1):136–159.

[221] Wengner, A. M., Höpken, U. E., Petrow, P. K., Hartmann, S., Schurigt, U., Bräuer, R., and Lipp, M. (2007). Cxcr5-and ccr7-dependent lymphoid neogenesis in a murine model of chronic antigen-induced arthritis. *Arthritis & Rheumatism*, 56(10):3271–3283.

[222] Wickham, H. (2009). *ggplot2: Elegant Graphics for Data Analysis*. Springer-Verlag New York.

[223] Wiedemann, A., Depoil, D., Faroudi, M., and Valitutti, S. (2006). Cytotoxic t lymphocytes kill multiple targets simultaneously via spatiotemporal uncoupling of lytic and stimulatory synapses. *Proceedings of the National Academy of Sciences*, 103(29):10985–10990.

[224] Willimann, K., Legler, D. F., Loetscher, M., Stuber Roos, R., Belen Delgado, M., Clark-Lewis, I., Baggiolini, M., and Moser, B. (1998). The chemokine slc is expressed in t cell areas of lymph nodes and mucosal lymphoid tissues and attracts activated t cells via ccr7. *European journal of immunology*, 28(6):2025–2034.

[225] Wotherspoon, A., Diss, T., Pan, L., Isaacson, P., Doglioni, C., Moschini, A., and de Boni, M. (1993). Regression of primary low-grade b-cell gastric lymphoma of mucosa-associated lymphoid tissue type after eradication of helicobacter pylori. *The Lancet*, 342(8871):575–577.

[226] Yokota, Y., Mansouri, A., Mori, S., Sugawara, S., Adachi, S., Nishikawa, S.-I., and Gruss, P. (1999). Development of peripheral lymphoid organs and natural killer cells depends on the helix–loop–helix inhibitor id2. *Nature*, 397(6721):702–706.

[227] Yona, S., Kim, K.-W., Wolf, Y., Mildner, A., Varol, D., Breker, M., Strauss-Ayali, D., Viukov, S., Guilliams, M., Misharin, A., et al. (2013). Fate mapping reveals origins and dynamics of monocytes and tissue macrophages under homeostasis. *Immunity*, 38(1):79–91.

[228] Yoon, S.-O., Zhang, X., Berner, P., Blom, B., and Choi, Y. S. (2009). Notch ligands expressed by follicular dendritic cells protect germinal center b cells from apoptosis. *The Journal of Immunology*, 183(1):352–358.

[229] Zabel, B. A., Zuniga, L., Ohyama, T., Allen, S. J., Cichy, J., Handel, T. M., and Butcher, E. C. (2006). Chemoattractants, extracellular proteases, and the integrated host defense response. *Experimental hematology*, 34(8):1021–1032.

[230] Zachmann, G. (2001). Optimizing the collision detection pipeline. In *Proc. of the First International Game Technology Conference (GTEC)*, volume 2.

[231] Zhang, J., MacLennan, I., Liu, Y.-J., and Lane, P. J. (1988). Is rapid proliferation in B centroblasts linked to somatic mutation in memory B cell clones? *Immunology letters*, 18(4):297–299.

[232] Zhang, Y., Meyer-Hermann, M., George, L. A., Figge, M. T., Khan, M., Goodall, M., Young, S. P., Reynolds, A., Falciani, F., Waisman, A., et al. (2013). Germinal center B cells govern their own fate via antibody feedback. *The Journal of experimental medicine*, 210(3):457–464.

Acronyms

AABB Axis-aligned bounding boxes

AID Activation-induced cytidine deaminase

ATR Ataxia telangiectasia and Rad3-related protein

BAFF B-cell activating factor

BALT Bronchus-associated lymphoid tissue

Bcl-2 B cell lymphoma 2 protein

BCR B cell receptor

Blimp-1 PR domain zinc finger protein 1

BP-3 BP-3 antigen; ADP-ribosyl cyclase 2

C3 Complement component 3

CCL19 Chemokine (C-C motif) ligand 19

CCL21 Chemokine (C-C motif) ligand 21

CCR7 C-C chemokine receptor type 7

CD Cluster of differentiation

CI Confidence interval

CLEC2 C-type lectin domain family 1 member b

CMV Cytomegalovirus

CTLs Cytotoxic T cells

CXCL13 Chemokine (C-X-C motif) ligand 13

CXCR4 C-X-C chemokine receptor type 4

CXCR5 C-X-C chemokine receptor type 5

DCs Dendritic cells

DZ Dark zone

E-NPP2 Ectonucleotide Pyrophosphatase/Phosphodiesterase 2

FasL Fas ligand

FDCs Follicular dendritic cells

FRCs Fibroblastic reticular cells

FTCS Forward central scheme

GALT Gut-associated lymphoid tissue

GCs Germinal centres

HEV High endothelial venules

HLA Human Leukocyte Antigen

iBALT Inducible bronchus-associated lymphoid tissue

ICAM Intercellular cell adhesion molecule

IgA Immunoglobulin A

IGFBP3 Insulin-like growth factor-binding protein 3

IgG Immunoglobulin G

IgM Immunoglobulin M

IKK2 Inhibitor of nuclear factor kappa-B kinase subunit beta

IL-1 Interleukin 1

IL-6 Interleukin 6

IL-7 Interleukin 7

ISL1 ISL LIM homeobox 1 gene

LT Lymphotoxin

LTis Lymphatic tissue inducers cells

LTo Lymphatic tissue organizers

LVs Lymphatic vessels

LZ Light zone

MAdCam Mucosal vascular addressin cell adhesion molecule

MALT Mucosa-associated lymphoid tissue

MCMV Murine cytomegalovirus

MECA79 Peripheral Node Addressin Antibody

Mgfe8 Milk Fat GlobuleEGF factor 8

MHC Major histocompatibility complex

MRCs Marginal reticular cells

MUC1 Mucin 1

MVA Modified Vaccinia Ankara

NF-κB Nuclear factor kappa-light-chain-enhancer of activated B cells

NK Natural killer

NKX2-5 Nk2 homeobox 5 gene

ODE Ordinary differential equation

p52 Tumor suppressor p52

p53 Tumor suppressor p53

PBs Plasmablasts

PCKR Per capita killing rate

PDE Partial differential equation

PDGFR Platelet-derived growth factor receptor

PDPN Podoplanin

PNAd Protein NH2-terminal asparagine deamidase

RANKL Receptor activator of nuclear factor kappa-B ligand

RelB v-rel avian reticuloendotheliosis viral oncogene homolog B

RSS Residual sum of squares

S1P Sphingosine-1-phosphate

SBB/La Sjörgen syndrome antigen B, autoantigen La

SCS Subcupsular sinus

SDF1 Stromal cell-derived factor-1

SHH Sonic hedgehog

SHM Somatic hypermutation

SLOs Secondary lymphoid organs

TBM Tingible body macrophages

Tfhs T follicular helper cells

TLOs Tertiary lymphoid organs

TLR Toll-like receptor

TNF Tumour necrosis factor

TNF-RI Tumour necrosis factor receptor 1

TNFR1 tumor necrosis factor receptor superfamily, member 1A

VCAM Vascular cell adhesion molecule

XAGE1 X antigen family member 1

List of Tables

List of Figures

Aleksei Uvarovskii

Date of Birth 3rd of August, 1989

Place of Birth Velikii Ustyug, Vologda region, Russia

Education

2006–2010 **Bachelor in Applied Mathematics and Physics**, *Moscow Institute of Physics and Technology*, Moscow, Russia.
Department of Molecular and Biologic Physics

2010–2012 **Master in Applied Mathematics and Physics**, *Moscow Institute of Physics and Technology*, Moscow, Russia.
Department of Molecular and Biologic Physics

2012-2016 **Graduate School**, *Helmholtz Centre for Infection Research and TU Braunschweig*, Braunschweig, Germany.
Department of Systems Immunology

Additional education

2011-2013 School of Data Analysis (Yandex), Moscow, Russia
Courses on fundamentals of algorithms and data structures, elements of statistical learning and programming

Work experience

2011–2012 **Intern**, *Institute for Systems Biology*, Moscow.
Mathematical modeling of neutrophil apoptosis

Referees

- Dr. Stephan Halle, Halle.Stephan@mh-hannover.de, +49 511 532-9725
- Dr. Esteban Vargas, esteban.vargas@helmholtz-hzi.de, +49 531 6181-5402
- Prof. Dr. Michael Meyer-Hermann, mmh@theoretical-biology.de, +49 531 6181-5402

Publications

Hernandez-Vargas, Esteban A., Esther Wilk, Laetitia Canini, Franklin R. Toapanta, Sebastian C. Binder, Alexey Uvarovskii, Ted M. Ross, Carlos A. Guzman, Alan S. Perelson, and Michael Meyer-Hermann. "Effects of Aging on Influenza Virus Infection Dynamics." Journal of virology 88, no. 8 (2014): 4123-4131.

Halle, Stephan, Kirsten Anja Keyser, Felix Rolf Stahl, Andreas Busche, Anja Marquardt, Xiang Zheng, Melanie Galla et al. "In Vivo Killing Capacity of Cytotoxic T Cells Is Limited and Involves Dynamic Interactions and T Cell Cooperativity." Immunity (2016).

✉ *alexey.mipt@gmail.com* • in *alexeyuvarovskii*